ANL/OEPM-79-14

ANL/OEPM-79-14

ANNUAL REPORT FOR 1979 ON RESEARCH, DEVELOPMENT AND DEMONSTRATION OF NICKEL-IRON BATTERIES FOR ELECTRIC VEHICLE PROPULSION

Contract No. 31-109-38-4141

by

Westinghouse Electric Corporation

ARGONNE NATIONAL LABORATORY

ARGONNE NATIONAL LABORATORY, ARGONNE, ILLINOIS

Operated for the U. S. DEPARTMENT OF ENERGY
under Contract W-31-109-Eng-38

DISCLAIMER

The facilities of Argonne National Laboratory are owned by the United States Government. Under the terms of a contract (W-31-109-Eng-38) among the U. S. Department of Energy, Argonne Universities Association and The University of Chicago, the University employs the staff and operates the Laboratory in accordance with policies and programs formulated, approved and reviewed by the Association.

MEMBERS OF ARGONNE UNIVERSITIES ASSOCIATION

The University of Arizona
Carnegie-Mellon University
Case Western Reserve University
The University of Chicago
University of Cincinnati
Illinois Institute of Technology
University of Illinois
Indiana University
The University of Iowa
Iowa State University
The University of Kansas
Kansas State University
Loyola University of Chicago
Marquette University
The University of Michigan
Michigan State University
University of Minnesota
University of Missouri
Northwestern University
University of Notre Dame
The Ohio State University
Ohio University
The Pennsylvania State University
Purdue University
Saint Louis University
Southern Illinois University
The University of Texas at Austin
Washington University
Wayne State University
The University of Wisconsin-Madison

Printed in the United States of America
Available from
National Technical Information Service
U. S. Department of Commerce
5285 Port Royal Road
Springfield, VA 22161

NTIS price codes
Printed copy: A06
Microfiche copy: A01

Distribution Category:
Energy Storage--Electrochemical--
Near-Term Batteries (UC-94ca)

ANL/OEPM-79-14

Annual Report for 1979 on

RESEARCH, DEVELOPMENT AND DEMONSTRATION OF NICKEL-IRON BATTERIES FOR ELECTRIC VEHICLE PROPULSION

Prepared for

The Office for Electrochemical Project Management
Argonne National Laboratory
Under Contract No. 31-109-38-4141

by

Westinghouse Electric Corporation
Pittsburgh, Pennsylvania

June 1980

79-9J31-EVBAT-R2

RESEARCH, DEVELOPMENT, AND DEMONSTRATION OF A NICKEL/IRON BATTERY FOR ELECTRIC VEHICLE PROPULSION

R. Rosey, Program Manager
W. Feduska, Technical Coordinator

CONTRIBUTORS:

L. A. Doggrell, J. F. Jackovitz, C. W. Maiden
N. J. Maskalick, W. Pollack, L. G. Romain,
J. Seidel, B. E. Taber

ANNUAL STATUS REPORT FOR FY '79
PUBLIC REPORT
CONTRACT NO. 31-109-38-4141

PREPARED FOR:

ARGONNE NATIONAL LABORATORY
Chemical Engineering Division
Office of Electrochemical Project Management
9700 South Cass Avenue
Argonne, Illinois 60439
N.P. YAO, Director
RONALD ELLIOTT, TASK LEADER

OCTOBER 15, 1979

WESTINGHOUSE R&D CENTER
1310 Beulah Road
Pittsburgh, Pennsylvania 15235

TABLE OF CONTENTS

LIST OF FIGURES

LIST OF FIGURES

LIST OF FIGURES

LIST OF TABLES

LIST OF TABLES

ABSTRACT

The program has progressed to the stage of evaluating full size (220 Ah) cells, multi-cell modules and 22 Kwh batteries. Nickel electrodes are now being prepared by an electroprecipitation process (EPP) that display stable capacities of up to 24 Ah/plate (at C/3 drain rate) at design thickness (2.5 mm) in tests ongoing at 200^{+} test cycles. Iron electrodes of the composite-type are also delivering 24 Ah/plate (at C/3) at target thickness (1.0 mm). Iron plates are displaying capacity stability for 300^{+} test cycles in continuing 3 plate cell tests. Best finished cells are delivering 57 to 63 Wh/Kg at C/3, based on cell weights of the finished cells, and in the actual designed cell volume. 6-cell module (6-1) performance has demonstrated 239 Ah, 1735 Wh, 53 Wh/Kg at the C/3 drain rate. This module is now being evaluated at the National Battery Test Laboratory (NBTL), Argonne National Laboratory.

The "2 x 4" battery has been constructed, tested and delivered to Jet Propulsion Laboratory for engineering test and evaluation. The battery delivered 22.5 KWh, as required (199 Ah discharge at 113 $\overline{V}$) at the C/3 drain rate. The battery has performed satisfactorily, under dynamometer and constant current drain tests. Some cell problems, related to construction, necessitated changing 3 modules, but the battery is now ready for further testing.

Reduction in nickel plate swelling (and concurrent stack electrolyte starvation), to improve cycling, is one area of major effort to reach the final battery objectives. Pasted nickel electrodes are showing promise in initial full-size cell tests and will continue to be evaluated in finished cells, along with other technology advancements in this area.

CONCLUSIONS

1. Fiber layups are now subjected to a needle-punching process, to reduce plaque lay-up thickness and, thereby, to improve the sintering furnace throughput.

2. The electroprecipitation process has been improved and 24 Ah full size nickel electrodes at target thickness (2.5 mm) have demonstrated cyclic stability at presently 200^{+} test cycles.

3. 2.00 mm thick thermal nickel electrodes have been fabricated which have demonstrated 23 Ah in full size electrode tests and have completed over 200 test cycles to date.

4. Composite-type, full-size iron electrodes have been prepared and demonstrated 21-26 Ah at target thickness (1.0 mm). No degradation has been experienced in some experimental plates in cyclic tests presently up to 300^{+} cycles.

5. Separator systems presently being used in the pilot line have produced cells in the 0.60 to 0.70 mΩ range, compared with cells of 1.2 to 1.4 mΩ, one year ago.

6. Full size iron-nickel cells have been constructed and tested that demonstrate 57-63 Wh/Kg at the C/3 drain rate. Degradation noticed in some of these cells seems to be related to nickel electrode swelling and subsequent stack electrolyte starvation during cycling. Increased plate porosity and improvements in the grid structure may alleviate the electrolyte starvation during cycling.

7. Full-size cells have remained stable, in 100% DOD cyclic testing, for over 120 test cycles to date, with testing continuing.

8. A 6-cell module, built in the pilot line, has demonstrated 239 Ah, 1735 Wh, 53 Wh/Kg at the C/3 drain rate. This module was delivered to NBTL/ANL for their evaluation.

9. The "2 x 4" battery has been built in the pilot line, tested in-house, and delivered to JPL for their test evaluation. The battery delivered 22.5 KWh at the C/3 drain rate (199Ah at 113 $\overline{V}$). The battery is performing satisfactorily at JPL in constant current, constant speed dynamometer tests and in SAE J227 driving cycle tests.

1.0 PROGRAM MANAGEMENT

In addition to providing technical and financial control of program activities, the program management tasks include preparation of special reports required by the Statement of Work. Since the technical and financial reporting elements are covered in other sections of this report, the information presented in this section will deal with the status of the special reports and other designated activites.

1.1 Program Management Report

A program plan was submitted on schedule, reviewed by ANL personnel and found acceptable with a few revisions and clarifications required. The revised plan incorporated the suggested revisions, was submitted in May 1978 and found acceptable by ANL personnel.

The detailed program plan for fiscal year 1979, which deals primarily with revisions to the Cost Plan (DOE Form 533P) and the Manpower Plan (DOE Form 534P), was submitted and approved in February 1979.

1.2 Quality Assurance (QA) Plan

A draft QA Plan was submitted to ANL/OEPM in April 1978 and reviewed by ANL personnel. Several elements of the plan required additional clarification. All questionable elements were resolved and a subsequent submission of the QA Plan was approved March 13, 1979.

1.3 Material Report

A Material Report was submitted on schedule to Dr. John Barghusen, the ANL/OEPM official administering the study. The report includes manufacturing process flow sheets, a complete breakdown of materials used in the manufacture of nickel-iron batteries (Kg/KWh), an estimate of quantities of material that could be recycled, projected market volumes, and a forecast of battery characteristics through the year 2000. The report will be updated to incorporate recent process changes.

1.4 Recycling Study

Several commercial vendors have been contacted to discuss the feasibility of recycling materials from used nickel-iron batteries and chemical compounds derived during the manufacturing process. Alternative materials reclamation procedures which are being evaluated range from a complete separation of cell components and subsequent raw material reclamation to total cell processing in a melt furnace with only a ferro-nickel alloy as the reclaimed material. The metals market supply/demand relationships between scrap and virgin metals appears to be the dominant factor in assessing financial feasibility of a suitable reclamation process.

Nickel is the major material of concern for reclamation. Three vendors were contacted in 1978 to evaluate feasible reclamation processes:

a) National Nickel Alloy Corporation, Greenville, Pa., is currently interested in processing only the nickel electrode as a ferro-nickel alloy for nickel reclamation. A sample nickel electrode was sent to them for materials evaluation and recycling feasibility analysis.

b) INMETCO, Ellwood City, Pa., is a wholly owned subsidiary of INCO established to reclaim nickel and other precious metals. Mr. Todd Grant, President, met with Westinghouse personnel in August 1978 to discuss metals reclamation. INMETCO has the capability to reclaim nickel from ferro-nickel compounds as either nickel or to refine the scrap to other ferro-nickel alloys. Process developments are currently being undertaken to remove other tramp metals, such as cobalt, from scrap compounds. The plant is currently under construction and is expected to be operational by late 1978. Sample electrodes were sent to INCO Research and Development Center for materials evaluation.

c) The Pesses Company, Solon, Ohio, is currently a major recycler of nickel-cadmium and nickel-iron batteries in the United States. A meeting was held with Dr. Marvin Pesses, President, to discuss recycling the Westinghouse nickel-iron battery. Edison-type nickel-iron batteries are presently smelted as a unit with no attempt to reclaim materials other than the ferro-nickel alloy obtained.

Nickel-cadmium batteries are handled differently. The tops are cut off the cells and plates are separated. The nickel and cadmium electrodes are processed separately to give high purity ingots which are then sold as such. An effort is currently underway to wash the thermoplastic case material and sell it as regrind. No attempt is made to reclaim the electrolyte.

In the case of the Westinghouse nickel-iron cell design, either of the above processes is viable, dependent on the final cell design. The following criteria would determine the process selection:

1) If copper terminals are used, the cell would be cut and stripped to remove the copper since it is considered an unwanted contaminant in ferro-nickel alloys.

2) If cobalt is used at the current ratio in the nickel electrode they may also be required to strip the cell and process to remove the cobalt. Since a bulk of the ferro-nickel alloys they sell to stainless steel manufacturers ends up in nuclear equipment applications, the cobalt is an unwanted "contaminant". Dr. Pesses stated that most of the cells they currently recycle have some trace amounts of cobalt (to 1-2%).

INMETCO analyzed several nickel electrodes and indicated >95% recovery of nickel from nickel metallics or nickel chemicals from the electrode processing. The value of nickel units for recycled material is approximately 85% of Class the II primary nickel price.

Since the above three companies are primarily interested in the metals reclamation and have no current interest in plastics, the case/cover and separator materials reclamation will be investigated with appropriate thermoplastic processers and manufacturers. Recycling applications for the cell electrolyte and the spent electrolyte from the EPP process will also be determined.

1.5 Environmental Impact Study

A computer assisted literature search was carried out on the Lockheed data base, centering on the following segments: APTIC, Chemical Abstracts, Energyline, Enviroline, Compendex, NTIS, and Pollution Abstracts. Words searched were selected with a view towards environmental impact statements and included components of the battery, compounds used in its manufacture and use, toxicity thereof, safety precautions, and disposal methods. The abstracts were evaluated and the pertinent abstracts were noted. Relevant information was then retrieved from the key abstracts.

The regional Federal EPA offices and Pennsylvania Department of Environmental Resources office have been contacted for appropriate effluent information and other relevant environmental standards. Currently no standards or guidelines exist at the state or federal level for nickel battery facilities. It appears to be the consensus of those involved that if a standard were imposed, it would closely adhere to the electroplating industry guidelines which are currently published in EPA document 440/1-75/040. The major Westinghouse concern is currently concentrated on nickel electrode processing and subsequent effluent treatment requirements.

An August 1978 meeting was held with ANL personnel from Biological and Medical Research Division and Environmental Impact Studies Division to discuss the Westinghouse nickel-iron battery manufacturing processes relative to their health assessment program on near-term batteries.

Results of Westinghouse nickel-iron battery pilot plant and personnel monitoring indicates present process techniques are in compliance with known applicable Allegheny County, Commonwealth of Pennsylvania, and Federal regulations.

A complete environmental draft report is planned for submission in the second quarter FY'80.

1.6 Safety Analysis

The battery system safety analysis information was collected and reported at the first design review. Experiences obtained as a result of previously operated electric vehicle battery systems and applicable safety standards followed by other industries utilizing battery system formed the basis for the analysis.

1.7 System Specification

The preliminary specification was submitted on schedule in June 1978.

The initial Nickel-Iron Battery Specification consists of four sections. The first section relates Cell and Battery Specifications to the initial near-term target of 50 Wh/Kg (23 Wh/lb), as well as the final goal on the contract of 60 Wh/Kg (27 Wh/lb). The second section details pertinent performance information, particularly cell charge, discharge, power and temperature characteristics. The third section addresses potential performance limiting characteristics in the cell and battery. Important factors here appear to be charging energy efficiency and total electrolyte weight. The fourth section lists 11 battery tests that are planned to be performed on the nickel-iron battery. These tests will establish efficiency as a function of drain rate, charge acceptance, voltage characteristics, internal resistance behavior, open circuit capacity losses, temperature effects on capacity and life, gassing, electrolyte displacement, and short circuit currents.

The data presented in the specification have been compiled from several sources: (1) extensive, in-house background experience and data obtained at Westinghouse, (2) recent development test results on small and full-size test electrodes, and (3) engineering projection based on the present state of technology.

2.0 TECHNICAL STATUS

The technical effort during the past year was aimed at meeting the objectives of the System Development Task of the program.

2.1 System Development

The objective of the System Development task of this battery program was to demonstrate improved performance capability in prototype cells, modules, and batteries. These improvements include attaining 53 Wh/Kg and 120 Wh/l in the overall cell, under 4-8 h charge and 2-4 h discharge conditions, while exhibiting short-term, stable cycling capability.

The System Development task encompasses 5 major subtasks:

(1) the nickel electrode

(2) the iron electrode

(3) cell components

(4) cell testing

(5) pilot plant operations.

The progress toward meeting the objectives of each of these subtask areas and their present status are now described.

2.1.1 Nickel Electrode

The nickel electrode development consists of:

- controlling electrode swelling during charge/discharge cycling
- improving active material utilization
- improving the loading factor and porosity

Concurrently all these developments are aimed at reduced materials, processing, and capital costs.

2.1.1.1 The Grid Structure Development

The goal of the grid structure development is to provide the structural basis on which the optimal balance of loading, active material utilization, and final electrode porosity can be achieved. This is being accomplished by investigating variations of starting grid density and thickness and their effects on electrode loading, loaded electrode thickness, and performance. The feasibility of eliminating or reducing high cost items (e.g., nickel plating the grid prior to loading) will be tested. In addition, the ability of the grid structure to control the nickel electrode swelling, without external aids, will be investigated.

New fabrication techniques, aimed at reducing costs and improving plaque uniformity, are also being investigated. Comparison of plaques made by modified techniques with the state-of-the-art will be used to select the candidate process to be pursued.

2.1.1.1.1 Nickel Plaque Preparation

The current collector and container for the active nickel oxide is formed from steel fibers which are sintered and nickel plated to form a coherent, porous, conductive structure.

Fabrication of the porous structure or plaque begins by assembly of a number of steel wool battes[1] into an array of many layers until a given fiber weight is attained. A batte is a very low density structure that is extremely bulky and must be compressed to at least 1/3 of its original thickness during the sintering operation. To attain the final desired thickness, the sintered plaque is compacted by a rolling operation. In this operation the steel fibers are bent, some sintered bonds are broken, and the plaque is now somewhat mechanically weak. Therefore, an additional sintering operation is employed to form new bonds between contacting fibers, making the plaque stiff again, and also increasing its electrical conductivity.

Needle-Punching

Experiments with a needle-punching process[2] have shown that the bulky fiber lay-up can be readily compacted to about 1/3 its original thickness (to 3.8 cm). Several of these thinner lay-ups can now be stacked onto sintering screens and processed at one time. Only one bulky fiber lay-up could be processed on a screen through the furnace before needle-punching was employed. The barbed, triangular needle in the needle-punching process, in pushing fibers through the thick fiber lay-up, causes many fibers to break. The steel fibers used are produced by a machining process which generates many surface irregularities which, in the work-hardened fiber, are sites for stress concentration. During the needle-punching operation, those fibers that are pushed by the barbed needle beyond their yield strength or into a sharp bend are readily broken. However, the surface irregularities on these fibers cause them to hook onto other fibers during the punching operation and results in an interlocking, thinner and more dense fiber structure.

Scale-up manufacture of needle-punched plaques has been transferred to a manufacturer of steel wool (International Steel Wool) who is equipped to produce needle-punched steel wool lay-ups of 38 by 51 cm. Their machine is capable of processing 150 cm widths, but, because of our sintering furnace width limitation, these larger lay-ups will have to be cut by them into smaller width sections. The fiber in these lay-ups will be oriented such that there will be two layers in the length direction (51 cm) to one layer in the width dimension. This cross-layer procedure was initiated when it was found in our laboratory that the fibers in the highly stressed region in the vicinity of the vertical tab could be readily broken when all of the fibers were oriented parallel to the vertical tab. This separation of fibers from the tab was discovered after the plaques had been processed through the nickel EPP process.

Modified Plaque Lay-Ups

A fiber structure, in which some of the fibers are positioned 90^{o}, to the surface of the plaque would be more desireable, because of the potential improvement in mechanical strength in the thickness dimension. This improved strength would be advantageous in resisting the expansion of the active nickel oxide which is dispersed in the pores of the plaque. To achieve this type of structure, however, will require some modification of the needle-punching equipment.

In addition to improving the mechanical integrity of a plaque fabricated with a vertical tab (see Figure 2.1), a cross layer of fiber improves the electrical conductivity in a direction perpendicular to the tab. The electrical conductivity of the porous, low density fiber structure is dependent upon the orientation of the fibers, the fiber density, and the degree of contact, or bonds, between the fibers. In the original design with a bus across the top of the plaque, all of the fibers were oriented perpendicularly to the tab and the electrical conductivity was maximized in this direction and minimized in the transverse direction. However, the total fiber resistance per unit area in a plate design with a tab across the top of the plate was estimated to be higher than a design in which a vertical tab is employed. Hence the plaque design was changed to one having a vertical bus and tab, as illustrated in Figure 2.1.

The present plaque design utilizes a vertical tab that is spot welded to the fiber plaque after the first sintering operation. This placement reduces the effective volume in the plaque for deposition of active material. This active area (and volume) is equivalent to that formerly used with a tab across the top of the plaque. However, these vertical tabs do not image the counterelectrodes in the same area and there results some expected but small loss in plate performance.

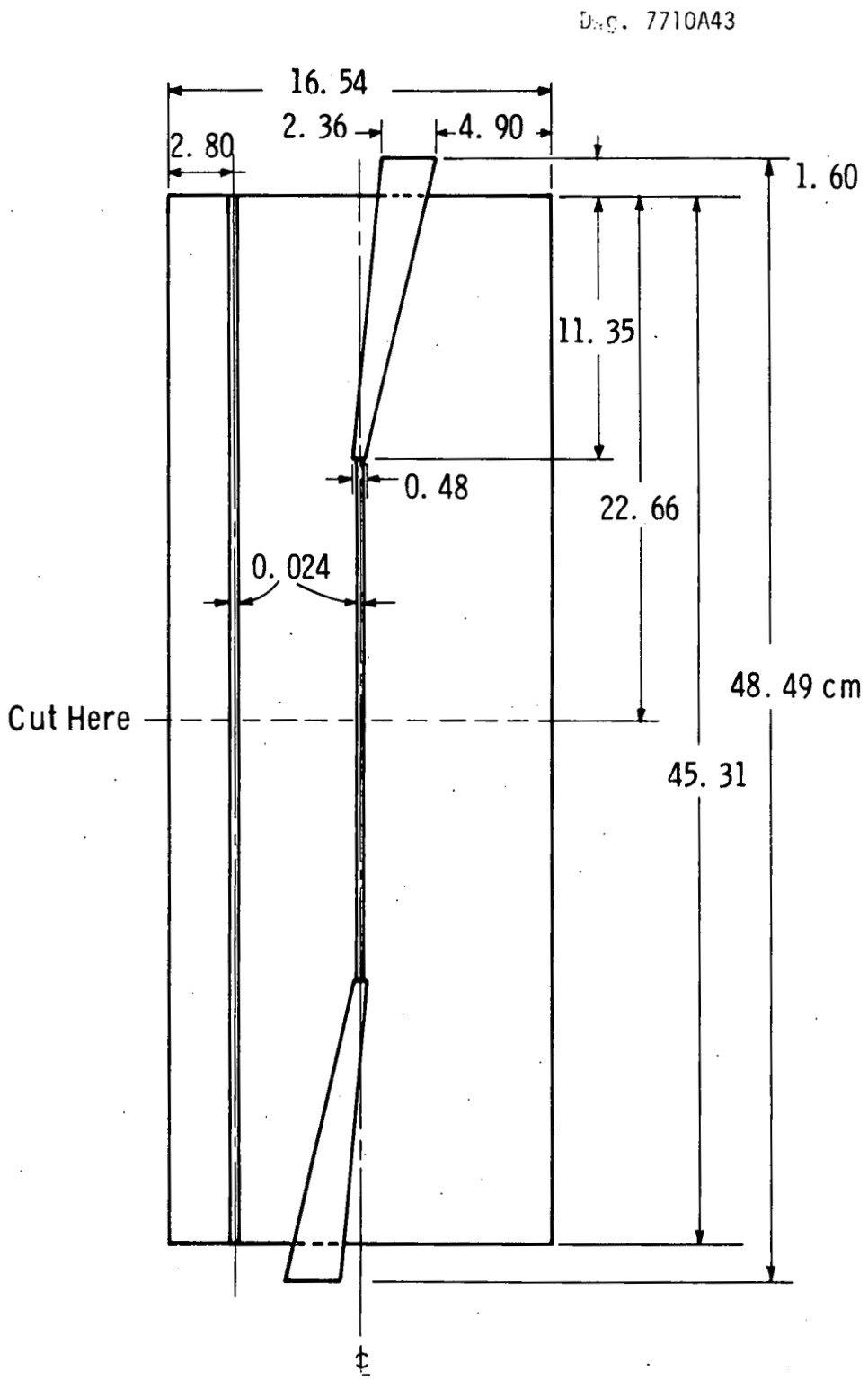

Fig. 2. 1 — Present outward plaque design for nickel electrodes. Thickness is 1. 91 mm prior to EPP active material loading, and 2. 54 mm after loading.

Experiments have been performed with plaques in which a tab is inserted between two needle-punched layers of fibers, prior to the sintering operation. This tab is attached to the fiber by a small spot weld at the top of the plaque prior to sintering. Additional fiber-tab bonds are formed during sintering. The primary benefit would be an increase of available volume for active material loading; however, the projected increase in manufacturing costs due to the more complex structure fabrication has led to the decision to terminate this development effort.

Plaque Electrical Resistance

The effect of fiber orientation and nickel plating, on the electrical resistance of the plaque is illustrated in Table 2.1. These measurements were made in the fiber area only, using a four-point voltage drop determination on a two plate plaque, as illustrated in Figure 2.2. The effect of either a single or a double sintering on the electrical resistance is shown to be somewhat insignificant after the sintered plaque has been nickel plated (Table 2.2). A very significant degradation of electrical conductivity is noted as a result of mishandling a fiber plaque (Table 2.2 - Plaque T 3/4) which caused some fibers to separate near the end of the vertical tab.

Measurements have shown small differences in electrical resistance, depending on the fiber orientation or type of tab (e.g., solid, split or spot welded to expanded metal). An attempt to follow several of these plaques through the EPP nickel process was not too successful, due to process variations. Similar difficulties were encountered with other plaques processed with the equipment at that time, indicating that other variables were being introduced into the experiment. Some 40 additional plaques, containing similar fiber processing variables, have been prepared and are ready to be processed.

Table 2.1

ELECTRICAL RESISTANCE OF FIBER METAL PLAQUES FOR NICKEL ELECTRODES

Plaque	As Sintered mΩ(a)	Nickel Plated mΩ	Remarks
1	0.26	0.18	Longitudinal and tube wound fibers. Bus welded on outside.
2A	0.31	0.21	Longitudinal and tube wound fibers. Bus between two needle punched layers.
2B	0.29	0.19	
3A	0.23	0.17	Longitudinal fibers. Bus between two needle punched layers. Exmet welded to bus. 1.2 x 2.0 cm
3B	0.22	0.17	

a) Measured at center between vertical tab buses - 15.24 cm apart (point 1 to point 1 in Fig. 2.2).

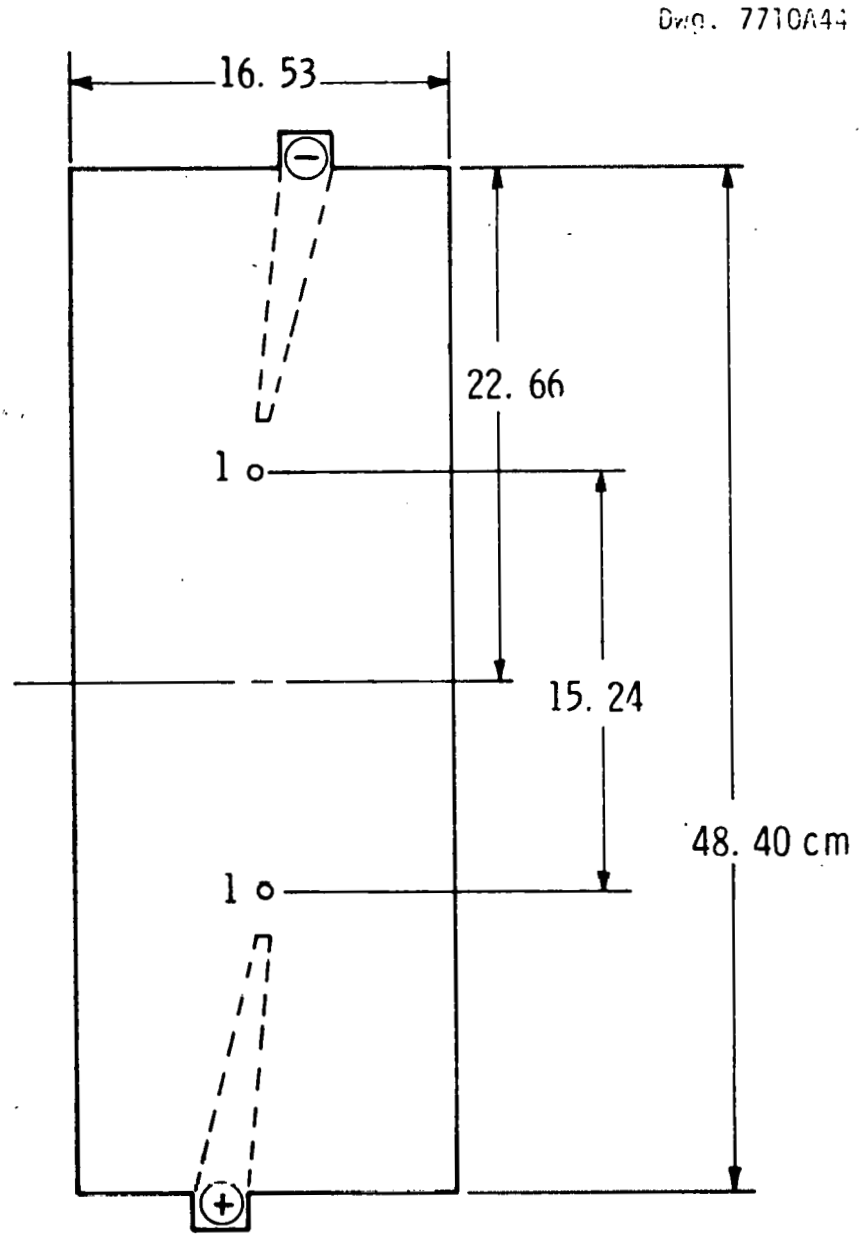

Fig. 2. 2 — Location of voltage probes (1-1) for electrical measurement of fibermetal plaques in a double-plaque processing configuration.

Feduska
b. m. - jd 11-19-79

Dwg 7710A44

TABLE 2.2

ELECTRICAL RESISTANCE OF FIBER METAL PLAQUES FOR NICKEL ELECTRODES, HAVING (1) IMBEDDED VERTICAL TABS, (2) 1 OR 2 SINTERINGS, (3) SINGLE OR CROSS-ORIENTED FIBERS

Plaque No.		Tab Type	Sinter	Resistance (MΩ) $R_{1\ 1}$
F1 11/12		Solid	1	0.17
F1 19/20		Solid	1	0.15
F1 13/14		Solid	1	0.18
F1 17/18		Solid	2	0.16
F1 15/16		Solid	2	0.15
F1 3/4		Spread	1	0.15
F1 9/10		Spread	1	0.15
F1 1/2		Spread	1	0.20
F1 5/6		Spread	2	0.15
F1 7/8		Spread	2	0.13
T 19/20	Cross Fiber	Welded	2	0.20
T 3/4	Cross Fiber	Welded	2	0.23
560/561		Welded	2	0.16
2087/8J		Welded	2	0.19
2076/5J		Welded	2	0.17

2.1.1.1.2 Iron Plaque Production

The current collector for the iron electrode is a porous structure presently formed from a combination of steel fibers and an expanded steel sheet. The expanded metal is the center layer for the fiber structure, which is formed on either side, using a similar fiber lay-up technique as developed for the plaque used for the nickel plate. The plaque is sintered in hydrogen, trimmed, and a tab seam welded to the plaque. An advantage of this composite porous structure is that the expanded metal appears to offer some stiffness in handling during the seam welding operation. The grid structure for the iron plate is not processed through a second sintering operation, as is the grid for the nickel plate. The change in plaque design to a vertical tab, instead of the horizontal tab across the top of the plaque, has changed the procedure for the welding operation. However, with a low density, porous fiber metal structure, such as the iron plaque, the expanded metal screen appears to give a better weld structure with the tab. Experiments have been initiated to evaluate an iron plaque without an expanded metal grid. Plaques from a needle-punched, fiber lay-up are being used in this latter experiment.

The effect of fiber orientation and fiber cross-section on electrical resistance are shown in Table 2.3. The lower density fiber structure has a significantly lower conductivity than the higher density structures, as would be expected. The difference shown for longitudinal and cross-layer plaques is for the unplated condition. Nickel plating would be expected to improve the electrical conductivity of the plaque and more significantly for a lower density plaque having a vertical tab since the plating, in effect, increases the fiber density.

Table 2.3

ELECTRICAL RESISTANCE OF FIBER METAL PLAQUES[a] FOR IRON ELECTRODES

Plaque	Orientation and Fiber Type	Resistance mΩ
A	longitudinal 1/0 size	0.43
B	longitudinal 1 size	0.44
C	Cross-layer 1/0 size	0.93
D	Cross-layer 1 size	0.95

[a]Single sintered and unplated.

2.1.1.2 The Nickel Electrode Electroprecipitation (EPP) Process

The objective of this subtask is to improve upon the established Westinghouse EPP process[3] for preparing nickel electrodes. Specifically, the work is aimed at developing nickel electrodes with 0.25 Ah/g active material, 0.14 Ah/g total electrode and 0.075 Ah/cm^2, all at the 3h discharge rate. These goals are to be attained in plates of 2.5 mm maximum thickness with 25 Ah capacity. The EPP process technology, at the onset of this program, made 343 cm^2 plates with the following specifications: 0.20 Ah/g active material, 0.12 Ah/g total electrode, 0.07 Ah/cm^2 at the 3h discharge rate, and 3.3 mm in thickness.

In addition, plate design and process techniques are being investigated both to improve plate dimensional stability and eliminate the need for the nickel plating step.

Also on the program, the EPP process is being further refined to meet the technical requirements of the nickel plate while minimizing process time and material losses.

Experiments conducted to date show EPP, as applied to fiber plaque substrates, is most consistently accomplished by employing two levels of impregnation. These levels are first "high" current, followed by "low" current.

According to the concept arising from our experiments, the "high" current step reaches a saturation level with respect to accomplished impregnation with $Ni(OH)_2$ in a short time. The "low" current step, which is required to complete the $Ni(OH)_2$ packing up to densities needed for target capacity, can take from 16 to 40 hours to reach completion, as presently executed.

It was found possible to further increase effective plate capacity by modifying the procedure by including a charge/discharge step between the two levels of EPP processing. The result is a high-capacity plate -- 25.0 Ah at a 2.5 mm plate thickness. Total elapsed processing time is approximately 48 hours. This plate processing has been

identified as a standard employed in positive plates for the "2 x 4" battery, and for all other positives manufactured during 1979.

2.1.1.2.1 Plate Swelling

EPP runs occasionally result in very high capacity plates, but with excessive swelling (up to 3.8 mm). This swelling during processing could be associated with incomplete nickel plate coverage of the steel wool fibers during the electrolytic nickel plate step. All plaques presently produced show less plate swelling as a result of extending nickel plating time. The additional plating also provides a stiffer structure which should reduce swelling during cyclic operation.

2.1.1.2.2 Maintenance of LiOH in the Formation Tank

LiOH content affects EPP $Ni(OH)_2$ formation by promoting β-NiOOH as the preferred product on charge and limiting the amount of less-desirable α-NiOOH[4]. Therefore, LiOH is maintained at 15 g/l in the KOH formation bath.

The composition of the KOH forming bath has been stabilized using a protective blanket of plastic spheres, employed to limit CO_2 absorption when the surface of the KOH solution is exposed to air. This method of maintaining the concentration of LiOH, via the use of a protective surface blanket of plastic spheres, is employed in the pilot line formation tank as a process control measure.

2.1.1.2.3 Effect of Fiber Density on Plate Performance

Nickel plaques, employing 1/0 size steel fibers and a three-groove surface on one side, were nickel plated. They were then evaluated for performance, after being carefully processed according to our current EPP schedule. Six plaques each, of high, regular and low density were processed. The loadings and performance measured at the 3 h rate on discharge #1 are as follows:

Table 2.4

EFFECT OF FIBER DENSITY ON NICKEL PLATE PERFORMANCE

Fiber Density	Act. Mtl Loading g/Plate	Capacity Ah/Plate	Ah/g Active
(high)	82	21.2	0.26
(reg.)	100	21.6	0.21
(low)	106	20.0	0.19

Final plate thicknesses were generally in the 2.3-2.4 mm designed range. Lowest plate loadings and highest active material efficiency are found with high-density fiber plaques. Judged on an economic basis substituting steel for some $Ni(OH)_2$ would appear to be advantageous since capacity-per-unit weight of plate (0.10 Ah/g of plate) is independent of fiber density.

These results were reproduced in subsequent EPP runs using groups of six high-density plaques and six low-density plaques. The results confirmed the trend reported in Table 2.4, with high-density fiber yielding higher active material efficiency.

A third rack of six plaques, employing high fiber density, was prepared and tested. The results continued to show that increasing fiber density enhances utilization of positive active material. In this run, plates having 23.1 Ah were produced. These higher fiber density plaques, due to their lower loading of $Ni(OH)_2$ and greater mechanical integrity, also promise to contribute to a design having less swelling characteristics.

Perforated Plate Design

To provide expansion space within the stackup and, thereby alleviate swelling pressure, a concept employing perforated plates is being evaluated. Nickel plates, each incorporating 100 holes, 6.4 mm in diameter, have been prepared and are being evaluated in full-size cells. A set of identical positive and negative plates, with the holes imaged, have been similarly prepared for evaluation in a 250 Ah cell featuring stackup constraining bolts. These design concepts should not only

demonstrate less swelling, but should also have the beneficial effect of providing increased electrolyte within the stackup.

2.1.1.2.4 Performance of Nickel Plates Having No Cobalt

Because of the present shortage and sharply increased cost of cobalt on the open market, the composition of the positive plate was critically examined. Evidence in the literature indicates that the present 20:1 Ni to Co ratio cannot be significantly changed without deteriorating life and capacity performance.[5,6]

Various candidate elements offer some promise as a substitute for cobalt. It is claimed, for instance, that much, if not all production of nickel positive electrodes in Russia is cobalt-free. Barium is directly mixed in the positive paste as the hydroxide. However, performance of these plates is reputed to be inferior to cobalt-containing plates.

Other additives which have been employed are manganese and cadmium. Various manufacturers in the United States have employed them, either exclusively or in combination with some reduced amount of cobalt. The effect appears to be one of enhancing capacity and extending cycle life, though not as effectively as cobalt does alone.[5,6,7]

A designated criterion for selection of candidate materials is the crystal habit of the hydroxide species. It is reasonable to expect that candidate hydroxides should be crystal analogs of $Co(OH)_2$ if they are expected to function like $Co(OH)_2$, as a capacity enhancer and cycle life extender for the positive plate.

Known crystal analogs of $Co(OH)_2$ are: $Mg(OH)_2$, $Fe(OH)_2$, $Mn(OH)_2$, $Cd(OH)_2$, $Ca(OH)_2$. The order listed is that of relative unit cell volume, although other criteria, such as free energy of formation, metal ion radius or solubility in KOH may be more important properties.

It will be our objective to determine whether incorporation of these alternate materials in EPP processing, as distinguished from

direct pasting methods which will also have to be considered, can equal or improve performance of positive plates using cobalt.

Finally, less-known candidates, such as zinc and, perhaps copper or silver, will be examined to determine their suitability. Since the actual mechanism of the cobalt effect is not known, these choices are determined largely by reports in the literature, and, to some extent by ionic radius or by phase-diagram evidence of compound formation with NiO or NiO_2.

In an initial phase of this work, we have prepared cobalt-free EPP plaques as control specimens. To date, six development plaques have been made. Initial capacities are, typically, 18 Ah. We know that comparably processed plaques with cobalt have a capacity range of 22-25 Ah. The cobalt-free plates will be cycled to determine the life degradation characteristics.

2.1.1.2.5 Plates With Reduced Thickness For 25-Plate Cell

An advanced cell, employing electrodes having 85% of the nominal thickness, is being processed to assess performance in a 25 plate stackup. This design should provide lower cell resistance (more power) and less total stackup swelling on cycling. Matching iron electrodes have also been prepared; special post and comb assemblies have been fabricated. Assembly of this cell will occur in September 1979.

2.1.1.2.6 EPP Nickel Plate Summary

Probably the most important design problem related to long service life of the nickel-iron cell is the stackup swelling, due to an increase in the positive plate thickness and resulting in stack electrolyte starvation during cycling. Three design approaches are under development and evaluation in order to circumvent and/or minimize positive plate swelling. These are:

(1) high-strength, low-loading, high active material utilization plates, via a high fiber density plaque design.

(2) in-plate expansion spaces, via a perforated plate design.

(3) new current collector concepts, e.g., wire brush type geometry.

As evaluation of full-size cells proceeds, regular measurement of plate shape change and of respective cell case expansions will provide figures of merit for each of these design approaches, from which ranking the best approach can be selected.

2.1.1.3 Thermal Nickel Process

The performance goals for the thermal nickel electrode are the same as those for the EPP nickel electrode. Thermal preparation of active material and subsequent pasting of this material into a grid can offer a reduction in total electrode cost and a significant decrease in capital equipment expenditure, relative to the EPP process. Refer to Appendix B for process description. Efforts during the past year have centered on study of methods for continuous, large batch preparation and formulation of an optimum active material paste composition that can be incorporated into a fiber metal plaque.

2.1.1.3.1 Preparative Methods

Several methods for large scale preparation of thermal nickel active material were explored. These included resistance and induction heating, using nickel crucibles as containers, plasma spray torches, and continuous reaction in a heated, rotating nickel tube. The most effective and reliable of these methods proved to be resistance heating in a nickel crucible. Sufficient material for 10 full-size cells can be prepared daily, using a laboratory size oven and nickel crucibles. This material is qualified using laboratory size electrode samples and performs comparable to EPP electrodes at 0.23 to 0.25 Ah/g at the three hour discharge rate.

2.1.1.3.2 Starting Materials

Several nickel oxide starting materials have been used in an attempt to reduce the overall cost of the final active product. The best oxide for consistent performance is INCO Black NiO. Another material marketed by INCO, named NOS-75, is a sintered nickel oxide containing 76% nickel and about 1% cobalt oxide. Since cobalt is an expensive EPP additive, this would help cut our costs even further. The NOS-75 material is priced at $1.96 per pound of contained nickel, compared to $2.15 per pound of black NiO on the same basis. However, the NOS-75 oxide contains small amounts of heavy metal impurities which appear to reduce active material performance 10-15% lower than that found for the black NiO. Therefore, no further evaluation of the NOS-75 is planned at present.

2.1.1.3.3 Process Modification

Development efforts were initiated for modifying the process for thermal nickel active material preparation. Experiments with partial and total substitution of sodium peroxide with sodium nitrate have been completed using a 2 kg batch. Results on small and full-size plate testing demonstrate that active material with a utilization of 0.25 Ah/g (at C/3 drain rate) can be prepared. Considerably less attack on the nickel container was noted when $NaNO_3$ was used. Significant cost reduction can be realized using the nitrate process, due to lower raw materials cost and possible recovery of exhaust gases which could allow regeneration of $NaNO_3$.

2.1.1.3.4 Electrode Construction

Thermal nickel active material is loaded into the fiber metal plaque structure using a roll pasting procedure. To assure uniform distribution and control over loading for a given plaque thickness, the paste must remain homogeneous during rolling. Test results indicate additives used to prevent curdling do not affect active material

performance. The target performance of thermal nickel electrodes in the nickel-iron battery is 0.14 Ah/g of finished plate at the C/3 discharge rate.

A large number of full-size (345 cm^2) electrodes have been constructed and tested. The loading procedure begins with plaques about 4.5 mm thick, the paste is then loaded, dried and then sized to 2.3 mm, or less. Loadings of 90-100 g active material per full-size plaque are achieved at 1.8 to 2.1 mm final thickness. These plates have shown stable performance in the 20 to 23 Ah (.20 to .24 Ah/g) range over hundreds of test cycles.

Initial full size cells were constructed using thermal nickel electrodes about 2.3 mm thick and with 105 g active loading. These electrodes increased in thickness to 2.6 mm on continued cycling which caused some swelling of the cell case, leading eventually to a loss of performance. A second set of cells were prepared, using nickel electrodes of 2.0 mm initial thickness wilh 95 g active material loading. These, surprisingly, gave outputs equivalent to the thicker, more-heavily loaded electrodes initially tested. Performance test results are summarized in Sections 3.1.2. Full size modules containing such nickel electrodes are currently being assembled for testing.

2.1.2 Iron Electrode

Iron electrode development was initially centered on two specific technologies, a briquet process which consisted of a pressed, sintered, powder metal approach and a composite process which consisted of a pasted, reduction process.

Iron electrode development is now restricted entirely to the composite type. The composite type electrode contains a fiber metal expanded metal conducting grid system to carry the current and to allow integral attachment of the connecting tab. This structure can provide excellent power characteristics for the iron electrode. The nickel-iron battery design required an iron electrode of 345 cm^2 active

area, approximately 1 mm in thickness, and having an output of 26.5 Ah at the C/3 discharge rate. The final program goal is to obtain 0.27 Ah/g of total iron electrode, entirely on the upper voltage discharge plateau. All full size cells to date contain composite type iron electrodes.

2.1.2.1 Iron Electrode Preparation

The current collector for the iron active material is a porous structure, presently formed from a combination of steel fibers and an expanded steel sheet. The expanded metal is the center layer for the fiber structure, which is formed on either side using a similar fiber lay-up technique as was developed for the nickel plaque. The single plaque is sintered in hydrogen, trimmed, and a tab is seam welded on one end. Since the expanded metal at present is available only in 22.9 cm width, plaques for single plates are being fabricated. The expanded metal appears to provide some stiffness in handling during the bus-tab seam welding operation giving an apparent process advantage. The grid structure for the iron plate is not processed through a second sintering operation, as is the grid for the nickel plate.

The subsequent process steps in the production of full size electrodes are: (1) the loading of the grid with oxide and phenolic, (2) the reduction of this mixture and (3) the pressing of the composite to a final thickness of 1 mm. The initial thickness of the sintered grid of about 5 mm is readily coined to 3.7 mm so as to limit the paste loading. At this thickness the paste is readily and rapidly loaded by means of rubber rolls. By means of hard rolls the loaded grid is then sized to 2.2 mm to remove the excess paste, so that the controlled volume of the retained paste is uniformly loaded within the voids of the grid. Control over the amount and uniformity of the loading is based on the expansive structure of the steel wool grid and upon the use of a suitable paste of the oxide.

Following the pasting step and prior to the reduction step, a drying operation is required to remove the paste water. With the water removed a rather open structure results which offering easier access for the hydrogen gas during the in-situ reducing step. A continuous-belt, hydrogen atmosphere furnace is used for the reducing step.

The overall dimensions of the electrode are not affected by the reduction step. In pressing to the final thickness, the reduced electrode with the requisite loading is readily pressed to 1 mm with no distortion to the other two dimensions.

2.1.2.2 Active Material

For the composite-type iron electrode, the starting active material consists of iron oxide and phenolic resin. Overall electrode performance is strongly dependent on the nature of the red iron oxide starting material. Initial success was obtained using Red Iron Oxide which is prepared by the calcination of ferric sulfate. Some residual sulfate remains after calcination and this imparting a degree of catalytic activity to the iron oxide.

Several suppliers were contacted to provide iron oxides produced to our specifications. Experiments with other calcined red oxides yielded 23-25 Ah in full size plate tests, which is comparable to the original material and at approximately 1/3 the projected material cost.

Evaluation of several types of phenolic additives has been completed in full size electrode tests. A wide variety in electrode performance was apparent, depending on the phenolic used. One of the candidate materials was incorporated into pilot line manufacturing of composite iron electrodes for the first full size battery. Full size electrodes, tested using this resin, gave 24-27 Ah -- meeting near term objectives for cell performance. More recently, some storage problems with this material, particularly caking, have incurred. Several options, discussed with the manufacturer, will be explored to overcome these handling problems. The higher level of capacity has been maintained to cycle 250, at 80% depth of discharge for the C/3 rates.

2.1.2.3 Iron Electrode Life Tests

Full size iron electrodes are currently on test to determine the effects of certain components on iron electrode life. The variables include nickel plating of the steel wool matrix, phenolic content of the active material and size of the steel wool fiber. These tests are designed to give insight into the reliability of these components over 1000 continuous test cycles. A summary of test results is given in Table 2.5. Electrode FX 907 was removed from continuous testing at 160 cycles at a capacity of 18.0 Ah. No expansion from the 1 mm initial thickness was measurable. This electrode retained its hard and smooth surface and showed only a very slight weakness in the tab junction. No corrosion in the main body of the electrode was observed. It is possible that the slightest degradation at the tab junction contributed to the 20% decline in capacity observed for this electrode.

Electrode FX 905 was removed from test after 130 cycles since its capacity had declined to 17.2 Ah. Examination revealed no apparent reasons for the capacity decline. The nickel counter electrodes were old and were found to be deteriorating severely. New nickel counter electrodes were inserted and cyclic testing was resumed. An immediate increase from 17.2 to 20.7 Ah was obtained This higher level of capacity has been maintained at cycle 400.

Simultaneously, new counter electrodes were inserted in test cells FX 901, 902, 903, 904 and 906, since these also had shown some steady decline. As is shown in Table 2.5, significant increases were noted for most cells. Voltage monitoring indicates that the iron electrodes continue to perform well at 400 continuous cycles. These life tests are continuing.

Table 2.5-Cyclic Stability for Composite Iron Electrodes in 25% KOH + 15 g/l LiOH Electrolyte at the C/3 Discharge Rate

	Ah Capacity vs. Cycle #					
	5	10	50	125	200	400
FX901	21.9	24.2	24.3	22.9	(22.2)*	21.9
FX902	17.5	19.1	23.6	20.6	(19.7)	15.7 (off @ 418)
FX903	24.6	24.7	24.5	20.0	(21.4)	17.5 (off @ 412)
FX904	24.9	25.1	24.7	22.6	(22.5)	21.8
FX905	17.6	21.1	22.4	17.2	(20.7)	21.7
FX906	18.7	22.6	24.3	22.1	(21.2)	22.1
FX907	19.3	22.9	23.0	20.9 (off at 160)		-

NOTES:

Active area = 53.2 in^2 = 345 cm^2

Thickness = 40 mils = 1 mm

Electrodes are discharged versus nickel counter electrodes to a final cell potential of 0.97 V for each test cycle.

*parenthesis ( ) indicate insertion of new nickel counter electrodes into 3 plate test cell.

2.1.3 Cell Components

Development work on cell components includes: cell and inter-cell connectors, separator(s), cell case and cover, and cell auxiliaries that deal with semi-automatic water feeding and/or electrolyte recirculating systems.

2.1.3.1 Separators

Efforts in separator development were concentrated on lowering cell resistance to (0.6-0.7 mΩ), needed to obtain suitable power from the full-size cells. At the start of the year the cell resistance range was too high (1.2-1.4 mΩ).

Separator resistance, per se, is only 2% of this high cell resistance, as is shown in the following calculation for a combination absorber-barrier-absorber separator, having a total resistance of 190 m $/cm^2$.

Positive plate area (one side) = 148 cm^2
Total separator area in 21 plate cell = 2950 cm^2
Separator component of cell internal resistance = 0.026 mΩ,
i.e., 2% of 1.3 mΩ.

In cell performance, however, separators have a much greater influence on internal resistance than can be attributed to their resistance measured on a separator resistance tester. As an example, cell 007CE was constructed with a low resistance nylon absorber, Pellon 2506K, and no barrier. The resistance of this cell was in the acceptable range, 0.66 mΩ. Another cell (008CE) was then constructed with the same type of absorber but with the addition of a barrier (balance 3501). The resistance of this cell was high, 1.07 mΩ. Thus the addition of a barrier, with a total resistance of 0.003 mΩ as calculated from separator resistance measurements, raised the resistance of the cell 0.41 mΩ (1.07-0.66).

The increase in resistance of cell 008CE beyond the resistance of the barrier added is difficult to explain. However, the increase in resistance may be explained by an increase in separator gas entrapment. More gas may be trapped by a separator with a barrier because the mobility of the gas escaping from the plates may be reduced i.e., the additional volume of the barrier physically reduces the space between the plates used by a bubble to escape.

To test the premise that gas entrapment in separators may be a factor in high cell resistance, a cell was attached to a vacuum pump while on discharge. The cell was discharged at 83A for 70 minutes. The cell was evacuated for 5 minutes after 46 minutes of discharge. Resistance readings were made before the vacuum was applied, while the vacuum was on and after the gas in the cell was returned to atmospheric pressure. Each time resistance readings were obtained by reading cell voltages at 83A, 43A and 23A. The results are shown in the following table.

TABLE 2.6

CHANGES IN CELL INTERNAL RESISTANCE CAUSED BY APPLYING A VACUUM WHILE ON DISCHARGE

Cell discharged at 83 amps. Vacuum on for 5 min., starting after 46 min. of discharge.

Time Of		Internal Resistance mΩ	
Discharge - Min.	Vacuum	83A-43A	43A-23A
45	off	1.02	1.2
50	on	.90	1.3
55	off	.70	1.0
70	off	.83	1.0

Two observations can be noted from this data:

(1) Internal resistance was lower at higher rates of discharge (corroborating earlier findings at Westinghouse.)

(2) Applying a vacuum during discharge, tended to lower cell internal resistance, particularily, after the vacuum was discontinued.

The results of this test supported the design decision to imprint vertical grooves in the plates faces to improve electrolyte circulation and assist the escape of gas formed during charging.

Cell 013CE was constructed with 3 vertical grooves in the positive plates, which resulted in a cell resistance of 0.71 mΩ. However, in subsequent cells, with 2 vertical grooves, we were not able to consistently obtain resistances this low.

New absorbers from Kimberly-Clark (KC) were tested which have a lower resistance on the separator test than Pellon 2506K nylon. Cells made with these new KC polypropylene fiber-based materials had internal resistances ranging from 0.71 to 0.85 mΩ.

A decision then had to be made as to which separators should be used on a run of 200 cells in the pilot line. Because there was no clearcut evidence as to which was best, we decided that three groups of cells would be made, each with a different separator system. These systems, and the reasons for using them were:

(1) Kendall absorber and Celanese barrier. This absorber was chosen because it was similar to the material that had performed satisfactorily in cells fabricated in previous iron-nickel battery projects.

(2) Kimberly-Clark absorbers and Celanese barrier. These absorbers were chosen because they have the lowest resistance of any we have tried, at comparable thickness.

(3) Celanese laminate. This is a laminated material made by Celanese with a barrier and an absorber made by Crown Zellerbach. The polypropylene fiber absorber is laminated to the barrier by a "point bonding" technique. The laminate has a somewhat higher resistance than unlaminated materials, but we have had very good experience on life tests of full-size cells made with such material.

Pellon 2506K absorber was not deemed satisfactory because it is made of nylon fibers which have a demonstrated low chemical resistance to electrolyte at the 60°C cell operating temperature limit.

The cells in which these separator systems were used were designed for circulating electrolyte, and were tested for internal resistance at higher drain rates than previous cells. They were tested between 200A and 100A, whereas previously, tested were between 83.3A and 41.6A. The internal resistances of all these cells were in the range 0.5-0.7 mΩ, which is better than the objective of 0.6-0.8 mΩ. From previous work, we know that internal resistance is lower when measured at higher rates and this is, most likely, the explanation for the lower internal resistance measurements.

In our work with nickel-iron cells we have mostly used Kendall absorbers. E 1583 was the standard separator in a previous project, but we have since found that cells built with other materials, such as 1645, have lower internal resistance. Unfortunately, Kendall was not successful in their last attempt to reproduce the 1645 material for us, and their substitute, 1003, has a resistance similar to E 1583.

2.1.3.2 Connector Development

The continuing objective of this subtask is the development of inexpensive, reliable, and highly conductive electrical connectors. Two types are distinguishable by environment, the internal connections, requiring caustic-resistant components, and the external connections. To date, more emphasis has been placed on the internal assembly. The

present internal design for the cell terminal assembly is a four piece component system, involving three joints: (1) electrode-to-tab, (2) tab-to-comb, and (3) comb-to-terminal post joining. Experimentation is being conducted on joining materials and techniques. The external intercell and intermodule connections are nickel-plated copper bus-bar with soldered joints.

Only one change has occurred with the electrode-to-tab joint. We found that plaques with the horizontal tabs were not as resistant to bending during handling as plaques with vertical tabs. The vertical tabs now comprise part of one vertical flow channel for the electrolyte in the finished cell. Until the tabs can be eliminated completely, no further effort will be expended on improving the electrode-to-tab joint.

The tab-to-comb joint has received much attention. At present we still use TIG welding with methods of keeping adjacent components, especially the separators, cool. Attempts have been made to identify alloys for brazing the connection in order to lower the tab-to-comb joining temperature. These braze alloys must be tested electrochemically. However, even the lowest melting temperature alloys tried have yet to provide sufficiently low local temperatures when the assembly is induction heated during the joining operation.

Effort has been placed on the development of a comb-to-terminal post joint which can be made prior to cell assembly and stacking. The connection made between the comb and terminal post, formerly made by TIG welding, went through several design changes, before a brazing technique could be implemented. Since the present post design is a steel-clad copper configuration the depth of the braze and the ratio of exposed steel to exposed copper had to be maximized. This was one of the few problems encountered with the change from the solid steel to the steel jacketed copper posts. Although brazing was initially used between steel combs and steel posts, it became necessary, with copper present in the bimetal post, to weld the joint. No difference in conductivity at the joint is perceived with either welding or brazing, but a reduction

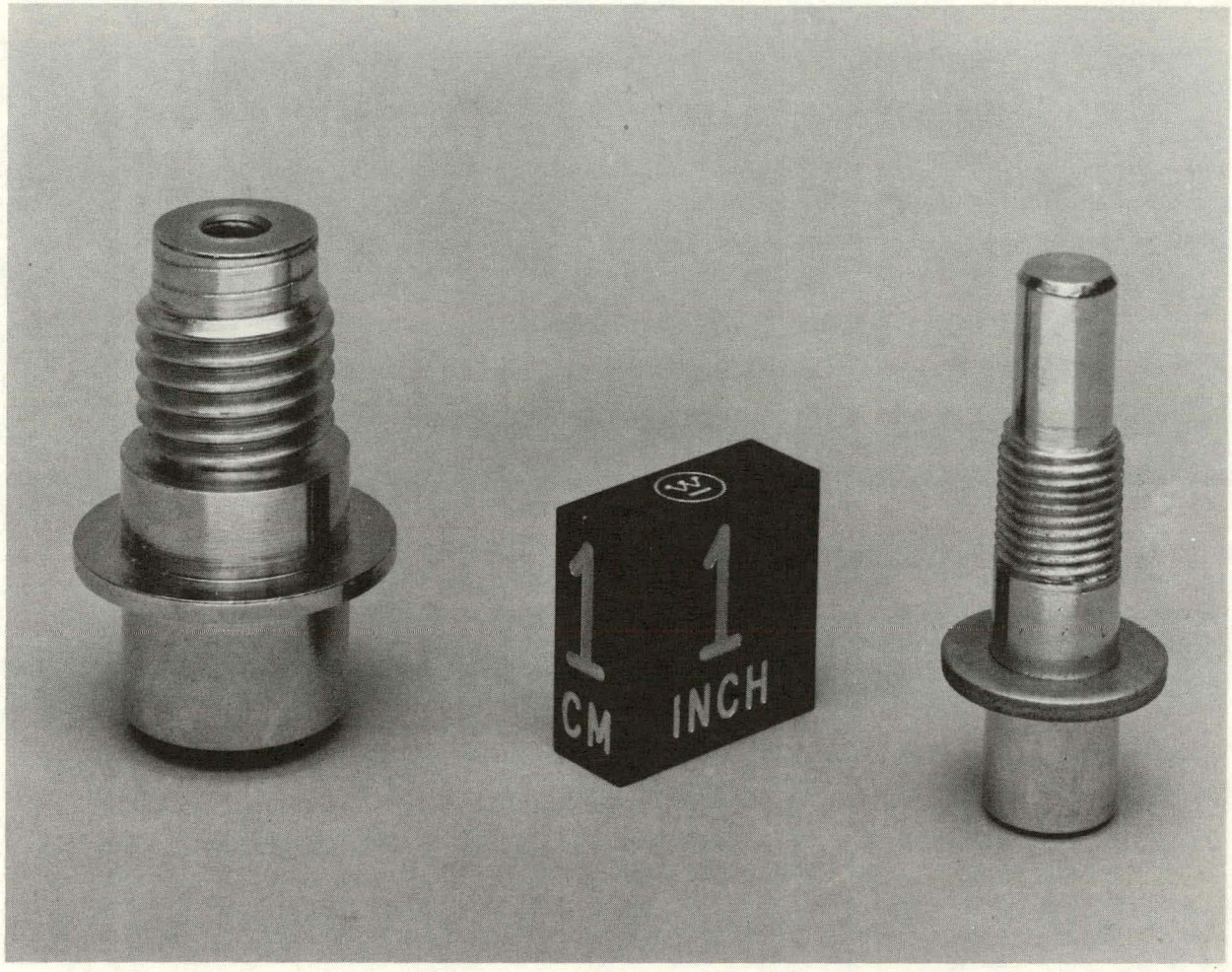

Figure 2.3

INITIAL ALL-STEEL POST (LEFT) AND PRESENT STEEL-CLAD COPPER POST (RIGHT) FOR FULL-SIZE IRON-NICKEL CELL

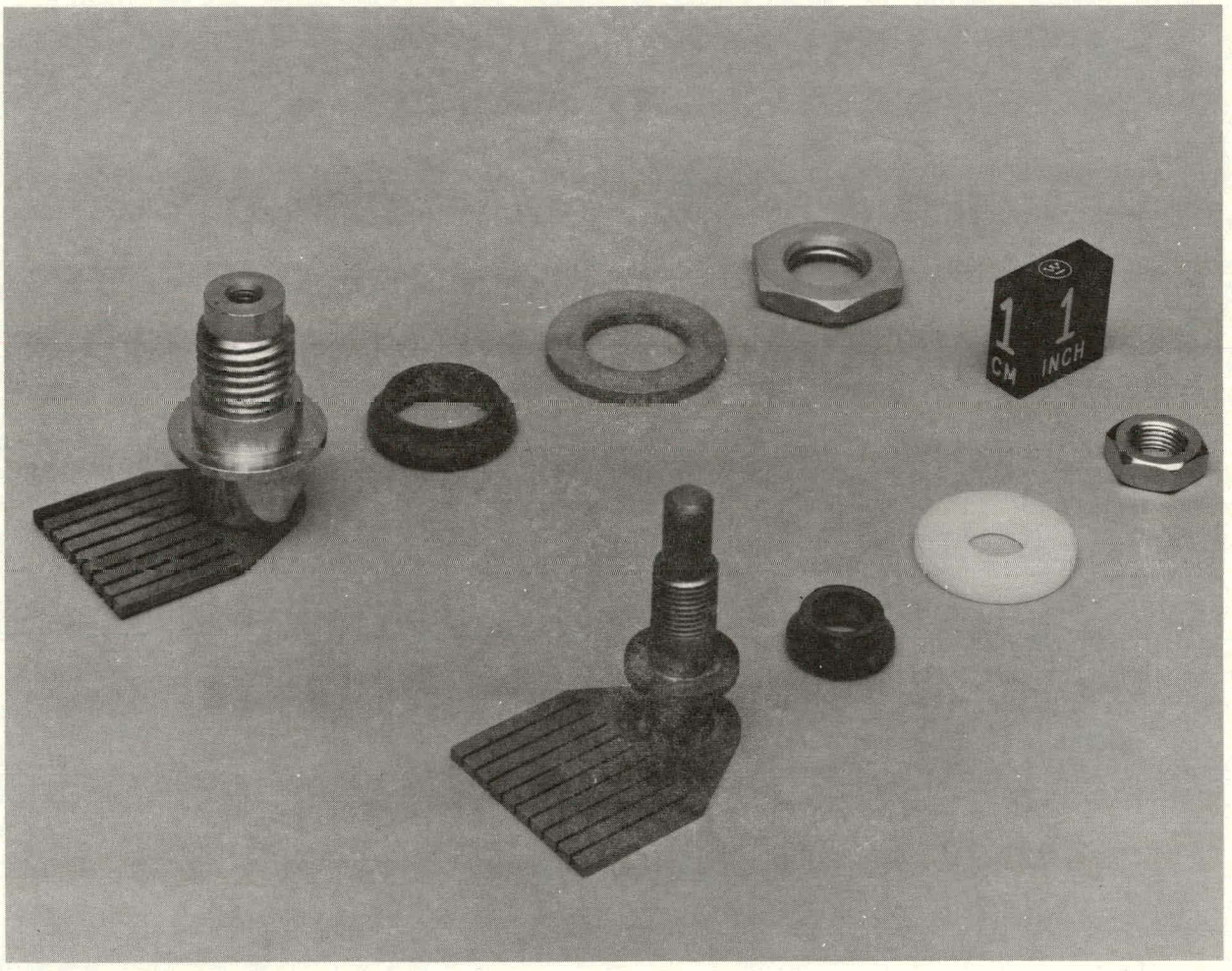

Figure 2.4

TERMINAL ASSEMBLIES, SHOWING WELDED POST-COMB ASSEMBLY, RUBBER SEALING GROMMET, NYLON WASHER AND NICKEL PLATEDSTEEL NUT. ALL STEEL (TOP) AND STEEL CLAD COPPER POST (BOTTOM).

in labor was needed. Figs. 2.3 and 2.4 are included to illustrate the significant difference in the component sizes, resulting from the smaller bi-metal post design.

Development work is now being focussed in two major areas: (1) cost reductions in comb fabrication, and (2) elimination of the tab and comb. Some promising results have been seen in (1) where combs have been assembly welded (rather than machined) from separate blanks and bar stock pieces to replace the expensive machined slot configuration. Preliminary work in (2) has involved a technique that utilizes cables and a through-the-cover cable collection terminal.

2.1.3.3 Cell Case and Cover

Work in this area is two fold: (1) design and procurement of molded prototype cell containers and covers, (2) development of new cover to case joining and sealing techniques, having compatability for use in a multicell module case and cover.

The design of the case and cover for the cells used in the first battery was completed in September 1978. The joint design chosen allowed for either an epoxy seal or an induction fusion weld. Several molding materials were tried, with Noryl 300 perferred. Difficulty was experienced in injection molding the case with all materials except nylon. The high aspect ratio of the container and the high viscosities of the preferred case and cover materials, combined to cause either incomplete or unbalanced filling of the case mold. An alternative modified polyphenylene oxide material, Noryl 225, with slightly lower heat deflection properties was chosen for its lower pressure and temperature molding requirements. Approximately 250 cases made of Noryl 225 were finally received for use with the first "2 x 4" battery, although the unbalance in face to face wall thicknesses was not eliminated (See Fig. 2.5). Several unsuccessful attempts have since been made by the vendor to lock the core in position. A very recent realignment of the mold has enabled a few uniform wall thickness cases

Design Thicknesses

Location	Ref.	Dimension
LIP	A	
FACE, TOP	B	.075
END, TOP	C	.075
FACE, MIDDLE	D	.0875
END, MIDDLE	E	.0925
FACE, BOTTOM	F	.100
END, BOTTOM	G	.110

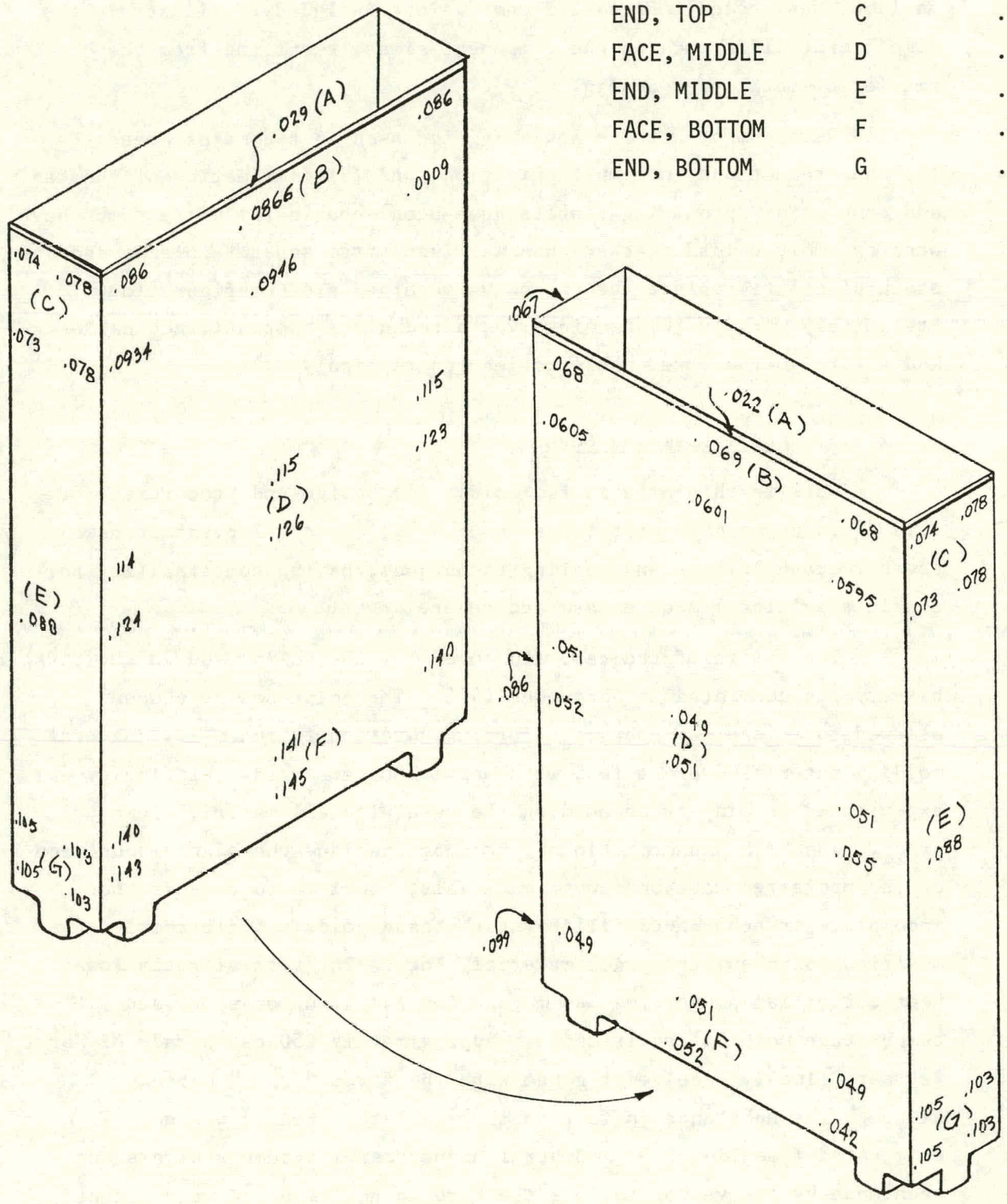

Fig. 2.5

CASE WALL THICKNESSES ILLUSTRATING MOLD CORE SHIFT

to be molded from Noryl 225 and the vendor feels there is a high probability the case molding problem has been solved.

Experimentation with an induction weld sealing process (cover-to-case) continues. The weld appears to be of a high quality, although a seal with high pressure integrity must be attained to accomodate the 5-10 psig required for electrolyte circulation This sealing technique is still in an elementary stage of refinement. As it is now performed, the process utilizes a Noryl 225 gasket, made with metal-impregnated strips, and a good joint seal is obtained everywhere, except the location at which the gasket ends abut. Since the continuous molded gaskets are not yet available, the technique not being perfected as yet, all the cases produced to date have been sealed with epoxy.

Design of a multicavity module case is in the conceptual stage. By this design the manifolding of the cells for gas and electrolyte maintenance, as well as the intercell electrical connecting, will be performed inside the module reducing sealing and manifolding difficulties. At present the individual cells are assembled together and joined via an external electrolyte inlet tube, an electrolyte and gas external exhaust tube, and external intercell electrical connectors. Fig. 2.6 shows a recent photograph of a 6-cell module assembly, having the present external hardware.

2.1.3.4 Cell Auxiliaries

Development work on cell auxiliaries relate to electrolyte water makeup and electrolyte recirculation. Emphasis is on an automated system.

2.1.3.4.1 Electrolyte Management

At the beginning of the program non-circulating electrolyte was tried. However, it became apparent that the benefits resulting from a circulating system, namely thermal balance and electrolyte composition control, justified a change in our design.

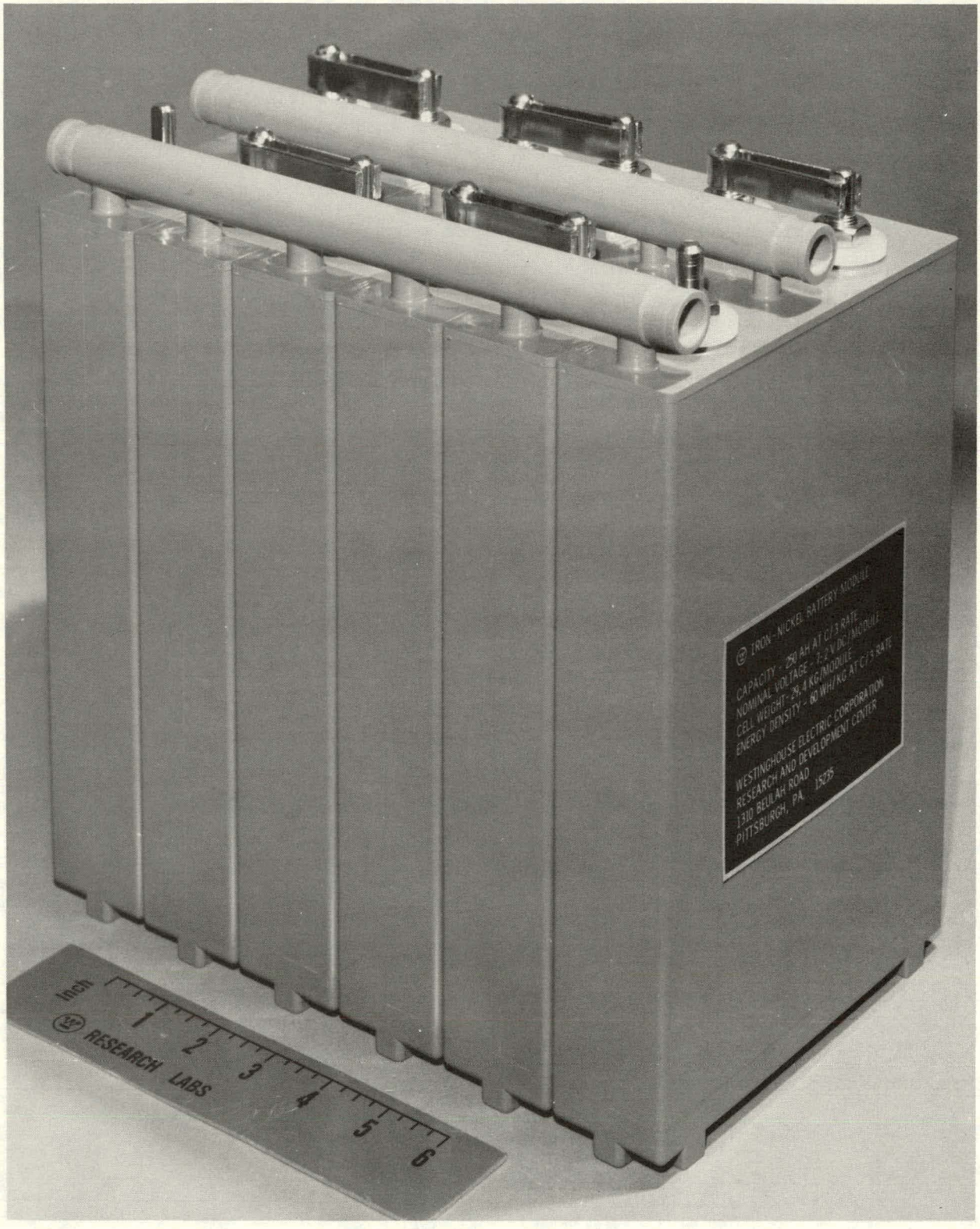

Figure 2.6

6-CELL MODULE FOR THE "2 x 4" NICKEL-IRON BATTERY

With electrolyte circulation the plenum volume in the cell above the electrode stack was no longer required, both electrodes were increased in height by 1.25 cm. and vertically coined electrolyte channels were incorporated into the electrodefores. The forced electrolyte convection not only removes heat during charge but increases electrolyte availability to the electrodes. The circulation system also replaces an automated watering system.

The decision to circulate the electrolyte impacted on all related design areas, e.g., changes were made in production procedures, as well as in the case/cover mold. Fig. 2.7 schematically illustrates the circulating electrolyte system. The auxiliary electrolyte management system consists of a pump, reservior, heat exchanger, water bubbler and associated flow controls/interlocks. Electrolyte is pumped in parallel through each cell during the charge cycle. The warm electrolyte and gas generated during charge is returned to the reservior and separated, with the gas discharged to the atmosphere through a water bubbler and electrolyte cooled by a heat exchanger in the reservior.

2.1.4 Cell Testing and Equipment

The ultimate purpose of the testing program is two-fold: (1) provide performance information in order to determine operating characteristics, suggest modifications, and reinforce design decisions; (2) provide information of interest to a potential user who needs to know performance, environmental and safety aspects of the system.

For Task 2, the System Development portion of the contract, testing concentrates in several areas. Full size 25Ah iron and nickel plate tests are being performed to assist in evaluating design, materials, and process changes by determining their effect on performance. Also, full-size nickel-iron cells are being tested, in finished, molded containers, against the target performance goals. 6-cell modules, as used for the "2 x 4" battery, were also tested for performance and design evaluation. Finally, the "2 x 4" battery was tested for performance prior to shipment to JPL.

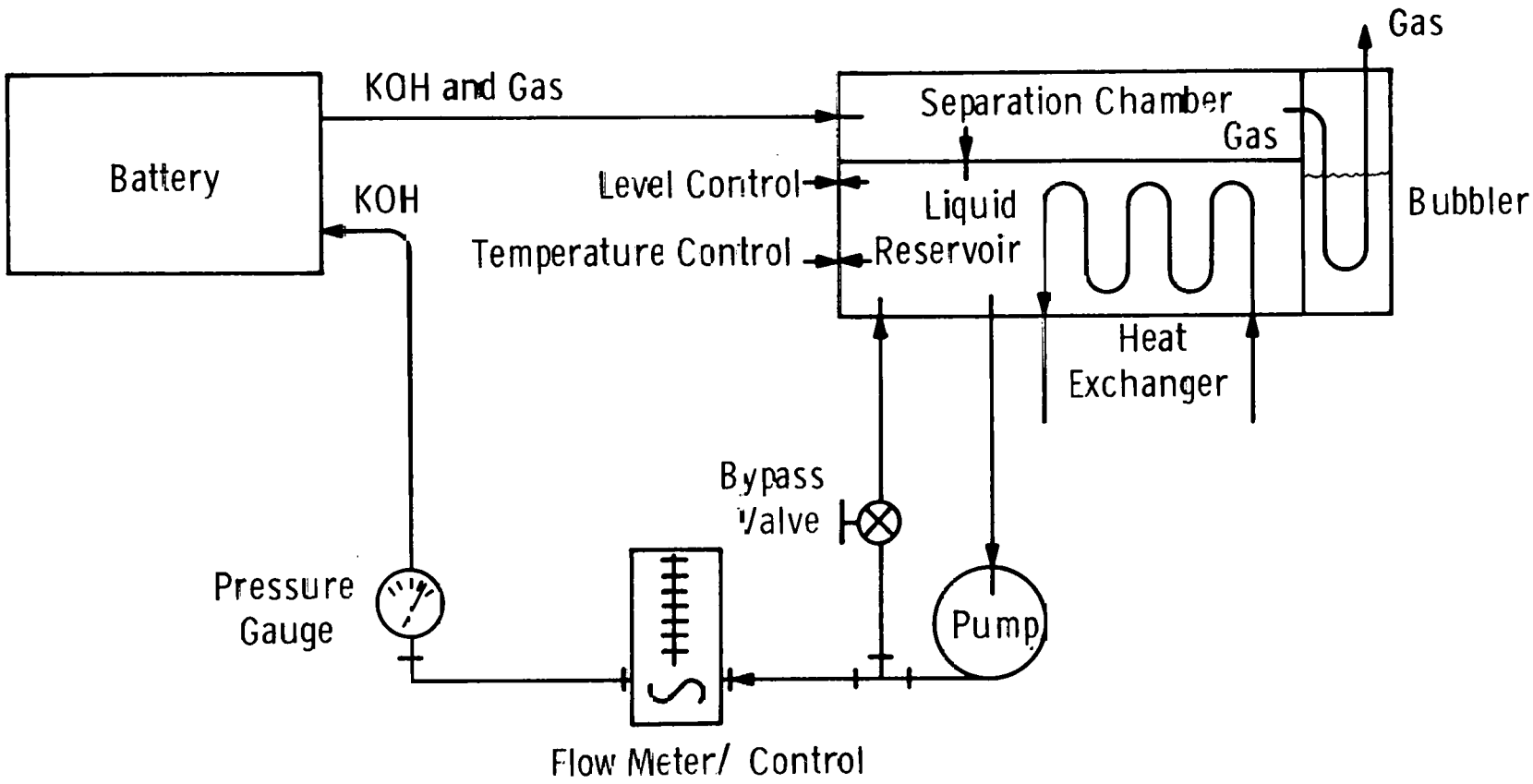

Fig. 2. 7 — Electrolyte circulation system schematic

This testing is to provide information on the operational and performance characteristics of the following areas: (1) pre-test, (2) charging, (3) capacity, (4) power, (5) charge retention, (6) life and (7) environmental aspects. A test plan was presented in the first annual report[8] which would provide the desired data.

Developmental cells are now being tested with circulation of electrolyte. Up to five charge/discharge 80% DOD cycles at C/3 rates (83.3A) can be run each day, with 10 tester positions available.

A special test station was designed to simultaneously test three 6-cell modules at various depths of discharge. Fabrication of the facility is expected to be complete by mid-October 1979. The system was chosen in an effort to cease the practice of testing cells at 100% DOD and to provide information on cells tested in a condition more closely approximating battery usage. These stations will assist in determining depth-of-discharge life data and temperature effects on performance.

Final specification of the minicomputer system for testing full cells is now on file. Purchases are delayed, pending procurement approval. The system was designed to provide automatic control, data acquisition, data reduction, and hard copy output for the entire battery lab. The minicomputer would be coupled with another, on-site file generating minicomputer system. The secondary system would create files for use by, but would not require the service of, the large on-site Univac computer.

2.1.5 Pilot Plant Operations

The nickel-iron battery pilot plant was designed and is utilized as a prototype module of a production facility. Task efforts for FY'79 were concentrated on the scale up of development processes in pilot plant equipment and the manufacturing of cells, modules, and a battery incorporating technology improvements made since the initiation of this program in December 1977. Process scale up entailed the determination of materials usage, process yields, and product quality to

provide a sound basis for manufacturing cost projections and estimates of production facility requirements. Cells were manufactured per documented process design specifications.

2.1.5.1 Iron Electrode Fabrication

Production of electrodes for the first battery began in January 1979. To date, 3245 composite-type iron electrodes were fabricated and collated into 295 cell stacks, of which 201 were assigned to the "2 x 4" battery program. The loading of the electrode plaque with the aqueous iron oxide paste was successfully controlled by the processes defined in Section 2.1.1.1. In the loading step, the plaque was purposely loaded with excess paste. In the sizing step, a controlled amount of the paste was retained in the plaque, by sizing it down to a predetermined thickness.

The two operations required the use of two separate facilities and two operators for each. A design study was undertaken to combine the loading and sizing operations to one operation using a single operator. The new operational design was also in the direction of lower material waste in addition to lower labor costs. Two approaches were considered in the design study. The roller type approach combined the loading and sizing operations into one facility and one operator. In this design the plaque is loaded with excess paste and then sized as it exits the system. The advantages of this design are that the paste supply is contained, unexposed to the air and that little paste is wasted. The disadvantages of this approach are the mechanical complexity, lack of flexibility, and cost.

The press type approach was proposed as an interim design. The key to this approach is in the use of porous dies, through which air is blown to release the loaded plaque. In this design the bottom die is first coated with excess paste, the plaque is placed on top of the paste, the top die is then lowered to force the paste into the plaque and to size the loaded plaque to a given thickness. To prevent the

paste water from being absorbed by the porous dies during loading, the dies were treated with highly hydrophobic materials. Sample dies, vacuum impregnated with an acetone solution of methacrylate, indicated no apparent water absorption during pasting while the air flow was sufficient to release the pasted plaque from the dies. Both approaches are still under consideration for producing iron plates in large quantities, while conserving manpower and material.

2.1.5.2 Maxi-Line

The electroprecipitation process (EPP) utilized for the pilot production facility, Maxi-line, is essentially the same as that for the development facility, mini-line, with some process modification to shorten the total electrode processing time.

Details of the EPP Maxi-line are shown in Fig. 2.8, 2.9, 2.10 and 2.11. Fig. 2.8 shows the entire line. The EPP tank is in the foreground with the rinse tank then the formation tank and the plating tank following in that order. Fig. 2.9 is a photo of the cascading rinse tanks. Fig. 2.10 shows the unfilled plating tank (left), the formation tank (center), and part of the rinse tank (right). Fig. 2.11 shows the unfilled plating tank.

Production of nickel electrodes for the first battery ("2 x 4") began in January 1979. 3270 plates were produced. A major setback in the start-up of EPP nickel electrode production was caused by a need for tank relining. An outside contractor relined the tanks, which were spark tested for leak tightness prior to their being loaded with the EPP solution.

The racks, used throughout the entire EPP process for suspending the electrodes, were disassembled, cleaned, and modified. Similar racks were also fabricated to increase the productivity of the line. With the addition of an extra set of anodes production capacity was increased 50%.

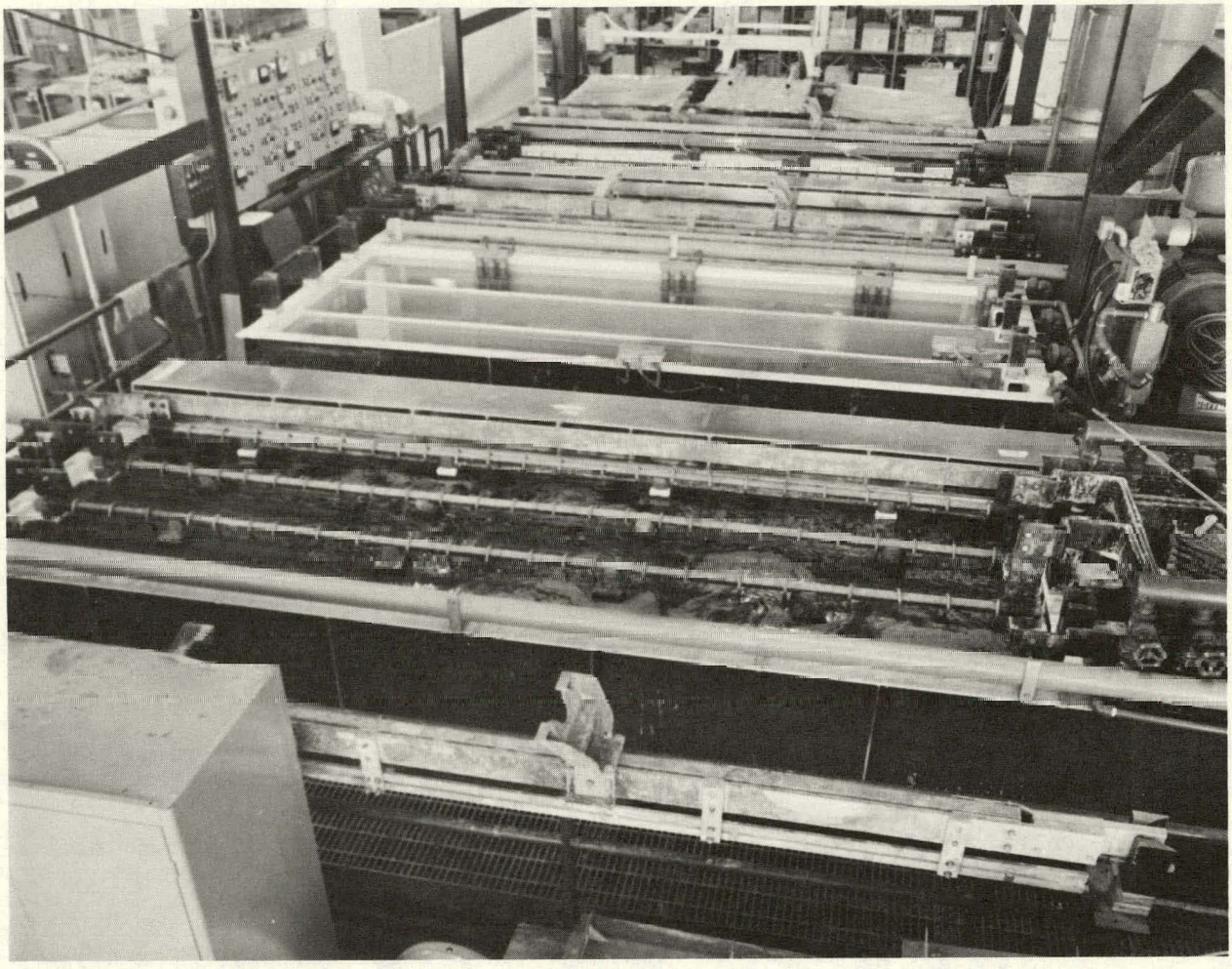

Figure 2.8

EPP MAXI-LINE

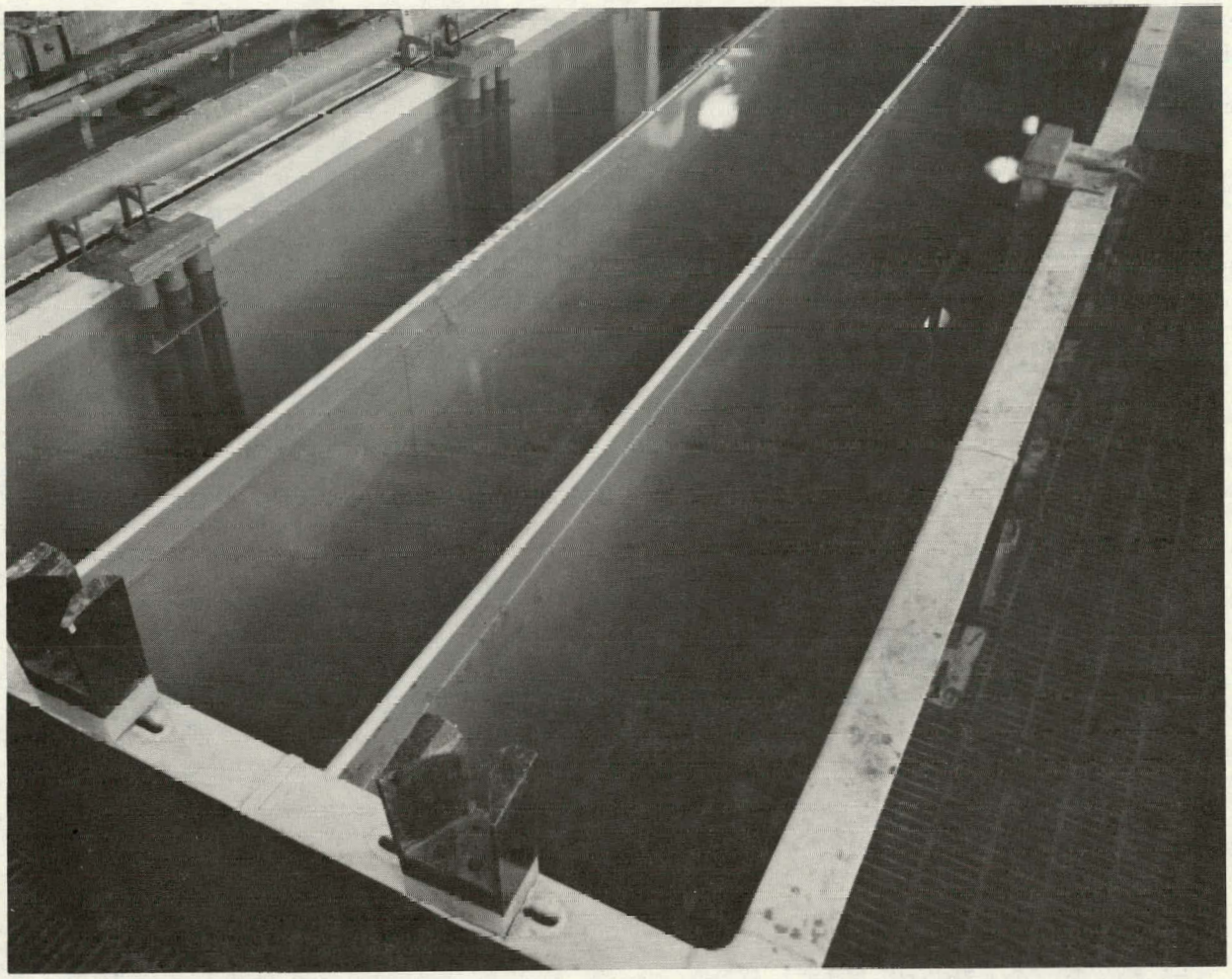

Figure 2.9
MAXI-LINE RINSE TANK

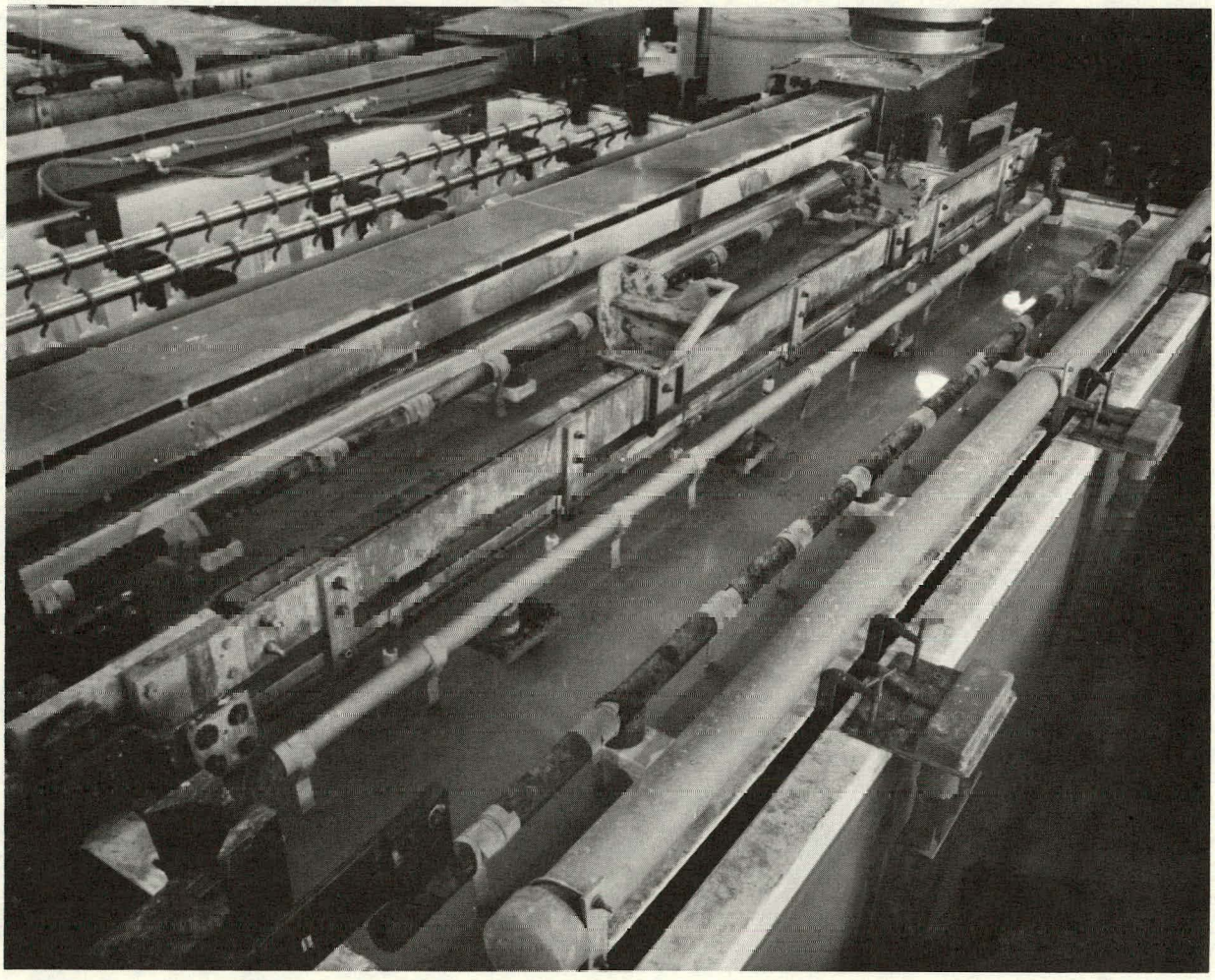

Figure 2.10

MAXI-LINE FORMATION TANK (CENTER)

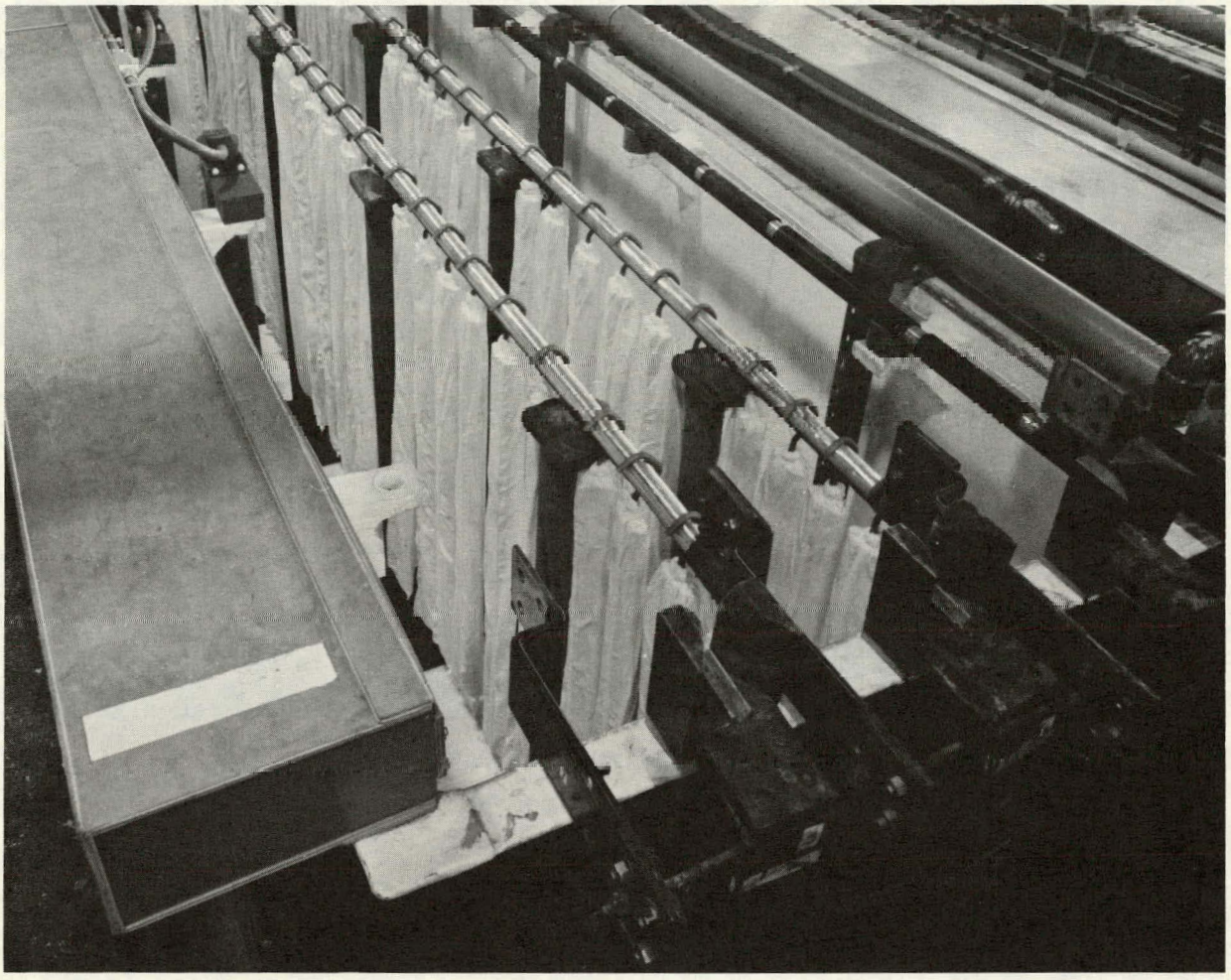

Figure 2.11

MAXI-LINE PLATING TANK (ANODES INSTALLED)

Data is gathered bi-weekly as part of Maxi-line solution QA/QC. Other data, taken for QA/QC, includes recording steel weight (grid plus tab), nickel plating weight, and thickness of the grids prior to EPP, as well as thickness and immersed electrode weights afterwards. Eight specified locations are measured for the thickness determination. The weights taken prior to EPP and the immersed weight of the finished electrode permit a calculation of the active weights. Both quantities are significant for QA/QC methods, and were determined for 10% of the electrodes in every run.

Fig. 2.12 illustrates the EPP nickel electrode production schedule and status.

2.1.5.3 Cell Assembly

Experimental test cells, modules, and the "2 x 4" battery were fabricated in the pilot line. Several cells have been made, incorporating a few changes in assembly technique, which reflect experience gained in fabricating the 2 x 4 cells. These include:

(1) channels are now cold pressed with a fixture

(2) the epoxy potting technique has been modified to prevent any blockage of the circulating electrolyte tubing. (An increase in the inlet tube size is also contemplated.)

2.1.5.4 Nickel-Iron Battery for "2 x 4" Program

As part of the DOE "2 x 4" program, battery modules, using the present cell technology were fabricated. A total of twenty-four modules are to be delivered to JPL, along with an off-board charger, the required maintenance equipment, and 3 sets of Operating and Maintenance Manuals. An additional four modules are to be delivered to ANL/NBTL for performance testing.

Figure 2.12

Nickel Electrode Production Schedule

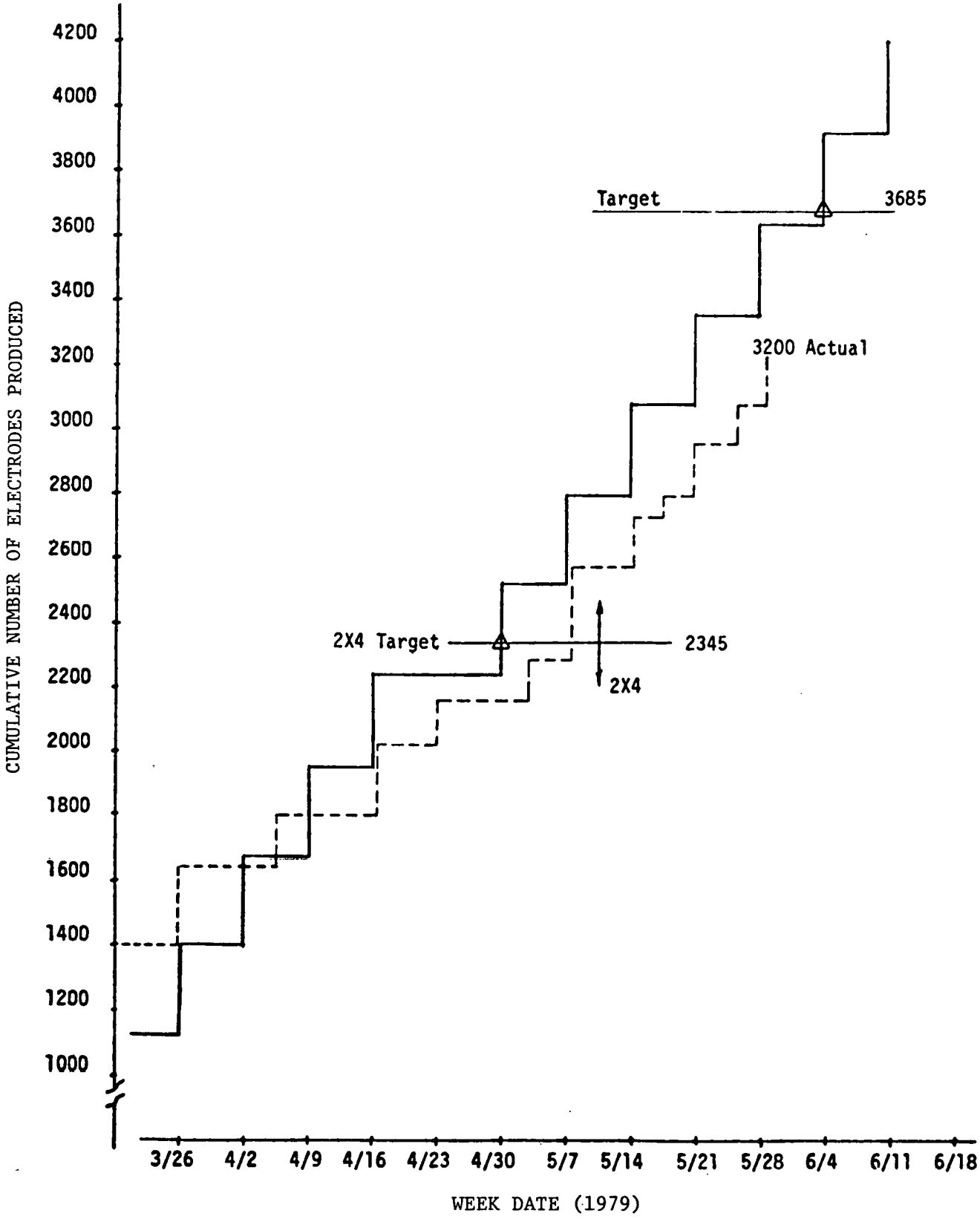

2.1.5.4.1 "2 x 4" Assembly

All of the cells scheduled for the "2 x 4" battery were assembled in the Pilot Line. The first module was shipped to ANL/NBTL in the middle of July for testing. Of the 28 modules scheduled for fabrication, 25 have been completed. The "2 x 4" battery was completed and shipped, along with the maintenance system, the charger and 4 extra modules, to JPL on August 10.

Fig. 2.13, 2.14, 2.15 and 2.16 have been included here to show the distribution of various performance characteristics of the 90 cells used in the "2 x 4" battery. Fig. 2.13 shows the spread of cell capacity; Fig. 2.14 shows cell weights; Fig. 2.15 shows pressure drop at the design flow rate; and Fig. 2.16 lists the cell internal resistances. The blocked in designated cells were those initially assembled in the "2 x 4" battery.

2.1.5.4.2 "2 x 4" Charger and Maintenance System

In March, an interface meeting was held at JPL, to assure compatible installation and operation of the near-term batteries in the four "2 x 4" vehicles. Interface data for the charger and maintenance system were also obtained at that time.

Maximum dimensions were received for an outer battery box, compatible with the JET and SCT vehicles, in which the nickel-iron battery was most likely to be first tested. A suitable battery tray and on-board electrolyle circulation system was designed to fit within the dimensional constraints established by JPL-86.4 cm w by 113.0 cmL x 32.0 cmH.

The circulation equipment was designed as part of the on-board battery system. In combination with the electrolyte reservoir is a gas/liquid separation chamber, an effluent gas scrubber, a heat exchanger and level and temperature monitors. A pump, a flow gage with a low pressure switch, and a bypass valve are also included. The battery with

FIG. 2.13 - DISTRIBUTION OF PRODUCTION CELLS BY CAPACITY

Notes: Charge 83.3A/4h
Discharge 83.3A to 1.0V

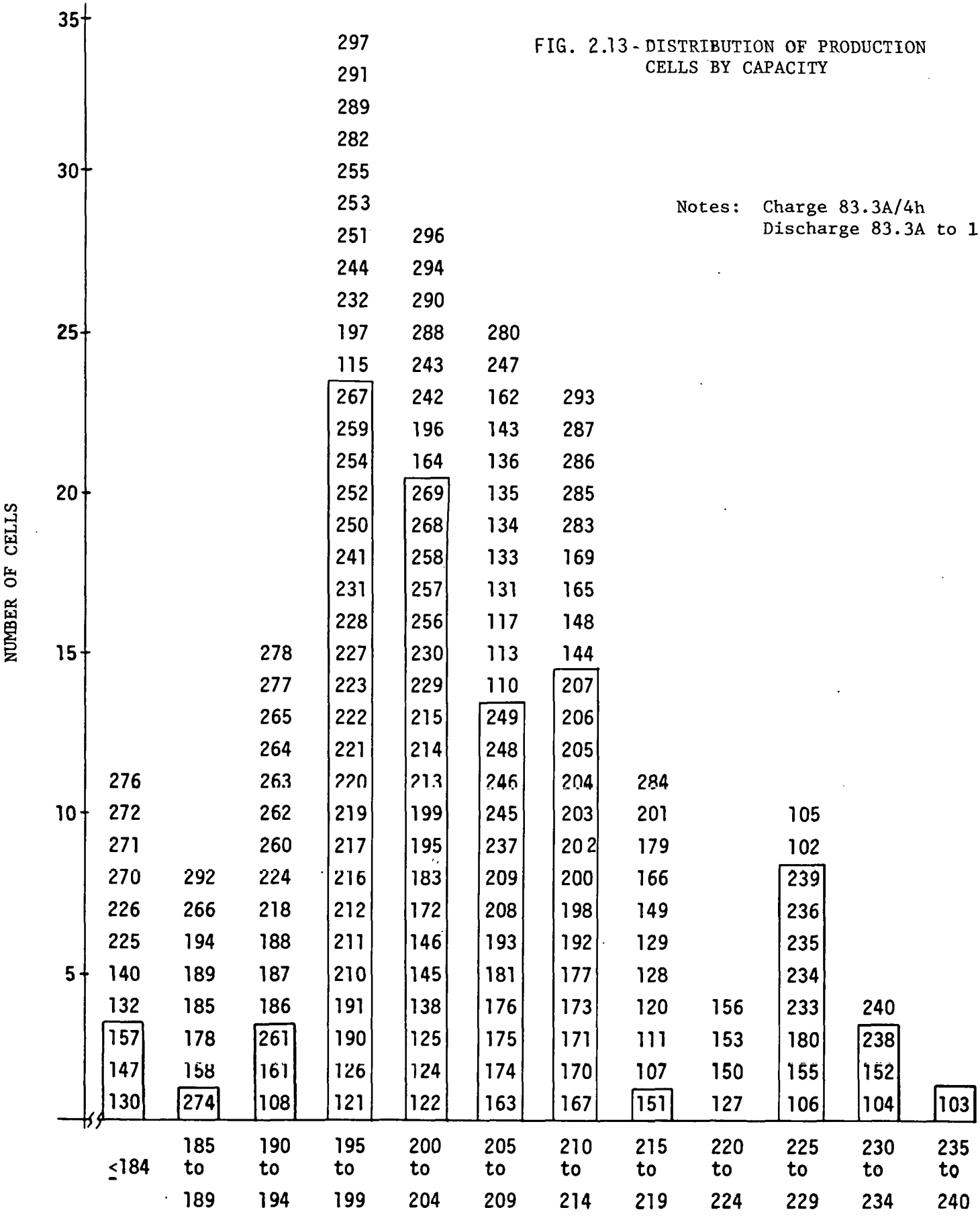

FIG. 2.14 DISTRIBUTION OF PRODUCTION CELLS BY FINISHED WEIGHT

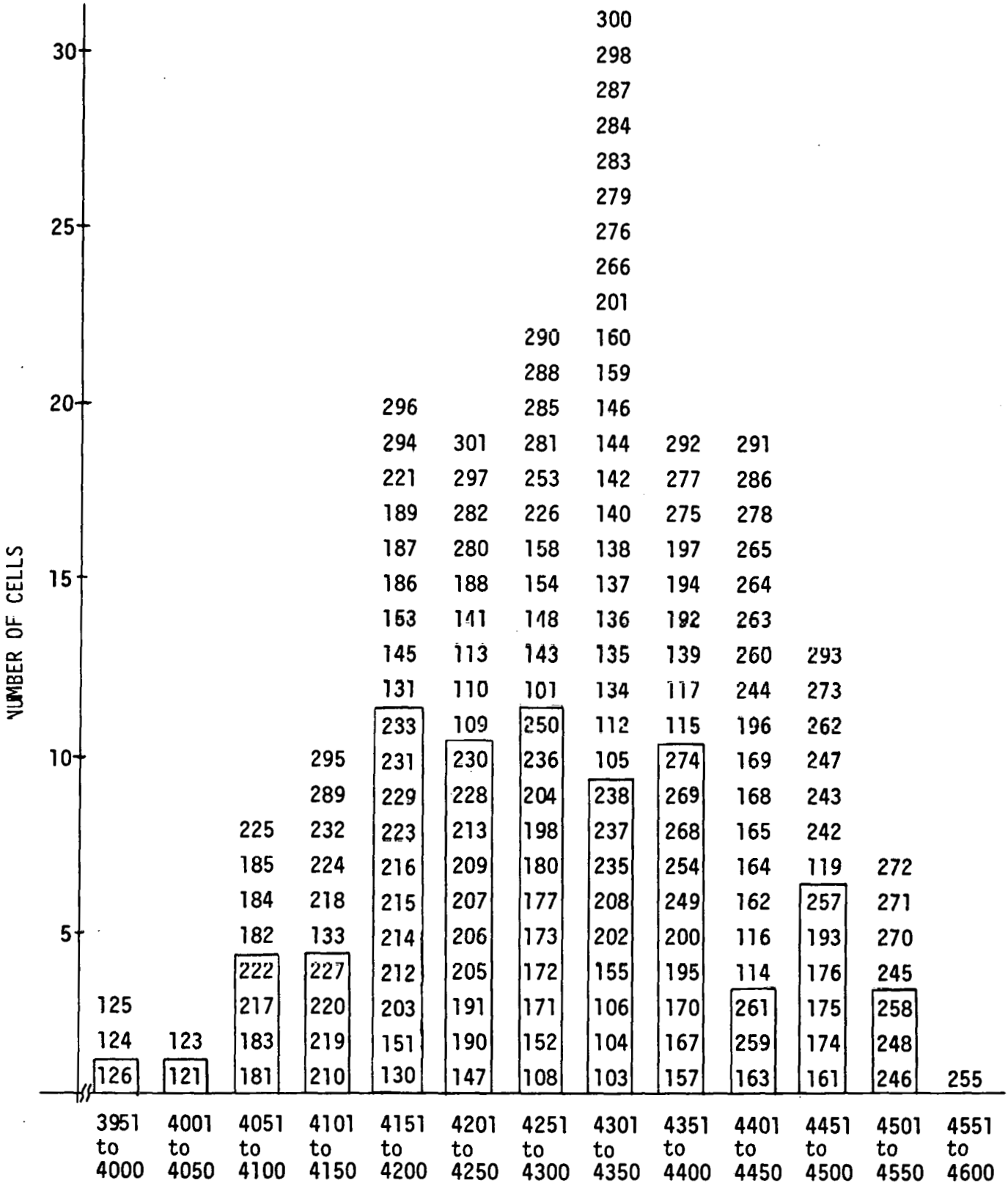

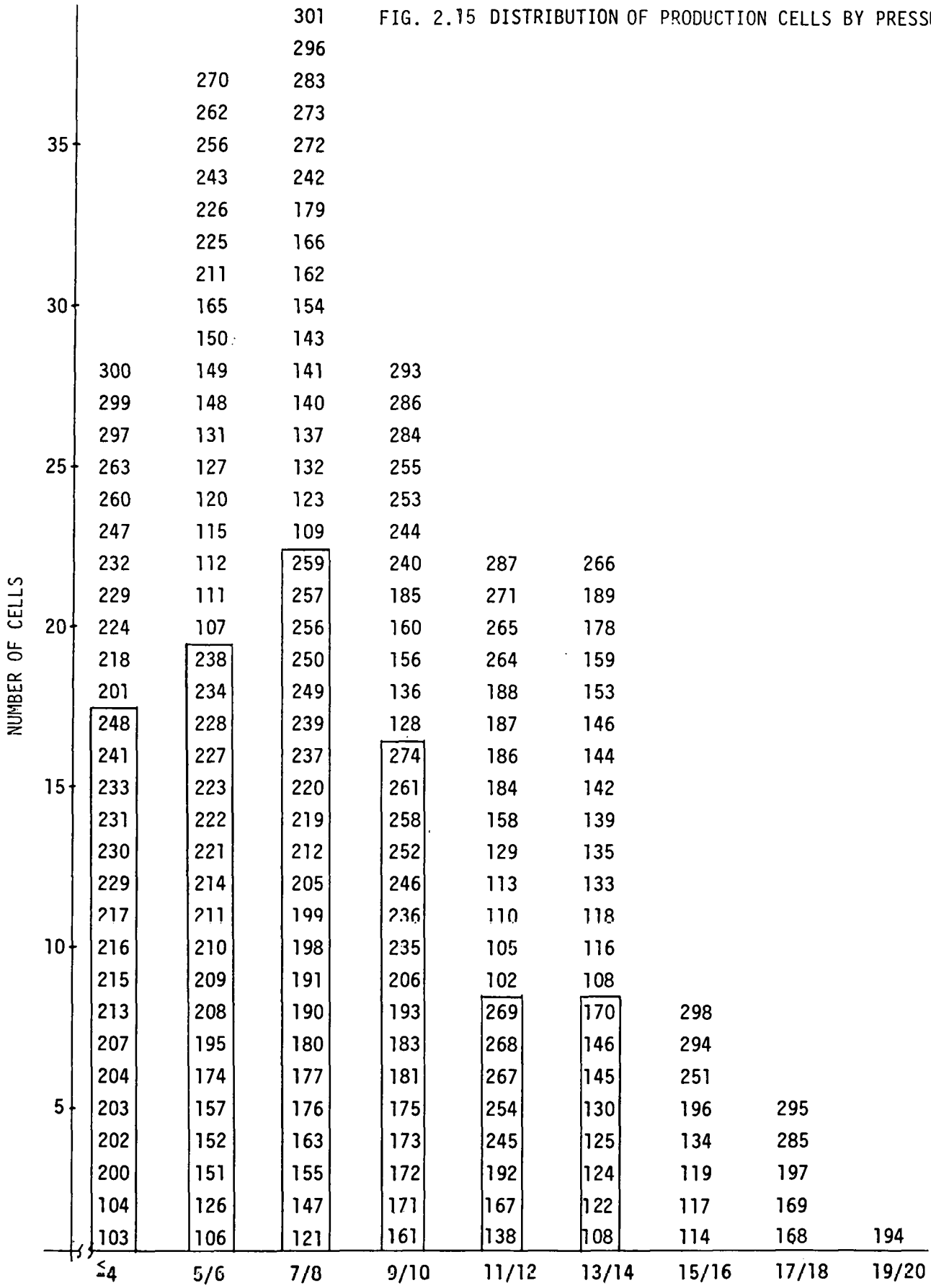

FIG. 2.15 DISTRIBUTION OF PRODUCTION CELLS BY PRESSURE DROP

FIG. 2.16 DISTRIBUTION OF PRODUCTION CELLS
BY INTERNAL RESISTANCE
(measured at 50A to 150A current increment)

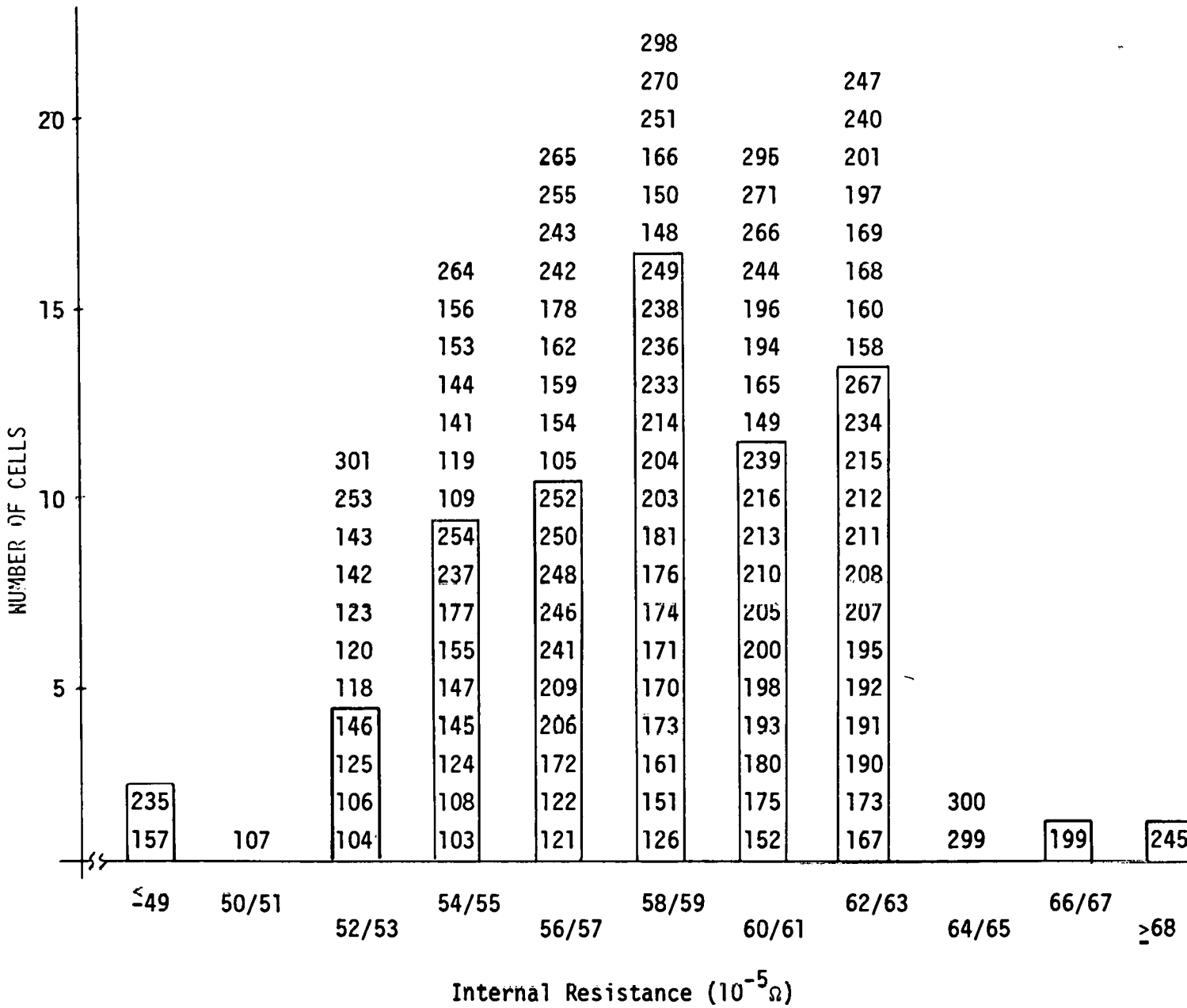

the maintenance system installed is shown in Fig. 2.17. The cell and module assignments for this battery are given in Fig. 2.18.

The charger was designed with a control system to monitor and provide interlocks for the on-board circulation system. The timers, temperature controller and pump are all operated from the charger panel. The power supply, which was initially provided, required 208V, 3 phase, 55A to operate. It is capable of a 50A maximum, continuous operation.

Two problems in the system were encountered during the battery testing at JPL. First, the electrolyte maintenance system, proved inadequate for handling the electrolyte volume changes throughout charge and discharge. Electrolyte is displaced by gas generated in the electrodes during the charge cycle. This additional volume of electrolyte must be stored in the reservoir and pumped back into the cells after discharge. The second problem was related to the electrical service available at the JPL Laboratory. It was discovered that 480 V, 3 phase, 35A service was available, which would permit charging the battery at greater than a 40A rate. Therefore, a 70A charger, shown in Fig. 2.19, was assembled and delivered to JPL. However the increased charge rate using this charger further increased the electrolyte volume and cooling capacity requirements. Even a temporary maintenance system fix was slightly undersized and the battery tests needed to be performed with an operator in attendance. Therefore, a much larger off-board electrolyte circulation system was sent to JPL. A redesign of the on-board circulating electrolyte system is underway.

Design changes that must be made include the replacement of the flow meter with a much smaller flow switch and pressure gage assembly, and the elimination of two cells to gain volume for the reservoir. These alterations and two inch increase in reservoir height should provide the extra volume needed to handle the electrolyte volume changes observed in testing. Other changes will include increasing the size of the heat exchanger and the relocation of some components. A new method of attaching and sealing the manifolding is also being investigated, to avoid leaks in the tube connections.

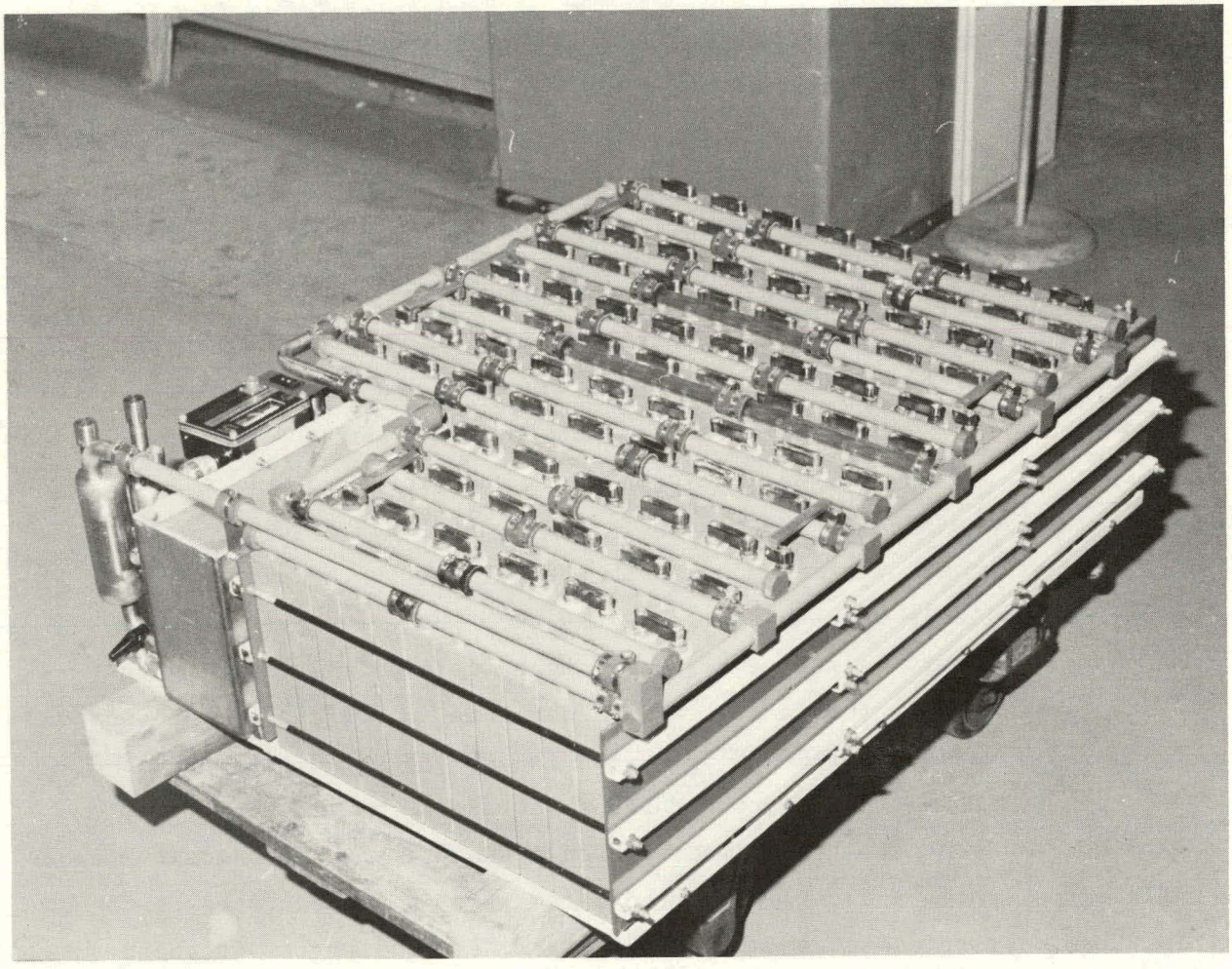

Figure 2.17

NICKEL-IRON BATTERY SYSTEM DELIVERED FOR
DOE/JPL "2 x 4" BATTERY PROGRAM

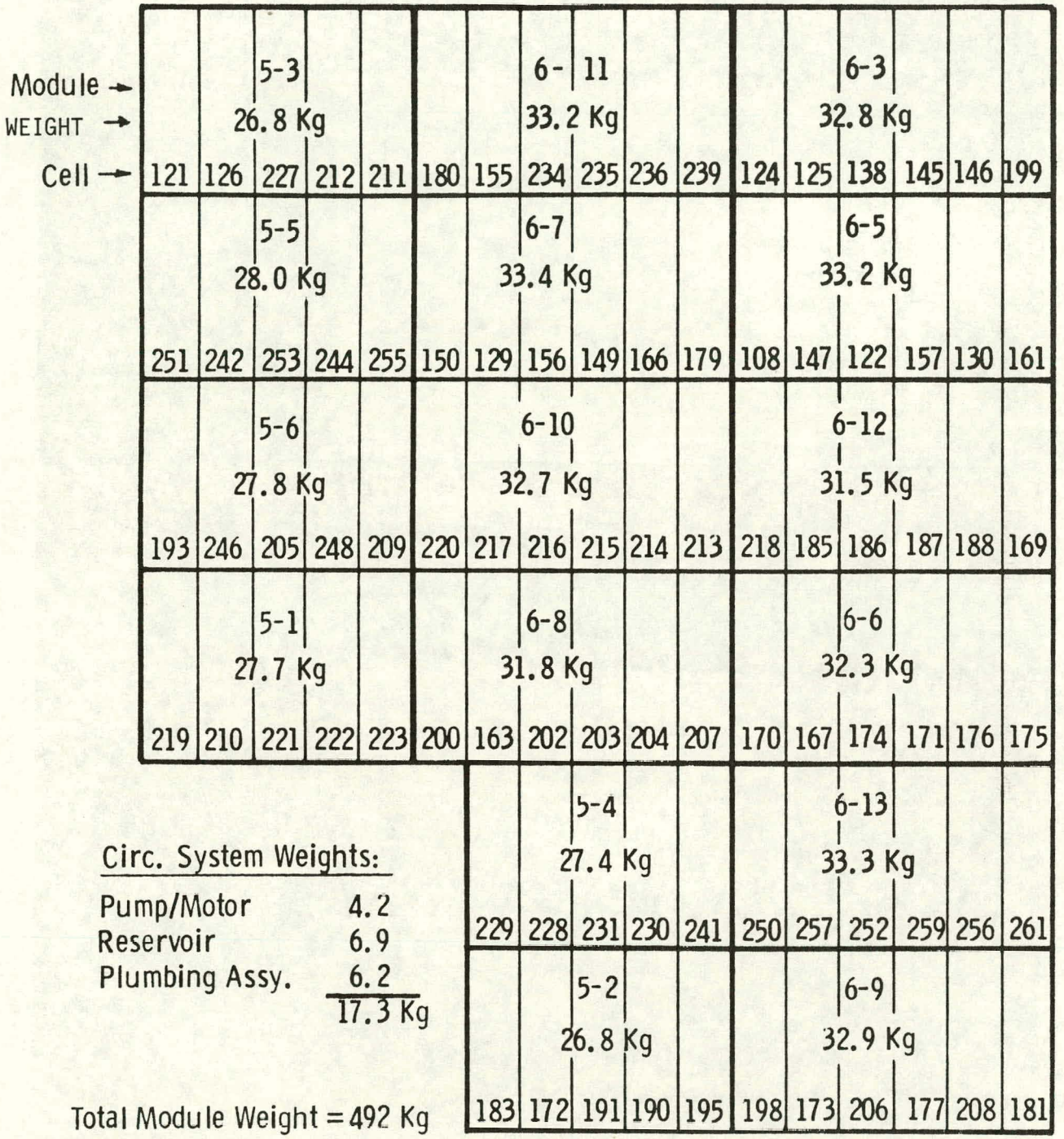

Circ. System Weights:

Pump/Motor	4.2
Reservoir	6.9
Plumbing Assy.	6.2
	17.3 Kg

Total Module Weight = 492 Kg

Fig. 2.18 – Cell and module plan for the DOE/ JPL 2×4 nickel-iron battery

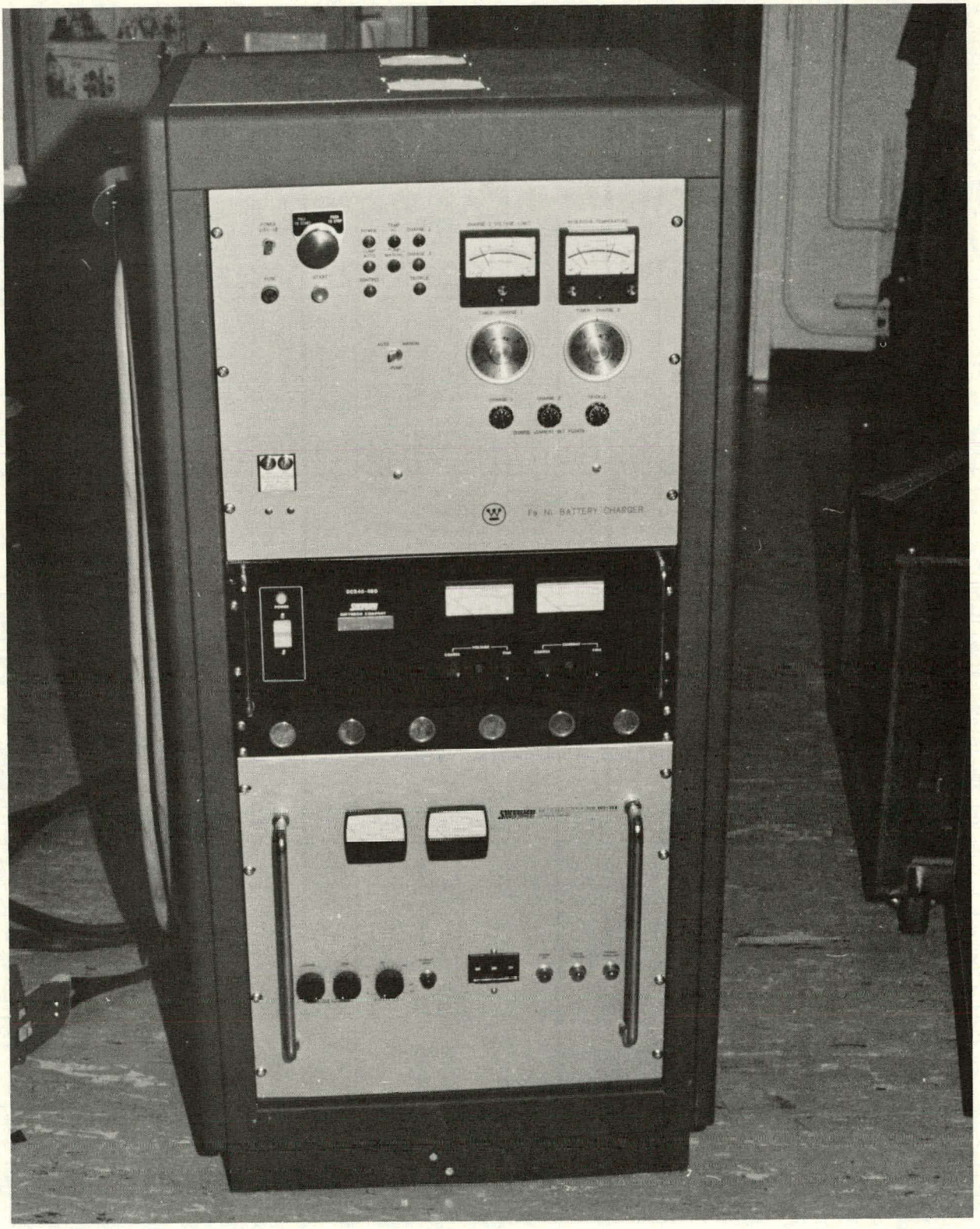

Figure 2.19

70 AMPERE RATE CHARGER FOR NICKEL-IRON "2 x 4" BATTERY

3.0 TECHNICAL PERFORMANCE

Initial program goals and projected demonstration values are presented in Table 3.1. Until recently, all full size cells and three plate cells have been on life cycle testing to 100% depth of discharge. These cycling test conditions were more stringent than those required for long life cycle testing currently envisioned as typical electric vehicle mission profiles. Cycle life test cells will require electrolyte circulation, electrolyte composition and temperature control, and minimization of $CO_3^=$ formation in the electrolyte. All these controls have been incorporated into a single cell test system and into a "closed" module test system which has been designed. This single cell test system has been installed into the auto make cycle life tester (see Figs. 3.1, 3.2).

All full size cells have been on test in containers of the proper volumetric constraints, according to our design specifications. Initially cells had containers made of plexiglas, with either oversized terminals and/or clamping fixtures and were, consequently, overweight. For these cells all cell gravimetric data was based on estimated cell weights, by taring out excess components and adding weights of final design components and adjusted electrolyte weights.

Cells made since May 1979 have molded cases and covers and are being rated for performance based on their actual weights, including electrolyte. Some Molded cases and covers made of styrene had been used to fabricate cells 030CE, 031CE, 032CE and 038CE. Presently, cells are being fabricated using GE Noryl 225 cases and Noryl 225 covers.

3.1 Three Plate Cell Tests

Three-plate test cells are used to evaluate both full-size 25 Ah iron and nickel electrode performances, to establish their state of development and to assist in the qualification of electrodes used in fabricating stack-ups for full-size prototype cell tests.

Table 3.1 - Iron-Nickel Battery Technical Goals
and Best Present Performance

	Characteristics	Contract Goals (Set Dec. 1977)	Best Present Demonstration[e]	Contractor Forecast[d] (for March 1979) Performance
1.	Battery Capacity (kwh) (100% rated)	25	26.5°, 24.3[s]	22.7[ℓ]
2.	Battery Dimension m H	0.28	0.28	0.28
	(m H x m W x m L) m W	0.38	0.38	0.38
	m L	2.21	2.21	2.21
	Volume (ℓ)	230	230	230
3.	Weight (kg)	417	420[f], 460[t]	445[k], 492[y]
4.	Volumetric Energy[a] (Wh/L)	100	143[g]	120[ℓ]
5.	Specific Energy[a] (Wh/kg)	60	63[h] 53[μ] 58[r], 46[x]	51[m]
6.	Specific Power (W/kg)			
	Peak Battery - with 17% Voltage drop for 30 sec.	100	175[i]	>100, <175[n]
	Sustained @ C/3	20	--	20[p]
7.	Duty Cycle			
	Charge (h)	4-8	C/3 for 4h	6
	Discharge (h)	2-4	3	3
8.	Lifetime			
	Deep Discharges[b]	2000	(to be established)[j]	→ 200 (still on test) Ⓦ
9.	Price/Energy[c] ($/Kwh)	<60	--	--
10.	Energy Efficiency (%)	>60	54[q] 53[v]	>50

Note: Letters refer to notes on the following page

TABLE 3.1. NOTES

[a]C/3 rate discharge; 4-8 h charge

[b]80% depth of discharge based on rated capacity

[c]Price delivered to auto manufacturer for production ~10,000/y

[d]First prototype

[e]Extrapolated from best available data. With finished molded cases and covers and final design cell terminals, grommets, etc. now available, data will be extrapolated from the same cell in this column when circulating electrolyte is employed in cyclic testing

[f]Based on Cell 013CE at 5.0 Kg

[g]Based on Cell 019CE performance, Cycle 31, 265 Ah, projected to design module volume

[h]Based on Cell 013CE, Cycle 22, 5.0 Kg/cell, cell weight only

[i]Based on test results on Cell 007CE (0.5-0.7 mΩ cell, nylon separator)

[j]Recent technology cell, with grooved Ni electrodes and most absorbent separator, at 62 test cycles and stable at 100% depth of discharge per cycle. Old state-of-the-art cells (at 40 to 44 Wh/Kg) have shown 1400 to 1800 stable test cycles, at 80 and 60% of discharge, respectively.

[k]Based on 5.3 Kg/cell

[l]Based on 270 Wh/cell projected to design module volume

[m]Based on 270 Wh/cell

[n]Based on a separator providing a cell of ~0.7 mΩ

[o]Based on Cell 013CE, Cycle 21, 315 Wh/cell

[p]Based on prior experience with Fe-Ni cells of 180 Ah, size

[q]Based on Cell 017CE, Cycle 39 (8 h charge), average charge V = 1.66 V, average discharge V = 1.20 V.

[r]Based on cell 031CE in molded, finished design case and cover; cycle 6, 246 Ah, at 5.1 Kg actual cell weight, including electrolyte, and average discharge voltage of 1.2 V.

[s]Based on Module 6-1, 1735 Wh on discharge cycle 2, 14 modules per battery

[t]Based on Module 6-1, 32.9 kg, including electrolyte, terminals and manifolds.

[u]Based on Module 6-1, 2nd cycle, 239 Ah, 1.21 V, 1735 Wh, 32.9 kg total module wieght

[v]Based on Module 6-1, 2nd cycle, 1735 Wh out, 3259 Wh in, charge not optimized

[w]Cell 194CE

[x]Based on "2 x 4" Battery, cycle 3.

[y]Based on "2 x 4" Battery, 32.7 Kg module wt. (including electrode, electrolyte manifolding, intercell connectors).

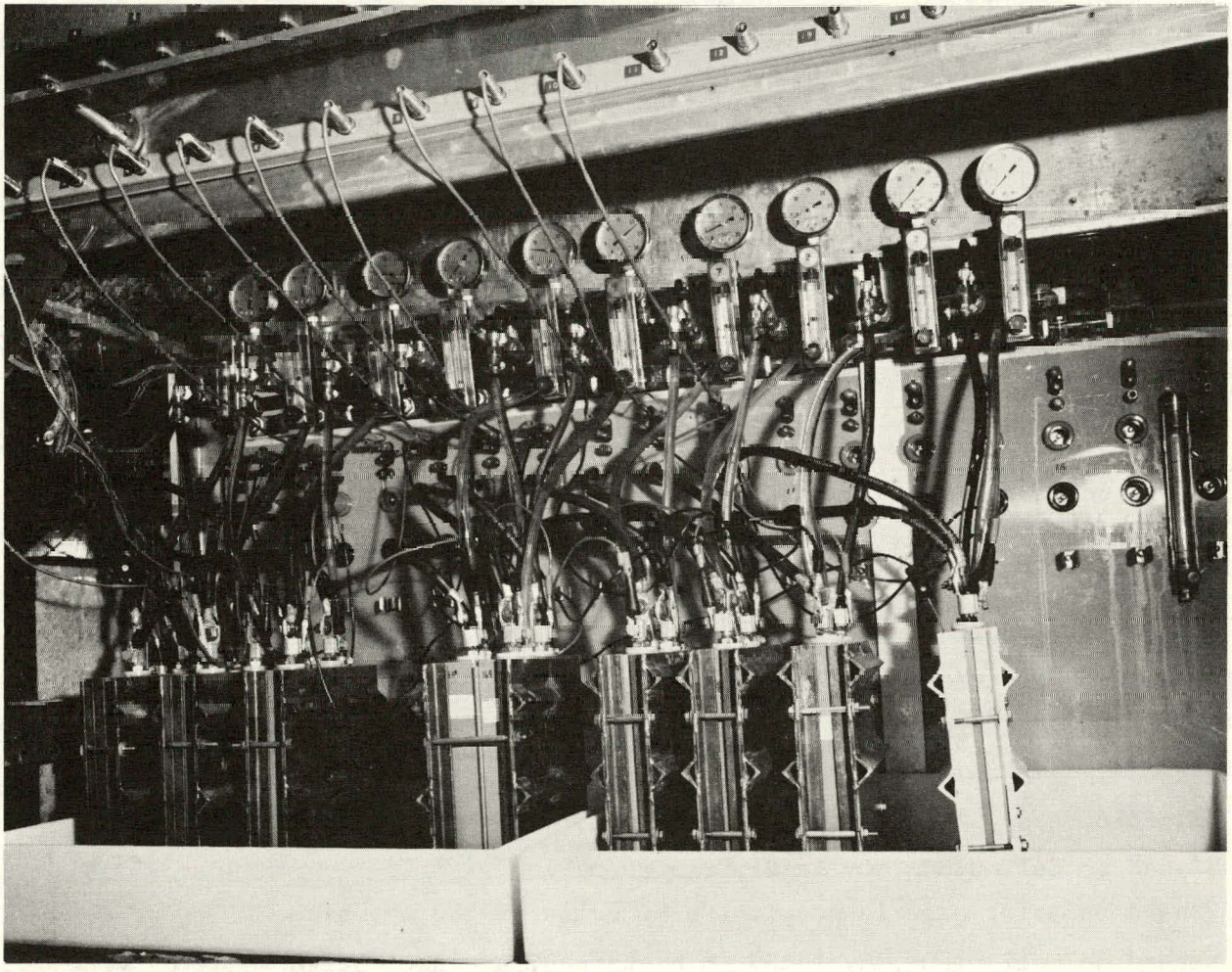

Figure 3.1

FULL-SIZE NICKEL-IRON CELL TEST SYSTEM HAVING
CIRCULATING ELECTROLYTE CAPABILITY

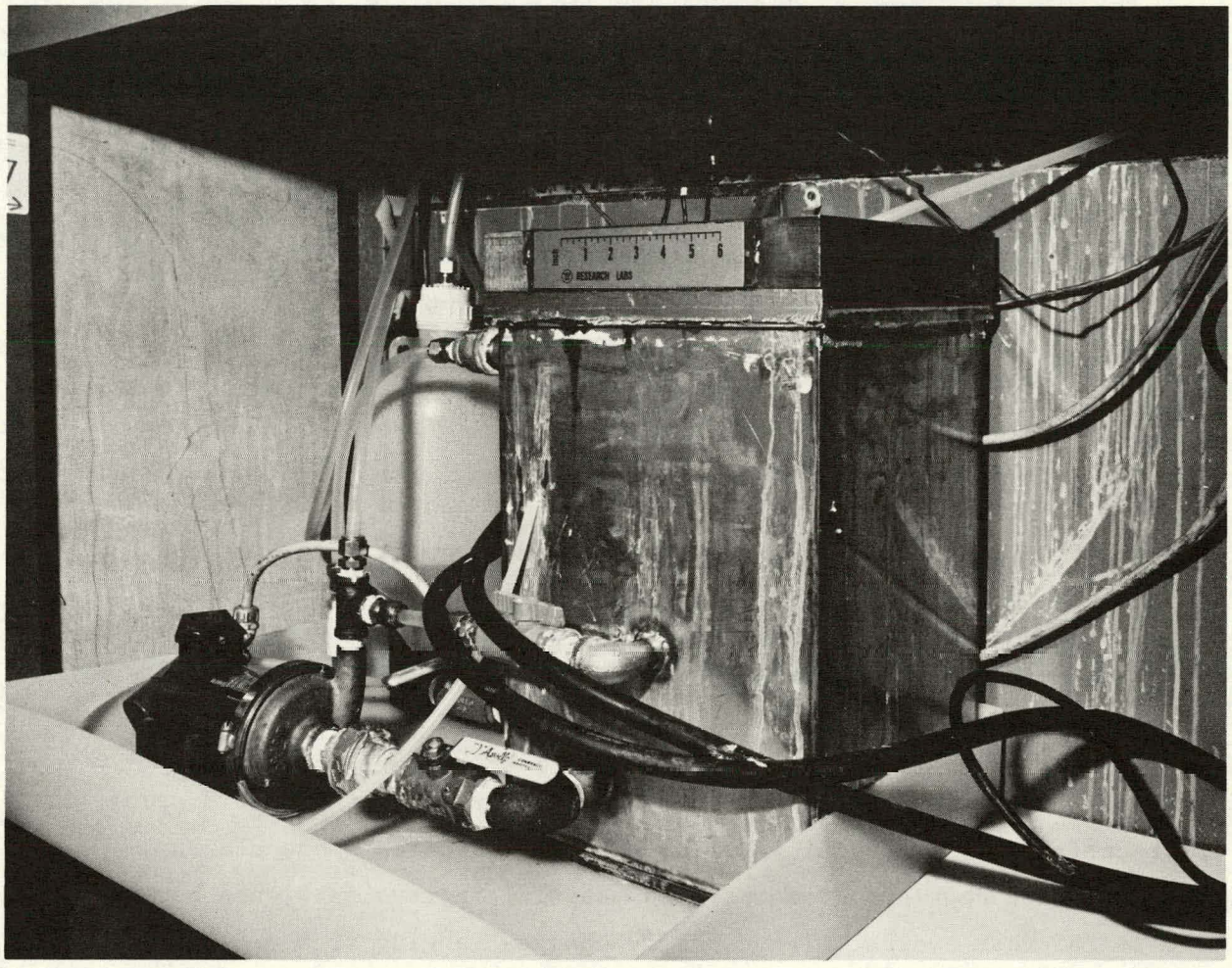

Figure 3.2

ELECTROLYTE RESERVOIR, PUMP AND GAS VENTING SYSTEM
INSTALLED IN THE AUTO CYCLE FULL-SIZE CELL TESTER

3.1.1 EPP Nickel Electrode Tests

Tables 3.2 and 3.3 summarize 3-plate cell test results on EPP and thermal nickel electrodes. Target nickel electrode capacity for the first ("2 x 4") battery was 23 Ah at the C/3 drain rate, to 1.0 V cutoff in the 3-plate test cell. These experimental electrodes deliver 21 to 26 Ah, depending on EPP processing conditions. Between 6 and 33% decline of Ah capacity has been noted after 200-300 test cycles. Experimental electrodes, 930E, 1134E, 1174E, 1180E and 11E are typical of the present state of EPP technology. The best test gave 6% decline in capacity (11E - with a crossed fiber plaque) up to 200 cycles (see Table 3.2.).

Maxi-line EPP plates are demonstrating capacities of 20 to 27 Ah in formation discharge, with the average (and majority) meeting the 23.5 Ah target specification at 2.54 mm plate thickness.

3.1.2 Thermal Nickel Electrode Tests

Full-size thermal nickel electrodes (2.0 to 2.3 mm in thickness) display 21 to 22 Ah capacity at the C/3 drain rate in the best 3 plate test cells to 1.0 V cutoff (see Table 3.3). Tests on these plates, which reflect continuing process and material improvements, are between 100 to 285 test cycles, with capacity changes ranging from a 4% loss in plate 12T to 30-33% decline in plates 10T and 11T. Plates 13T and 14T exhibit 10-16% decline in capacity at the 200 test cycle level.

3.1.3 Briquet Iron Electrode Tests

All effort on the briquet-type electrode has been deferred and all iron electrode effort has been concentrated on the composite-type.

3.1.4 Composite Iron Electrode Tests

Results on full-size test plates have been summarized in Table 2.5, Section 2.1.2.3. The composite-type iron electrodes have demonstrated stable capacities of 21 to 22 Ah at up to 250 test cycles.

TABLE 3.2

EPP-Type Nickel Electrode 3 Plate Cell Test Results

Plate Designation	Initial Capacity[c] Ah	Life Characteristics Ah Eff. % [b]	Cycles [c]	% Decline AHR Capacity [d]
391E	23.0	69	189	9
402E	20.9	63	129	11
438E	22.1	66	237	13
482E	23.9	72	123	5
544E	21.2	64	157	26
549E	24.4	73	197	30
633E	20.6	62	157	10
779E	22.3	67	157	31
831E	27.4	83	76	2
930E	23.8	71	252	20
1114E	22.2	67	136	20
1134E	25.2	76	163	26
1174E	22.3	67	213	33
1180E	23.9	72	213	30
27E	25.7	77	> 304	28
2114E	23.9	72	> 337	29
11E	25.2	76	> 188	6

a. C/3 discharge , C/3 charge for 4h.
b. Based on at least 5 consecutive cycles.
c. "Greater than" symbols denote continuing operation.
d. Percent decline from initial.

TABLE 3.3

Thermal-Type Nickel Electrode 3 Plate Cell Test Results

Plate Designation	Initial Capacity[a] Ah	Initial Ah Eff. %[b]	Life Characteristics Cycles[c]	Life Characteristics % Decline Capacity[d]
10T	21.7	65	255	33
11T	21.9	66	285	30
12T	21.6	65	96	4
13T	21.9	66	217	16
14T	20.4	61	179	10
16T	16.5	50	123	-7

a. C/3 discharge, C/3 charge for 4h.

b. Based on at least 5 consecutive cycles.

c. "Greater than" symbols denote continuing operation.

d. Percent decline from initial, minus sign denotes increase.

This stability has been maintained in plates having variations in nickel plating, steel wool fiber type and phenolic content of the active material paste, suggesting none of these factors are critical to stable performance.

3.1.5 Summary of Three-Plate Test Results

With respect to individual electrode gravimetric performance goals, the composite iron electrodes are approaching target performance, (.40 Ah/g active and .27 Ah/g electrode), at .36 Ah/g active and .20 Ah/g electrode, based on 26.0 Ah capacity obtained in some plates. EPP plates are wet and cannot be precisely measured in this regard. Based on plates of 24.6 Ah capacity, performance is estimated at .21 Ah/g active and .11 Ah/g electrode (target performance is .25 Ah/g active and .14 Ah/g electrode). However, as projected results in full-size cells show in Section 3.3, overall cell performance, using EPP nickel and composite-type iron electrodes in the specified cell volumetric constraint, are meeting and exceeding the initial goal of 53 Wh/kg at C/3 drain rate. The best composite irons exhibit no capacity loss in up to 400 cycles. The best nickel EPP electrodes indicate 6 percent loss over initial capacity in 190 test cycles. Thermal-type nickel electrodes have shown 15% degradation in capacity in 220 test cycles in one test electrode.

Work is continuing, to improve the performance of the iron and nickel electrodes by modifications in plate construction and/or active material formulation.

3.2 Full-size Cell Test Results

Fig. 3.1 shows the present full-size test station used to evaluate Westinghouse nickel-iron cells. Each cell contains, per the design specification, 10 nickel plates and 11 iron plates in the design volume specified for the cell. The cell has provision for electrolyte circulation and gas venting.

Table 3.4 presents data obtained in testing full-size cells. Table 3.5 summarizes some of the best full-size cell data.

Couloumbic efficiencies have not been optimized in the test results reported in these tables, since the cells were cycles by in-house standard procedures, primarily to obtain performance as a function of cycling. Some of the cells were fabricated to gain experience toward evaluating cell construction variables and do not necessarily represent attempts at maximizing gravimetric performance.

These cell results have indicated the feasibility of attaining 50 to 60 Wh/Kg at the C/3 drain rate in full-size iron-nickel cells, having the design volumetric constraint and using EPP nickel and composite-type iron electrodes.

Cyclic life testing (our initial testing had been at 100% depth of discharge per cycle) has been modified to 80% depth of discharge per cycle at the C/3 drain rate and has been further modified to permit electrolyte composition, circulation and temperature control.

These modifications should enhance cell cyclic life, since this property is highly dependent on stack thermal balance (temperature control) to enhance nickel plate charge acceptance, electrolyte composition control and electrolyte availability within the plate stack. Electrolyte circulation was used in prior long-time cyclic tests (to 1400 cycles) conducted at Westinghouse on iron-nickel cells of 180 Ah capacity. Furthermore, these earlier tests were performed in a CO_2-controlled environment, to minimize CO_3 = pickup in the electrolyte, and this control will also be employed in the future cyclic tests.

Test evidence being compiled suggests that the following factors, singly or in combination -- thermal balance, electrolyte composition control and availability within the plate stack, and CO_2 control -- are conducive to long cycle life. Two cells in finished molded cases, showing cyclic capacity degradation, have been unclamped from their test fixtures to permit electrolyte penetration into the stack-up (at least for an overnight period), and then reclamped and

TABLE 3.4

Test Results Obtaired on Full-Size Iron-Nickel Cells

Plate Designation	Initial Capacity[a] Ah	Wh	Initial Ah Eff. %[b]	Life Characteristics Cycles[c]	% Decline Capacity[d]
004CE	211	243	63	56	11
006CE	252	290	75	48	26
009CE	227	261	68	34	47
010CE	235	287	71	73	23
011CT	204	245	61	31	5
012CE	243	297	73	88	44
013CE	241	294	72	104	52
014CT	211	253	63	20	-5
015CE	218	262	65	77	61
016CE	237	284	71	92	55
017CE	215	258	65	91	44
018CE	230	276	69	28	13
019CE	238	286	71	89	20
020CE	228	274	68	56	55
021CT	220	260	66	63	9
022CE	217	258	65	78	34
023CE	237	284	71	78	38
025CE	232	281	70	> 125	30
026CE[j]	243	292	73	84	48
029CT	199	245	60	> 94	51

TABLE 3.4 (Continued)

Test Results Obtained or Full-Size Iron-Nickel Cells

Plate Designation	Initial Capacity[a] Ah	Wh	Initial[b] Ah Eff. %	Life Characteristics Cycles[c]	% Decline[d] Capacity
030CE	200	240	60	63	-12
031CE	246	295	74	62	13
032CE	213	254	64	48	1
038CE	214	-	64	10	(tbd)
105CE	222	-	67	101	20
140CE	210	-	63	> 111	21
169CE	225	-	68	> 91	24
186CE	194	-	58	> 78	-6
194CE	192	-	58	> 104	-23
270CE	187	-	56	> 46	14
284CE	218	-	65	> 33	17
287CE	215	-	65	> 33	23

a. c/3 discharge c/3 charge for 4h.

b. Based on at least 5 consecutive cycles.

c. "Greater than" symbols denote continuing operation

d. Percent decline from initial, minus sign denotes increase

Table 3.5

SUMMARY OF BEST GRAVIMETRIC ENERGY DENSITY RESULTS
OBTAINED TO DATE ON FULL-SIZE PROTOTYPE NICKEL-IRON CELLS
(CAPACITIES AT C/3 DISCHARGE RATE TO 1.0V CUTOFF,
CHARGE AT C/3 FOR 4 h.)

Cell	Best Ah	Cycle	Wh	Wh/g	Total Cycles*	% Ah Cell Dedgradation Initial-to-Final
010CE[a]	250	16	305	62	73	23
012CE[a]	266	25	325	63	88[b]	44
013CE[a]	259	26	317	64	103[b]	52
017CE	254	32	305	60	90[b]	44
019CE	270	33	321	61	89[b]	20
021CT	246	16	289	57	56[b]	9
025CE	262	25	314	61	(>125)	30
194CE[c]	236	117	272	50	(>117)	na

(>) = still on test

*Cycling discontinued due to capacity degradation

a "static" electrolyte cell - non circulating electrolyte

b mostly full discharge cycles, to 1.0 V/cell cutoff

c circulating electrolyte cell from start of testing

further tested. Results of these tests are shown in Table 3.6. These data indicate that the stack is able to deliver capacity, but is being starved for electrolyte, which, if made available, will restore capacity to a high level (for example, from 114 to 210 Ah in the case of cell 025CE at test cycle 120).

Cause(s) for the starvation are being determined, but nickel electrode swelling is likely. Fabrication techniques are being modified to deepen and widen the vertical electrolyte flow channels in the nickel plates. Calculations and tests to increase pore volume are being made on EPP and thermal nickel electrodes and compared with data on older design nickel electrodes (which cycled 1400 times to 80% DOD in 180 Ah cells). It appears that less pore volume may be available, for electrolyte in the present EPP nickel electrodes. If this is proven to be the case, in plates that have undergone numerous test cycles, the plate design and the EPP process will be modified to more closely match the E-180 nickel plate porosity, while still maintaining suitable plate capacity.

Some full-size cell data are now showing increased performance with cycle life. Cell 194CE is presently demonstrating 231 Ah capacity at 117 test cycles (100% DOD cycles in this case) with testing continuing.

Performance data were obtained on full-size nickel-iron cells when discharged at the C/6 rate, as compared with the C/3 rate. These data, illustrated in Figs. 3.3 and 3.4, indicate from little change up to 12 to 13% improvement in performance (capacity, energy available and gravimetric energy density).

A deep discharge test cycle (discharge to 1.0 V/cell cutoff) is illustrated in Fig. 3.5. Fig. 3.6 presents the performance characteristics of full-size cells when subjected to an 80% depth of discharge cyclic test regime. About 10 to 20 mV improvement in average cell discharge voltage occurred, during the 80% DOD discharge.

Table 3.6

TESTS SHOWING CAPACITY RESPONSE IN FULL-SIZE NICKEL-IRON CELLS, AFTER UNCLAMPING AND RECLAMPING THE STACK
(220 Ah Nominal Capacity)

	Before			After	
Cell	Ah	Cycle	Unclamped	Ah	Cycle
025CE	82.0	114	Overnight	210	120
169CE	100	75	Overnight	206	81

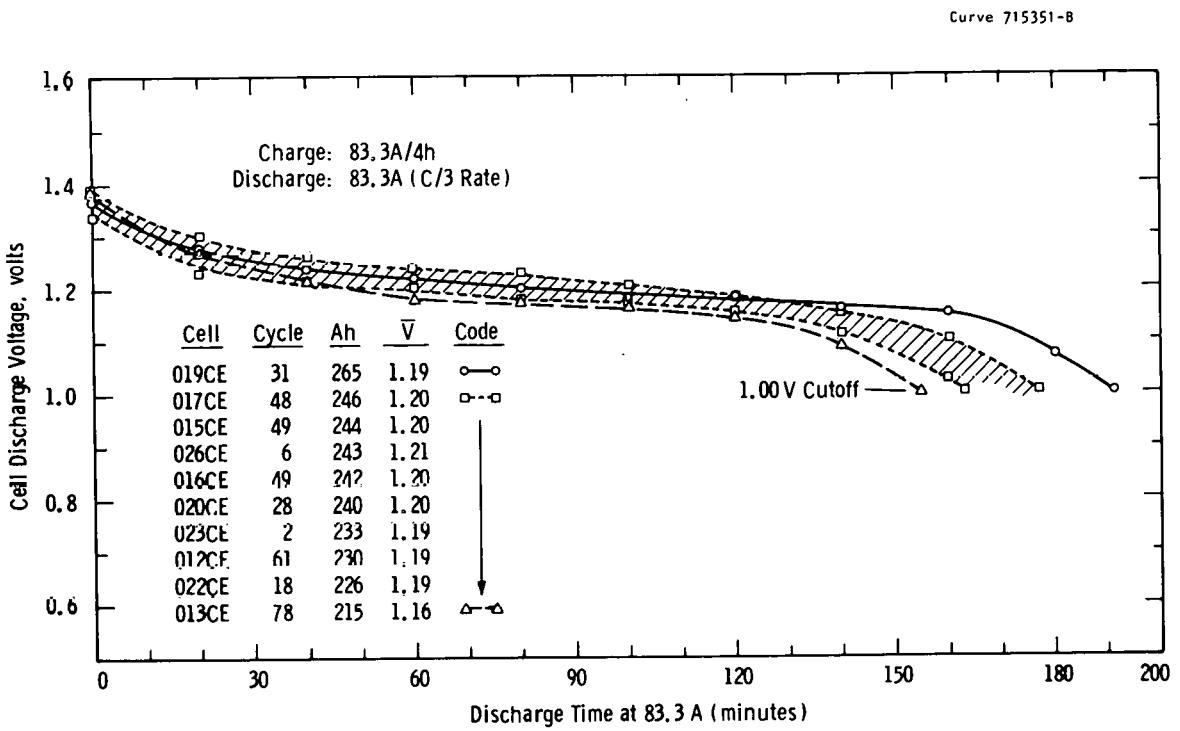

Figure 3.3

DISCHARGE CHARACTERISTICS OF FULL-SIZE NICKEL-IRON CELLS AT THE C/3 RATE

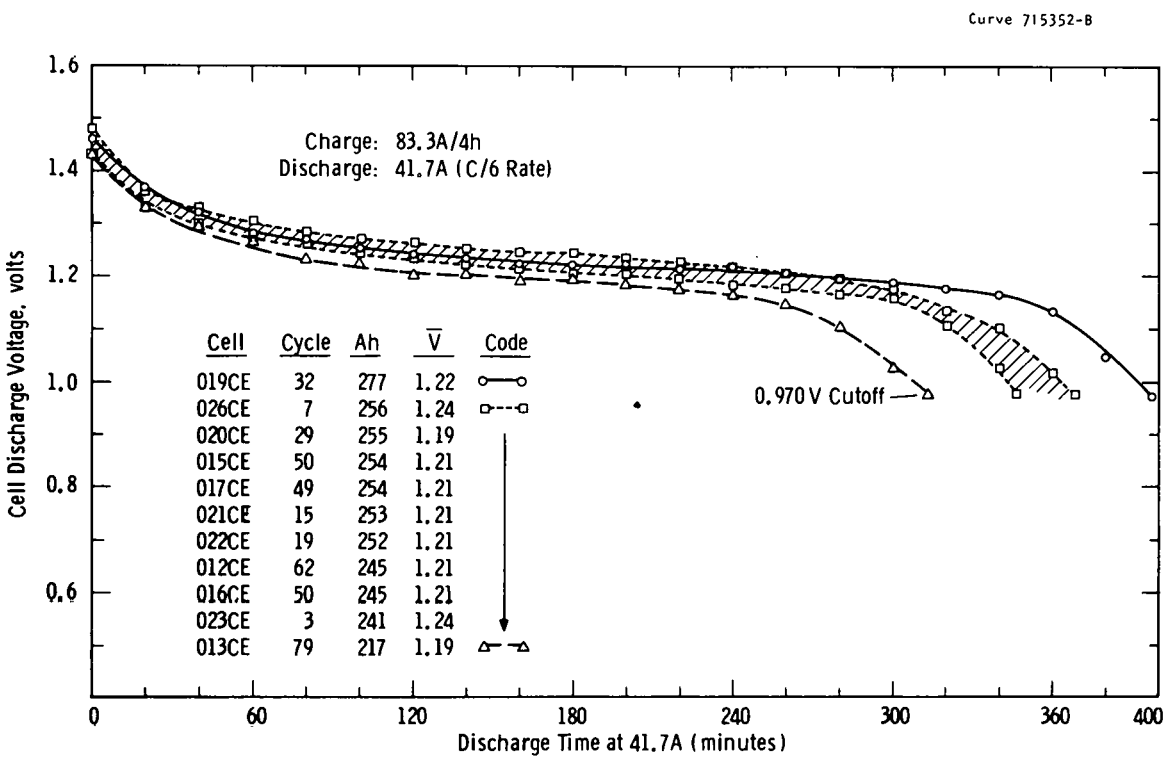

Figure 3.4

DISCHARGE CHARACTERISTICS OF FULL-SIZE NICKEL-IRON CELLS AT THE C/6 RATE

Power characteristics obtained on cell 007CE (0.70 mΩ) are given in Fig. 3.7. The peak power profile shown is determined by stepping the discharge current up in 200 Amp increments, holding for 5-10 seconds at each level, stepping down in the same manner and repeating this cycle at various depths of discharge during an otherwise constant current C/3 discharge. These data indicate that, in the nearly fully charged state, up to 175 W/Kg peak power is attainable in the cell. At 72% depth of discharge, about 100 W/Kg was obtained in testing this cell.

3.2.1 Summary of Full-Size Cell Tests

Cell results have indicated the feasibility of attaining 50 to 60 Wh/Kg at the C/3 drain rate in full-size cells, having the design volumetric constraint and using EPP nickel and composite iron electrodes.

Cyclic life testing (our initial testing had been at 100% depth of discharge per cycle) has been modified to 80% depth of discharge per cycle at the C/3 drain rate and has been further modified to permit electrolyte composition, circulation and temperature control.

These modifications should enhance cell cycle life, since this property is highly dependent on stack thermal balance (temperature control) to enhance nickel plate charge acceptance, and electrolyte composition control and availability within the plate stack. Electrolyte circulation was used in prior long-time cyclic tests (to 1400 cycles) conducted at Westinghouse on iron-nickel cells of 180 Ah capacity. Furthermore, these earlier tests were performed in a controlled CO_2 environment, to minimize $CO_3^=$ pickup in the electrolyte. This same control will also be employed in the future cyclic tests.

Cyclic testing has been resumed on cells having electrolyte circulation capability. Best data to date have shown cell 194CE with stable capacity (230 Ah) after 120 deep discharge cycles, with testing continuing.

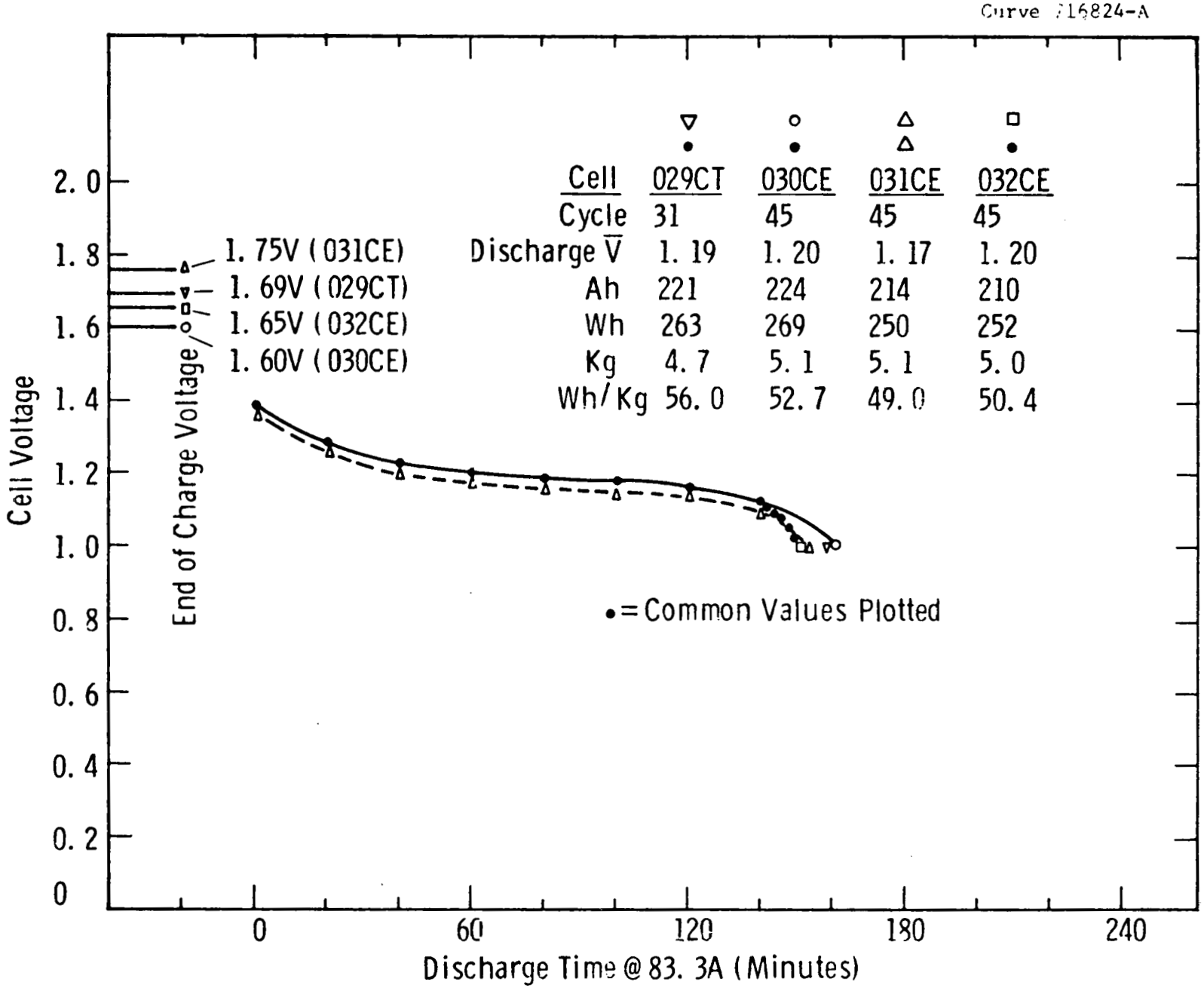

Fig. 3.5 — Performance characteristics of thermal nickel (029CT) and production (030, 031, 032CE) nickel-iron cells at C/3 drain rate

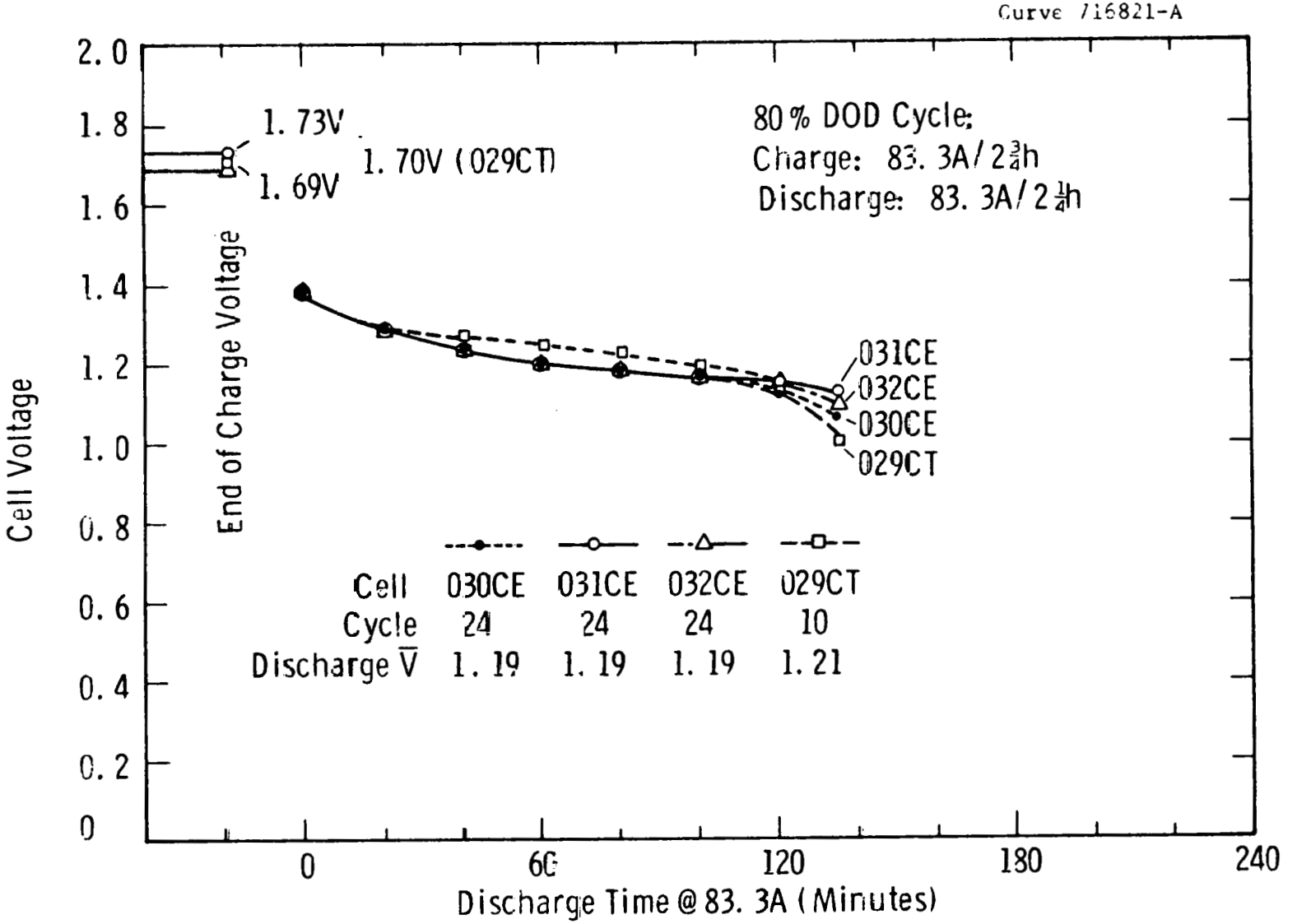

Fig. 3.6 – Performance characteristics of pilot line production nickel-iron cells (030CE, 031CE and 032CE) and thermal nickel cell 029CT at C/3 drain rate during an 80% DOD test cycle

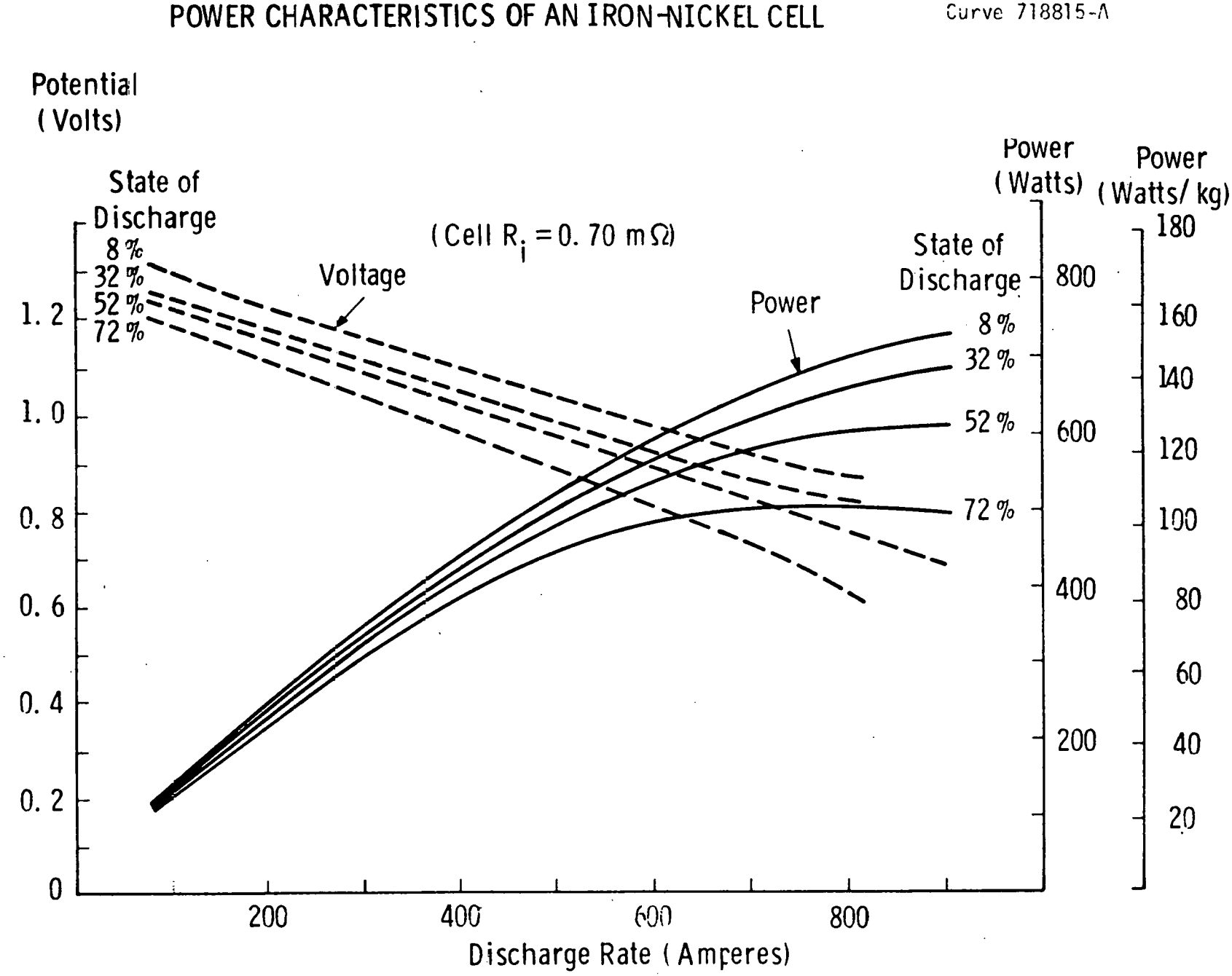

Fig. 3. 7 — Power characteristics of cell 007CE

Noryl 225 cell cases and Noryl 225 covers are being used in constructing full size cells. Bench tests on such cells have delivered up to 58 Wh/Kg at the C/3 drain rate at target cell weight (5.0 Kg).

New separators are being investigated, aimed toward reducing total cell resistance and eliminating the need for a separate barrier layer, as used in our present separator system. Pilot Line cells, tested with electrolyte circulation for capacity, can consistently display target cell resistances of 0.50 to 0.70 mΩ, at 1/2h into discharge at 83.3A.

Cells at 0.70 mΩ, or less, are expected to provide up to 175 W/Kg, near full charge, as demonstrated in cell 007CE (with nylon separator) of 0.70 mΩ resistance.

3.3 Cell Failure Examinations

Of six cells given failure examinations, three (116CE, 118CE and 139CE) had shorts near the plate tabs. The three shorts occurred at the top of the plates under the comb to which the plate tabs were welded. In cell 139CE the short extended to the nearest top corners of the plates and melted the case, causing a hole through which electrolyte leaked. In each cell the separators above the plates, under both positive and negative combs, were melted down to below the tops of the plates when the plates were welded to the combs. The separator used in all three cells was Kimberly-Clark 49696 absorber with a Celgard barrier. The method of welding plate tabs to combs is being studied so that excessive meltdown of separators can be prevented.

Two cells had shorts at the bottoms of the plates. The short in cell 105CE was found on cycle 101 when a hole burned through the case. On the cycle before the short was found, this cell had a capacity of 148 Ah (initial capacity 220 Ah). A short had been found in this cell just after it was assembled, caused by the arc, during welding, which grounded through the cell to the welding fixture. This original short was covered by a layer of separator prior to stack insertion into the

cell case, but it probably initiated the short on cycle 101. After the original short the weld tooling fixture was coated with an insulating material to prevent further shorts in cells during assembly.

The second cell with a short (187 CE) also developed a hole in the bottom. A hole, one inch in diameter, had been burned in five adjacent plates. The short in this cell had burned to the extent that no specific cause for it could be found. One possible cause, poor sealing of the separator envelope, will be precluded by an alternative wrap now being considered for separators.

Cycling of cell 260CE was discontinued after 38 cycles because its capacity had fallen to 25 Ah. The cell stood for several days with the restraints removed; then the restraints were replaced and cycling was continued. On the next cycle it had a capacity of 208 Ah. The low capacity on cycle 38 is attributed to electrolyte starvation, which was alleviated when the restraints were removed. Cycling on this cell is being continued.

3.4 Nickel-Iron Battery Module Tests

Fig. 2.6 illustrates the standard 6 cell module that is fabricated in the pilot line. Module 6-1 was constructed in the Pilot Line and pretested at (W), prior to shipment to DOE/ANL in mid July, 1979 for their test evaluation at NBTL. Module 6-1 construction, similar to the modules being built for the "2 x 4" battery, is comprised of 6 series connected cells (with EPP nickel and composite-type iron electrodes), complete with electrolyte circulation capability and exhaust gas venting (Fig. 2.6). Cell resistances in Module 6-1 ranged

from 0.53 to 0.61 m at 1/2 hour into discharge at 83.3A.* OCV's of the cells ranged from 1.245 to 1.296 V (7.478 V/module), except for cell 120CE (1.175 V), which experienced some overheating during construction.**

The module was fitted to an electrolyte circulating and cooling system, instrumented and tested for performance through 2 full charge and discharge cycles. Fig. 3.8 illustrates the performance and behavior of module 6-1, during its second test cycle. The module, classified as CB (see Table 3.7), performed very well, despite the initial OCV problem with Cell 120CE. The module delivered 239 Ah at the C/3 drain rate, which corresponded to 1735 Wh (7.26 $\overline{V}$, calculated for the module, 1.21 $\overline{V}$, calculated for the cells). The module, classified as CB (see Table 3.7), performed very well, despite the initial OCV problem with Cell 120CE. The module delivered 239 Ah at the C/3 drain rate, which corresponded to 1735 Wh (7.26 $\overline{V}$, calculated for the module, 1.21 $\overline{V}$, calculated for the cells). At 32.9 kg, total module assembled and electrolyte filled weight, 6-1 delivered 52.7 Wh/kg. With no attempt made to optimize the charge, 6-1 displayed 72% Ah and 53% Wh efficiencies. Maximum charge temperature was controlled at 42°C for this test cycle. Assembly, pretest and test procedures, actual and projected performance data have been supplied to DOE/ANL, regarding module 6-1, where it is undergoing test evaluation in the NBTL facility.

---

*Prior to module assembly, cells are tested on the formation bench in groups of 2 cells, each, utilizing electrolyte circulation and temperature control. All cells are ranked with respect to their formation bench capacity, internal resistance and flow characteristics on the formation bench (see Table 3.7). Cell resistances are determined by a 100-200-100A sweep test at 1/2 h into discharge.

**Most likely, during comb-to-tab welding, some separator melt down occurred at the plate-to-tab interface, which could lead to a slight short in this region and cause a lower cell voltage. However, the cell was stable at this lower voltage.

Fig. 3.9 illustrates the performance and behavior of another module, 6-6, during its second test cycle. This module, comprised of lower capacity cells (Classification BB), was tested to evaluate its acceptability for inclusive into the "2 x 4" battery. Module 6-6 delivered 226 Ah, 1602 Wh, 49.6 Wh/kg at the C/3 drain rate -- acceptable performance. Bulk electrolyte temperature was controlled at 31°C, throughout this test. Cell resistances ranged from 0.58 to 0.63 mΩ. Electrolyte flow impedance was high (18.5 psi, gage) for the module and, perhaps, this behavior may be related to the lower cell and module average voltages (1.18 $\overline{V}$ and 7.08 $\overline{V}$, respectively) obtained on 6-6. Module flow impedance and cell resistances will continue to be compared with average voltage behavior, to determine if a correlation does exist.

3.5 "2 x 4" Battery for JPL Evaluation

The "2 x 4" battery (Figure 2.17), along with its on-board electrolyte reservoir and pumping system and charger, was assembled and delivered to Jet Propulsion Laboratory, Pasadena, California, for their test evaluation in August 1979. The battery contains 16 modules (10 with 6 cells and 6 with 5 cells) and 90 total cells, of the module configuration illustrated in Fig. 2.18. Prior to delivery, the battery was tested at Westinghouse R&D Center for 3 test cycles, to check the charger capabilities, evaluate the performance of the cells, modules and battery, test the circulating electrolyte system, and to determine some of flow and the thermal characteristics of the battery on charge and discharge. Fig. 3.10 and 3.11 illustrate the charge-discharge,

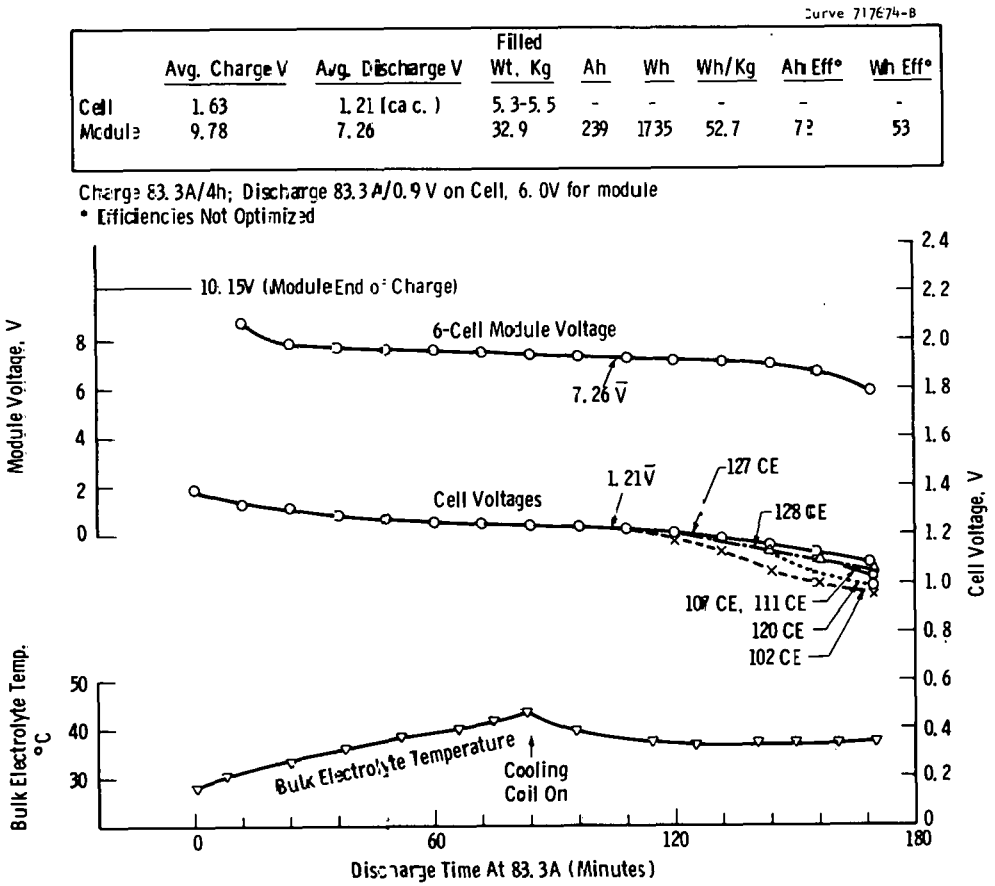

Fig. 3.8 - Cell and Module Voltages, Bulk Electrolyte Temperature Obtained During Testing of Nickel-Iron Battery Module 6-1, Cycle 2

Table 3.7

CELL CLASSIFICATION FOR 6-CELL MODULE ASSIGNMENT FOR THE "2 X 4" BATTERY

A. CELL CAPACITY RANGE (C/3 Rate)	DESIGNATION
$\leq$ 205 Ah	A - (reject for battery)
206 → 215	B
216 → 225	C
226 → 235	D
236 → 245	E
246 → 255	F
> 255	G

B. CELL ELECTROLYTE FLOW IMPEDANCE	DESIGNATION (end of charge)
$\leq$ 5 psi	A
6 → 10	B
11 → 15	C
16 → 20	D
> 20	E - (reject for battery)

C. CELL INTERNAL RESISTANCE RANGE	DESIGNATION	
$\leq$ 0.85 mΩ	Accept	@ 100-200-100A sweep and @ 1/2 h into discharge at 83. A (C/3 rate)

circulation, temperature data obtained on the battery for test cycles 1 and 3, respectively. The battery delivered 199 Ah on cycle 3, 113.0 $\overline{V}$, 22.5 KWh, at about the C/3 drain rate. Maximum bulk electrolyte temperature, without cooling during discharge, was 62°C. Figure 2.29 also lists module and circulation system weights. Total module weight was 492 Kg,the on-board electrolyte system weight was 17 Kg for a total battery system weight of 509 Kg. Final weight goal for the Prototype I battery is 445 Kg.

During August 1979, at JPL, the battery was subjected to another 11 test cycles. Table 3.8 provides a summary of the 2 x 4 battery test and performance history. These tests were conducted under cognizance of Westinghouse personnel on field assignment at JPL. There, the battery delivered between 181 to 192 Ah at, approximately, the C/3 drain rate when charged at the 35 and 70A rates. Dynamometer test results (battery coupled with South Coast Technology's converted VW Rabbit) indicated about a 75 miles range at a constant 55 mph and 115 miles range at 35 mph. When driven according to the SAE J227a B and D driving cycles, 68 and 48 miles, respectively, were obtained.

After these tests, several problem cells were isolated in the battery. These cells (146, 138, 219, 221 and 172) were located in 3 modules of the battery -- 6-3, 5-1 and 5-2. Cells 146 and 138 indicated extremely low open circuit voltages (.006 and .001 V), cells 219, 221, (module 5-1) and 172 (module 5-2) indicated abnormally high charge voltages (3.8 volts) even at low charge current (1-10A). These modules were removed from the battery and replaced by spare modules. The modules were returned to Westinghouse for examination. Post operational examination revealed cells 219, 221 and 172 had their inlet electrolyte circulation tabs blocked by epoxy and the cell stacks had dried out. The technique and tube design are being modified on present future cells to eliminate this blockage. Cells 146 and 138 were found to have faulty separators coverage over the plates in the tab region, leading to shorts in these cells.

Table 3.8 PERFORMANCE DATA OBTAINED ON NICKEL-IRON "2 X 4" BATTERY AT JPL

ORGANIZATION	TEST CYCLE	RATE(A)	INPUT(Ah)	DISCHARGE RATE(A)	DISCHARGE OUTPUT(Ah)	TEST MODE	DYNAMOMETER TEST RESULTS
(W)-R&D Center	1	40	293	73	193	Resistor Bank	--
	2	70	280	73	191	Resistor Bank	--
	3	70/40	280	73	199	Resistor Bank	--
JPL Pasadena, CA	4	30/35	250/320	81-75	191	Light Bank	
	5	35/50	295/325	124	164	SCT @ 55 mph.	73 miles
	6	50	270	80-71	192	Light Bank	
	7	50	260	80	185	Light Bank	
	8	70	270	79-73	181	Light Bank	
	9	70	254	53	184	SCT @ 35 mph	121 miles
	10	70	252	119	166	SCT @ 55 mph	76 miles
	11	70	253	N.A.	161	SCT @ SAE D Cycle	48 miles
	12	80/70	90/245	N.A.	191	SCT @ SAE B Cycle	62 miles
	13	75	256	N.A.	157	SCT @ SAE D Cycle	48 miles
	14	75	211	N.A.	157	SCT @ 35 mph	105 miles

Curve 717883-B

	Avg. Charge V	Avg. Discharge V	Filled Wt., Kg	Ah	Wh	Wh/Kg	Ah Eff*	Wh Eff*
Cell	1.61	1.18 (Calc.)	5.50-5.55	-	-	-	-	-
Module	9.66	7.09	32.3	226	1602	49.6	68	50

Charge 83.3A/4h; Discharge 83.3A/6.0 V on Module
* Efficiencies Not Optimized

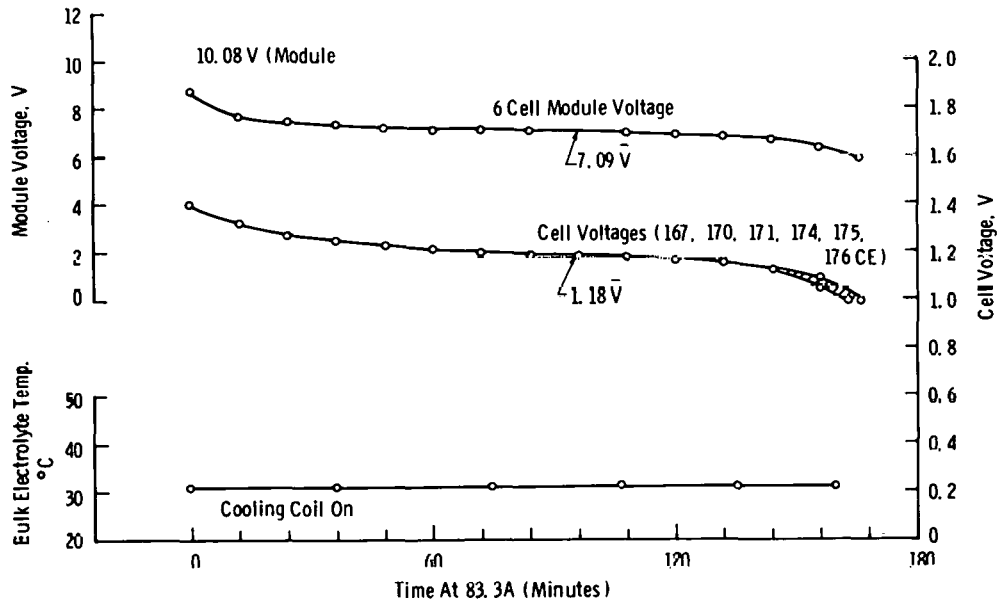

Figure 3.9

CELL AND MODULE VOLTAGES, BULK ELECTROLYTE TEMPERATURE OBTAINED DURING TESTING OF NICKEL-IRON BATTERY MODULE 6-6, CYCLE 2. CIRCULATED ELECTROLYTE, C/3 DRAIN RATE

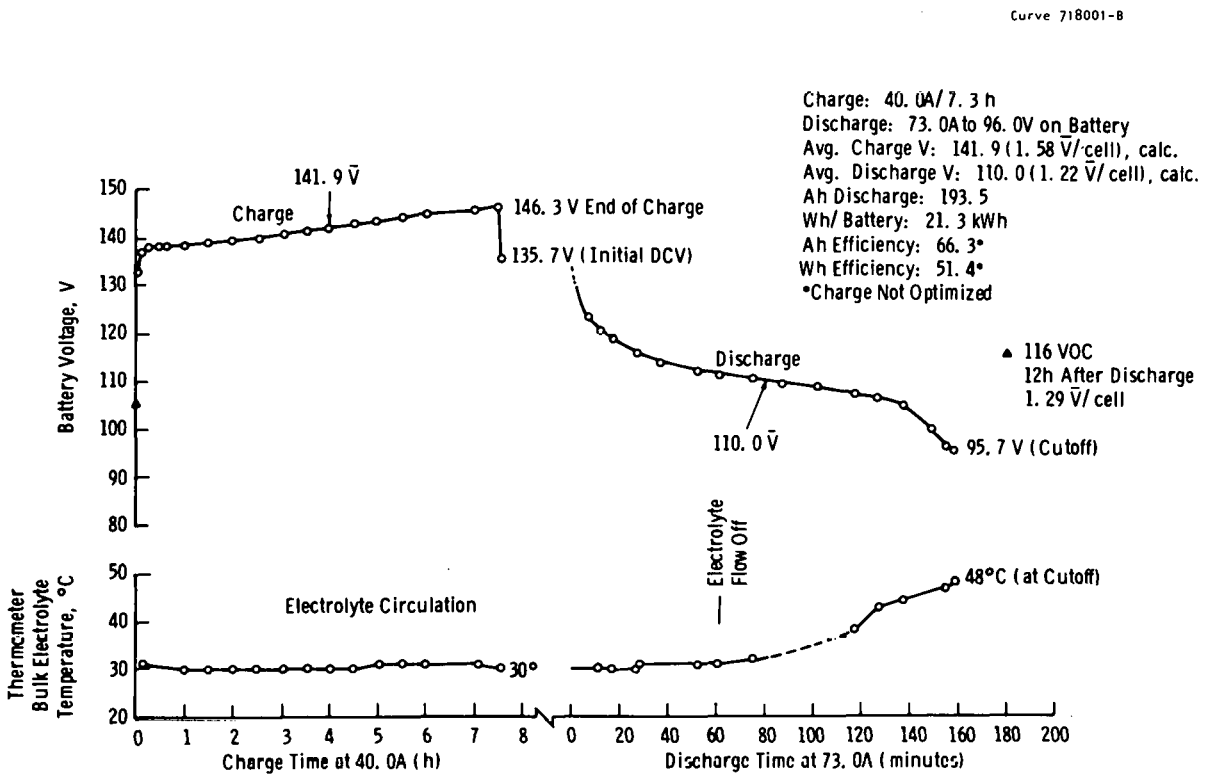

Figure 3.10

(W) NICKEL-IRON "2 x 4" BATTERY
PERFORMANCE CHARACTERISTICS -- CYCLE 1

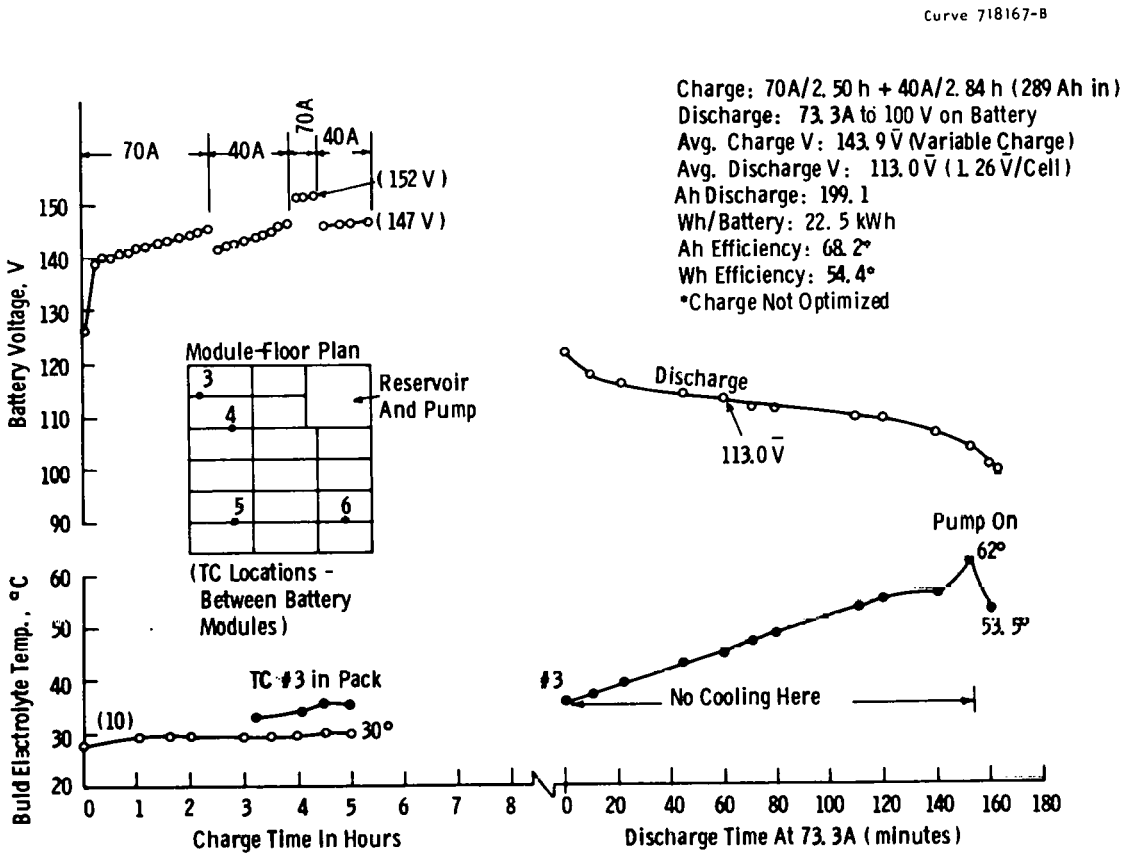

Figure 3.11

(W) NICKEL-IRON "2 X 4" BATTERY PERFORMANCE CHARACTERISTICS - CYCLE 3

4.0 REFERENCES

(1) Annual Status Report for FY '78, Research Development and Demonstration of Nickel/Iron Battery for Electric Vehicle Propulsion, ANL/DOE Contract No. 31-109-34-4141, August 31, 1978, p. 13.

(2) Ibid, p. 12

(3) Hardman, C. C., U.S. Patent 3,600,227, Method of Impregnating Flexible Metallic Battery Plaques, August 17, 1971.

(4) Falk, V. and Salkind, A., Alkaline Batteries, John Wiley and Sons, 1969 , p. 48,49.

(5) Weininger, J. L., "Nickel Hydroxide Electrode Research" 1st Interim Technical Report, Dec. 1969. Report #5-70-1025, Dept. of the Air Force, Aero-propulsion Lab, Wright-Patterson AFB, Ohio.

(6) Weininger, J. L. and Ruzzo, J. G., Jr., "Effect of Additives on Nickel Hydroxide Electrode Capacity and Cycle Life", Abstract #3, Detroit Meeting of the Electrochemical Society, Oct. 1969.

(7) Pickett, D. F. "Fabrication and Investigation of Nickel-Alkaline Cells; Part I. Fabrication of Nickel Hydroxide Electrodes Using Electrochemical Impregnation Techniques", AFAPL-TR-75-34, Part I, Oct. 1975.

(8) "Research, Development and Demonstration of a Nickel-Iron Battery for Electric Vehicle Propulsion - Annual Status Report for FY-'78", R. Rosey, et al., Public Report ANL Contract No. 31-109-34-4141.

5.0 APPENDIX A

ELECTROPRECIPITATION EPP SIDE REACTIONS

The side reactions which are of importance in the nickel plate electroprecipitation process are:

a. $2\ NO_3^- + 8\ H^+ + 6\ e^- \longrightarrow 2\ NO + 4\ H_2O$

b. $2\ NO + 2\ H^+ + 2\ e^- \longrightarrow N_2O + H_2O$

c. $N_2O + 4\ H^+ + H_2O + 4e^- \longrightarrow 2NH_2OH$

d. $2\ NH_2OH + 6\ H^+ + 4\ e^- \longrightarrow 2\ NH_4 + 2\ H_2O$

The above, when summed, yield the overall reaction:

e. $2\ NO_3^- + 20\ H^+ + 16e^- \longrightarrow 2\ NH_4^+\ 6\ H_2O$

Reactions a. and b. initiate the sequence necessary for the production of NH_4^+ ions. These NH_4^+ ions, per se, are not desirable, since the literature data specify maximum limiting concentrations of NH_4^+ ions of approximately 2 g/l, above which the formation of nickel-amine complexes inhibit the deposition of $Ni(OH)_2$. Analysis of our presently utilized EPP solutions shows that NH_4^+ ion content is approximately 4 g/l.

If reactions a. and b. are permitted to proceed at high rates, as evidenced by extensive gassing during EPP, then not only is NH_4^+ ion production accelerated, but obstructive gases are included in the plaque pores, blocking $Ni(OH)_2$ deposition. Therefore, visual control and voltage control are applied to keep these reactions minimized, or eliminated.

6.0 APPENDIX B

THERMAL NICKEL ACTIVE POWDER

The initial reaction in the thermal nickel preparation process is the fusion of a nickel oxide-cobalt oxide powder mixture with sodium peroxide. The fusion takes place in a suitable high-temperature resistant container in an oxidizing or inert atmosphere. A heating temperature range between 850 and 1000 C to form Na_2O which oxidizes the NiO-CoO mixture, resulting in a black crystalline single-phase material which may be defined as sodium nickelate and sodium cobaltate. This reaction product is then hydrolyzed to cause a decomposition reaction and formation of hydrated nickel and cobalt higher oxides. The active material settles quickly, is washed to neutral, and is dried at a temperature that will not degrade activity; e.g., between 50 to 110 C. (The NaOH formed can be drawn off and concentrated by evaporation into a saleable product.) A set of equations which schematically describe the chemistry of this process can be given as:

$$NiO + CoO + Na_2O_2 \longrightarrow NaNiO_2 + NaCoCO_2 \quad (950\ C,\ 1\ hr)$$

$$2\ NaNiO_2 + NaCoCO_2 + 3H_2O \longrightarrow Ni(OH)_2 + CoOOH$$

$$+ NiO_2(^1/_2H_2O) + 3\ NaOH$$

The temperature and time of fusion reaction of the NiO-CoO and Na_2O_2 have a decided influence on the performance of the final active product. Active material was incorporated into electrodes of 6.5 cm^2 area. They were then sized to a desired thickness of approximately 2 mm and were subjected to cycling testing, to determine the performance characteristics of the material, prior to using it in full-size test plates.

7.0 ACKNOWLEDGEMENTS

The members of the program team who contributed to the work described in this report, and their major areas of responsibility were

L. A. Doggrell - Separators, failure analysis of tested cells.

J. F. Jackovitz - Composite iron electrode, thermal nickel electrode,.

C. W. Maiden - Electrical testing sytems, module life test system design and construction.

N. J. Maskalick - EPP nickel electrode process development, advanced EPP concepts, cobalt substitution in the nickel active material.

W. Pollack - Electrode plaque process development, advanced plaque concepts.

L. G. Romain - EPP pilot line process, cell and module fabrication, formation line cell testing, cell and module testing.

J. Seidel - Composite iron electrode and process, thermal nickel electrode and process, advanced concept cells.

B. E. Taber - Component, cell, module and battery design, battery auxiliary systems design, comb-to-post terminal design and fabrication, testing facilities design, battery testing, cell testing, under various operating regimes.

Members of the support team include:

D. R. Hart, Pilot Line Coordinator
P. T. Bair
J. F. Buchholz
J. H. Dugan
L. W. Martz
S. L. Karaffa
V. J. Mulvehill
E. A. Pantier
T. M. Valko

8.0 FY-1979 PUBLICATIONS AND PRESENTATIONS:

1. "Westinghouse Iron-Nickel Battery Development", R. Rosey ACS/CSJ Chemical Congress Symposium, Apr. 1979.

2. "Westinghouse Iron-Nickel Battery Characteristics", R. Rosey Presentation at Second DOE/LLL Workshop on Energy Storage Systems for Automobile Propulsion - Electrochemical Panel, June 1979.

3. "Design of an Iron-Nickel Battery for Electric Vehicles", W. Feduska/R. E. Vaille, ECS Battery Division Proceedings of the Symposium on Battery Design and Optimization, Vol. 79-1, Edited by S. Gross p 299-310.

4. "An Advanced Iron-Nickel Battery for Electric Vehicle Propulsion", W. Feduska, et al, Electrochemical Society, Oct. 1979.

5. "Fabrication of High Capacity Nickel Electrodes Using a Pasting Technique", J. Seidel/J. F. Jackovitz, Electrochemical Society, Oct. 1979.

6. "Westinghouse Iron-Nickel Development Program", W. Feduska, panel presentation at Third DOE Battery and Electrochemical Contractors Conference - Session III Near Term Batteries, Dec. 1979.

7. "Research, Development and Demonstration of a Nickel-Iron Battery for Electric Vehicle Propulsion - Annual Status Report for FY-'78", R. Rosey, et al, Public Report ANL Contract No. 31-109-34-4141.

Distribution for ANL/OEPM-79-14

Internal:

J. J. Barghusen
D. Barney
C. Bean
E. C. Berrill
R. Biwer
A. Brown
L. Burris
G. Chapman
A. A. Chilenskas
C. C. Christianson
G. Cook
D. Corp
E. Creamer
S. A. Davis
W. DeLuca
R. C. Elliott
M. Farahat
P. R. Fields
F. Foster
D. Fredrickson
B. R. T. Frost
E. C. Gay
J. Geller
M. Genger
F. Hornstra
C. C. Hsu
J. Klinger
V. Kremesec
A. B. Krisciunas
M. Kronenberg
W. W. Lark
T. S. Lee
M. Liu
R. Loutfy
W. Massey
J. Miller
W. Miller
P. A. Nelson
M. V. Nevitt
E. G. Pewitt
D. Poa
J. Rajanwitt
J. J. Roberts
M. F. Roche
H. Shimotake
R. K. Steunenberg
C. Swoboda
Z. Tomczuk
A. Tummillo
R. Varma
P. D. Vashishta
D. R. Vissers
D. S. Webster
N. P. Yao (44)
ANL Contract File
ANL Libraries
TIS Files (6)

External:

DOE-TIC, for distribution per UC-94ca (318)
Manager, Chicago Operations and Regional Office, DOE
Chief, Office of Patent Counsel, DOE-CORO
V. Hummel, DOE-CORO
J. Purcell, DOE-CORO
Argonne Universities Association
President
C. B. Alcock, U. of Toronto
W. L. Worrell, U. of Pennsylvania
W. Ahmad, KW Battery, Skokie, IL
R. Alkire, University of Illinois, Urbana
M. Allen, Mechanical Technology Inc., Latham, NY
E. T. Ames, TRW Systems, Redondo Beach, CA
L. Andrews, Electric Vehicle Council, Washington, DC
S. J. Angelovich, Mallory Battery Co., Tarrytown, NY
G. M. Arcand, Idaho State University, Pocatello, ID
R. Aronson, Electric Field Propulsion Corp., Troy, MI
G. N. Ault, NASA-Lewis Research Center, Cleveland
J. D. Baker, Stewart Warner Corp., Chicago
W. Bales, Jet Industries, Inc., Austin
H. Balzan, Chattanooga, TN
K. F. Barber, DOE, Office of Transportation Programs, Washington
T. Barber, Jet Propulsion Laboratory, Pasadena

R. J. Barkley, Compass Industries, Inc., Hermosa Beach, CA
J. W. Barlass, Westinghouse Electric Corp., Skokie, IL
T. M. Barlow, Lawrence Livermore Lab.
D. Barron, Delco-Remy Div., GMC, Anderson, IN
R. Bassett, Sandia Labs, Albuquerque
W. Bauer, KW Battery, Skokie, IL
E. Baumann, LILCO, Mineola, NY
W. C. Beasley, Union Carbide Corporation, New York, NY
H. Bell, Arizona Public Service Co., Phoenix
J. Bellack, Cleveland Electric Illuminating Co., Cleveland
L. Belove, Marathon Battery Corp., Waco, TX
C. Berlsterling, C. Franklin Institute, Philadelphia
W. R. Benn, Great Lakes Carbon Corporation, New York, NY
D. N. Bennion, Brigham Young University, Provo, UT
C. Berger, Electrochemical & Water Desal. Technology, Santa Ana, CA
D. Bergmann, GM Transportation Systems Center, Warren, MI
J. Birk, Electric Power Research Institute, Palo Alto
W. S. Bishop, Air Force Aero Propulsion Lab, Wright-Patterson AFB
K. Blurton, Institute of Gas Technology, Chicago
D. P. Boden, C&D Batteries, Plymouth Meeting, PA
J. Bolger, University of California, Berkeley
D. Borello, Die Mesh Corp., Pelham, NY
A. Borucka, Borucka Research Co., Livingston, NJ
P. Bowen, C & D Batteries, Plymouth Meeting, PA
D. Bowman, United States Postal Service, Washington
J. C. Boylan, Electric Dynamics Corp., Plainwell, MI
B. J. Bragg, Bell Laboratories, Murray Hill, NJ
J. Brennand, General Research Corp., Santa Barbara
A. F. Brewer, Malibu, CA
D. C. Briggs, Philco-Ford Corp., Palo Alto
P. Bro, J. R. Mallory & Co., Inc., Burlington, MA
J. Broadhead, Bell Laboratories, Murray Hill, NJ
R. Brodd, Union Carbide Corp., Cleveland
E. P. Broglio, Eagle-Picher Industries, Joplin, MO
A. D. Brown, EVE Electric Motor Car, Inc., East Lansing, MI
P. J. Brown, DOE, Office of Transportation Programs, Washington
R. A. Brown, Eagle-Picher Industries, Joplin, MO
S. B. Brummer, EIC Corporation, Newton, MA
R. Buchholz, Honeywell Corp., Minneapolis
T. Burgess, Lucas Industries, N. A. Inc., Troy, MI
H. Burghart, Cleveland State University, Cleveland
D. Burns, Onan Corporation, Minneapolis
B. W. Burrows, Gould Inc., Rolling Meadows, IL
M. Burtgon, Delco Remy Div. of GMC, Anderson, IN
J. D. Busi, USA Foreign Science & Tech. Center, Charlottesville, VA
E. Buzzelli, Westinghouse Electric Corp., Pittsburgh
W. P. Cadogan, Emhart Corp., Hartford, CT
E. Cairns, Lawrence Berkeley Lab.
E. Campbell, Electric Vehicle Consultants, Inc., New York, NY
P. Campbell, University of Southern California, Los Angeles
J. Campbell, DOT/UMTA, Washington, DC
R. T. Carpenter, Kimberly Clark Corp. Neenah, WI
T. V. Carvey, Hughes Aircraft Corp., Culver City, CA
A. Charkey, Energy Research Corp., Danbury, CT

L. D. Christian, General Electric, Gainesville, FL
R. C. Chudacek, McGraw Edison Co., Bloomfield, NH
R. Clark, Sandia Labs., Albuquerque
J. E. Clifford, Battelle Memorial Institute, Columbus
J. A. Consiglio, Solva-Tek Associates, Topsfield, MA
A. R. Cook, ILZRO Inc., New York,
J. E. Cooper, Aero Propulsion Laboratory, Wright-Patterson AFB
K. E. Cooper, Trojan Battery Co., Santa Fe Springs, CA
G. Coraor, E. I. Du Pont de Nemours & Co., Inc., Wilmington, DE
R. E. Corbett, Lockhead Missiles & Space Co., Sunnyvale
K. E. Cox, University of New Mexico, Albuquerque
W. W. Craig, Edward Harding and Co., Chicago,
D. Crane, United States Postal Service, Washington
R. A. Crawford, PPG Industries, Barberton, OH
H. H. Crist, AM General Corp., Wayne, MI
R. H. Dare, Battronic Truck Corp., Boyertown, PA
D. Davis, Lawrence Livermore Lab.
R. J. Dawson, ESB Inc., Madison, WI
J. Devitt, Denver, CO
A. N. Dey, P. R. Mallory & Co. Inc., Burlington, MA
G. A. DiBari, INCO, Suffern, NY
W. J. Dippold, DOE, Office of Transportation Programs, Washington
T. P. Dirske, Calvin College, Grand Rapids, MI
D. DiVirgillo, Lockhead Missiles and Space Co., Inc., Sunnyvale, CA
D. Douglas, Electric Power Research Institute, Palo Alto
D. Dow, Detroit, MI
D. Dunoye, Reston, VA
T. Dwyer, Corning Glass Works, Corning, NY
E. F. Echolds, AiResearch Manufacturing Co., Torrance, CA
M. Eisenberg, Electrochimica Corp., Mountain View, CA
D. B. Eisenhaure, Charles Stark Draper Lab Inc., Cambridge, MA
T. Eissenberg, Oak Ridge National Lab., Oak Ridge, TN
M. W. Ellison, Hughes Aircraft Corp., El Segundo
D. Elson, Black and Decker Inc., Towson, MD
R. English, General Battery Co., Reading, PA
B. Enserik, Dynamic Science, Phoenix
R. Enters, McGraw Edison Co., Bloomfield, NJ
H. Espig, Gould Inc., Rolling Meadows, IL
A. Ewing, DOE, Office of Transportation Programs, Washington
G. Farbman, Westinghouse Electric Corp., Pittsburgh
F. Fedor, Bell Laboratories, Murray Hill, NJ
R. Fedora, Gould Inc., Rolling Meadows, IL
W. Feduska, Westinghouse Electric Corp., Pittsburgh
W. H. Fengler, Meteor Research Limited, Roseville, MI
F. Feres, KW Battery Company, Skokie, IL
R. Ferraro, Electric Power Research Institute
D. T. Ferrell, Exide Corporation, Yardley, PA
E. Fiss, Duke Power Company, Charlotte, NC
A. Fleischer, Orange, NJ
C. W. Fleischmann, C&D Batteries, Plymouth Meeting, PA
R. F. Fogle, North American Rockwell, Anaheim
R. T. Foley, American University, Washington, DC
J. S. Fordyce, NASA-Lewis Research Center, Cleveland
H. A. Fuggiti, Exide Management and Technology Co., Yardley, PA

T. Fujita, Pasadena, CA
B. Ganji, KW Battery Co., Skokie, IL
G. Gelb, Advanced Ground Systems, Long Beach, CA
J. H. B. George, Arthur D. Little, Inc., Concord, MA
S. Geppert, Eaton Corporation, Southfield, MI
L. J. Gerlach, United States Postal Service, Rockville, MD
J. A. Gilchrist, Chloride America, Tampa
W. Gillespie, Structural Plastics Inc., Tulsa
C. Glassman, Transportation Research Center, East Liberty, OH
H. Glixon, Chevy Chase, MD
M. Globerman, General Services Administration, Washington
W. Goldman, Electric Vehicle Engineering, Lexington, MA
G. Goodman, Globe-Union Inc., Milwaukee
R. E. Goodson, Purdue University
J. Gould, Unique Mobility Inc., Englewood, CO
L. B. Gratt, IWG Corp., San Diego
H. Grepke, TurElec Inc., Bradenton, FL
D. Griter, Solar Centra, Mechanicsburg, OH
E. E. Grough, Lucas Industries Inc., Troy, MI
R. Guess, General Electric Research Lab, Schenectady
R. G. Gunther, General Motors Research Labs, Warren, MI
M. Hadden, Billing Energy Corp., Provo, UT
G. Hagey, DOE, Division of Technology Overview, Washington
N. Halterm, Chrysler Corporation, Detroit
H. Hamilton, University of Pittsburgh
R. Hamilton, Institute for Defense Analysis, Arlington, VA
W. Hamilton, General Research Corp., Santa Barbara
B. Hamlen, Exxon Enterprises Inc., Florham Park, NJ
D. Hanify, Fiat, Chicago
K. L. Hanson, Genearl Electric Co., Philadelphia
W. Harhay, Electric Vehicle Associates, Cleveland
J. H. Harrison, Naval Ship R&D Center, Annapolis, MD
G. Hartman, Exide Management and Technology Co., Yardley, PA
J. Hartman, General Motors Research Labs, Warren, MI
E. A. Heintz, Airso Speer Carbon Graphite, Niagara Falls, NY
E. V. Hellman, Gould Inc., Langhorne, PA
R. Heppenstall, Penn Jersey Suburu Inc., Pennsauken, NJ
A. Himy, Naval Sea Systems Command, Washington
V. Hlavin, NASA-Lewis Research Center
G. Hobbib, Exide Management and Technology Co., Cleveland
A. Hodgman, General Electric, Gainesville
R. Hoenburg, Mechanical Technology Inc., Latham, NY
R. Hudson, Eagle-Picher Industries, Joplin, MO
J. R. Huff, US Army Mobility Equipment R&D Command, Fort Belvoir, VA
H. L. Hughes, Oklahoma State University, Stillwater, OK
J. R. Hunt, International Nickel Co., Washington
H. R. Ivey, Wood-Ivey Systems Corp., Winter Park, FL
J. Jacus, Moore Haven, FL
M. A. Janse, Allegheny Power Service Corporation, Greensburg, PA
G. H. Jantz, Rensselaer Polytechnic Institute
L. Jenney, Office of Technology Assessment, U.S. Congress, Washington, DC
A. W. Johnson, General Electric Co., Philadelphia
F. Johnson, Department of Industry, Trade and Commerce, Ottawa, Canada
L. Jokl, MERADCOM, Fort Belvoir, VA

K. R. Jones, Thiensville, WI
W. J. Jones, Westinghouse Electric Corp., Pittsburgh
R. E. Jordan, Omega Motors Corp., Garden Grove, CA
D. Kane, National Motors Corp., Lancaster, PA
E. Kanter, Gulton Battery Corp., Metuchen, NJ
N. Kaplan, Harry Diamond Laboratories, Washington
V. Kapur, Arco Solar Inc., Chatsworth, CA
R. Kaylor, Kaylor Energy Products, Menlo Park
J. Keith, Kamon Sciences, Colorado Springs, CO
H. C. Kelly, OTA, U.S. Congress, Washington
J. G. Kennard, NASA-Lewis Research Center
R. L. Kerr, Aero Propulsion Lab., Wright Patterson AFB
J. A. Kerrella, Delco-Remy Division/GMC, Anderson, IN
R. A. Keyes, Robert A. Keyes Associates, Martinsville, IN
R. A. Kingery, Oconomowoc, WI
R. S. Kirk, DOE, Office of Transportation Programs, Washington
M. Klein, Energy Research Corporation, Danbury, CT
G. B. Kliman, General Electric Co., Schenectady
G. B. Klinean, General Electric Co., Schenectady
R. C. Knechtli, Malibu, CA
R. A. Knight, AMF Inc., Stamford, CT
O. R. Kozak, American Battery Corp., Long Beach, NY
J. G. Krisilas, Aerospace Corporation, El Segundo, CA
P. E. Krouse, Exide Management & Technology Co., Yardley, PA
R. R. Kubalek, St. Joe Lead Co., Clayton, MD
L. Kulin, Whirlpool Corp. Benton Harbor, MI
C. M. Langkau, Union Carbide Co., Cleveland
H. Lauve, Electric Auto Corporation, Troy, MI
J. Lee, RAI Research Corp., Hauppauge, NY
I. J. Levine, Consolidated Edison, New York
K. Levine, St. Joe Minerals Corp., Pittsburgh
H. Lim, Hughes Research Lab., Malibu, CA
D. Linden, Little Silver, NJ
E. L. Littauer, Lockhead Palo Alto Research Laboratory
A. Long, Zeonics Corp., Fairfax, VA
E. Long, St. Joe Minerals Corp., Monaca, PA
M. Lugash, Maxon Industries, Huntington Park, CA
J. T. Lundquist, W. R. Grace & Co., Columbia, MD
T. Lynch, Fiber Materials, Inc., Biddeford, ME
E. N. Mabuce, Union Electric Co., St. Louis
J. MacDougall, AT&T, Basking Ridge, NJ
D. E. Mains, Naval Weapons Support Center, Crane, IN
J. Maisel, Cleveland State University, Cleveland
J. S. Makulowich, Electric Vehicle Council, Washington
V. Manson, National Aeronautics and Space Adm., Washington
L. S. Marcoux, Hughes Aircraft Company, Los Angeles
K. Marshall, KW Battery Company, Skokie, IL
T. W. Martin, United States Postal Service, San Bruno, CA
A. Masters, Packaged Promotions Inc., Chicago
S. Matsuda, Thermo Electron Corp., Waltham, MA
C. E. May, NASA-Lewis Research Center, Cleveland
E. Meeks, Derl Manufacturing Co., Compton, CA
N. Merriman, Army Picatinny Arsenal, Dover, NJ
S. Meschkow, Franklin Research Institute, Philadelphia

J. D. Meiggs, Kaman Sciences Corp., Colorado Springs
P. Mighdoll, Booz-Allen & Hamilton, Cleveland
R. P. Mikkelson, General Dynamics, San Diego
D. G. Miley, U.S. Naval Ammunition Depot, Crane, IN
H. Miller, Department of Transportation, Cambridge, MA
D. K. Miner, Copper Development Associates, Birmingham, MD
L. J. Minnick, Industrial Research Consultant, Plymouth Meeting, PA
L. G. Morin, Tarrytown, NY
F. Morse, University of Maryland, College Park
A. Moss, Leesona Moos Laboratories, Warwick, RI
R. Mueller, University of California, Berkeley
J. H. Muir, Dimension V Inc., Indialantic, FL
J. P. Mullin, National Aeronautics & Space Administration, Washington
G. Murphy, Northwestern University
B. McCormick, Los Alamos Scientific Lab.
L. R. McCoy, Energy Systems Group, Canoga Park
R. McKee, McKee Engineering, Palatine, IL
F. McLarnon, Lawrence Berkeley Lab.
P. McRay, ILC Technology, Sunnyvale
W. J. Nagle, NASA-Lewis Research Center, Cleveland
H. V. Nadham, Bogue Batteries, El Segundo
L. Nalley, Creative Research Co., Roebuck, SC
J. Newman, Univ. of California, Berkeley
J. S. Newton, Newton Engineering Co., Glen Ellyn, IL
M. M. Nickolson, Atomics International Division, Canoga Park
A. O. Nilsson, NIFE Incorporated, Lincoln, RI
J. Norberg, Exide Management & Technology Co., Philadelphia
A. C. Occhipinti, Kenner, LA
L. G. O'Connell, Lawrence Livermore Lab.
G. Odom, Georgia Power Company, Atlanta, GA
R. Oglesby, GM Transportation Systems Ctr., Warren, MI
L. Omohundro, Kingery Research & Development, Wake Forest, NC
E. I. Onstott, Los Alamos Scientific Lab
R. Osteryoung, Colorado State University, Fort Collins
B. N. Otzinger, North American Aviation, Downey, CA
J. P. Overman, Hammond Lead Products Inc., Hammond, IN
J. E. Oxley, Gould Inc., Rolling Meadows, IL
E. Papandreas, RET, Lake Worth, FL
J. S. Parkinson, Johns-Manville R&D Center, Manville, NJ
J. M. Parry, Arthur D. Little Inc., Cambridge, MA
E. Patagalia, General Services Administration, Washington
S. Pauling, Naperville, IL
J. E. Pavolsky, NASA/Lyndon B. Johnson Space Ctr., Houston
C. Pax, DOE, Office of Transportation Programs, Washington
E. Pearlman, Exide Management and Technology Co., Yardley, PA
G. F. Pezdirtz, DOE, Energy Storage Systems, Washington
A. G. Plunckett, General Electric R&D Center, Schenectady
R. A. Powers, Union Carbide Corp., Cleveland
V. J. Puglisi, Yardney Electric Corp., Pawcatuck, CT
E. Ramirez, Amectran, Dallas
E. Raskin, USAF Cambridge Research Laboratory, Bedford, MA
A. D. Raynard, AiResearch Manufacturing Co., Torrance, CA
E. C. Read, Exxon Enterprises, Linden, NJ
H. L. Recht, Atomics International Division, Canoga Park

N. Richie, KW Battery Co., Skokie, IL
C. Ridgway, Walt Disney World Co., Lake Buena Vista, FL
E. Rizkalla, DOE, Office of Controller, Washington
R. A. Rizzo, Globe-Union Inc., Milwaukee
R. Robert, The MITRE Corporation, McLean, VA
F. T. Rooney, Bureau of Automotive Maintenance, Norfolk, VA
L. Rosenblum, NASA-Lewis Research Center, Cleveland
N. Rosenburg, Department of Transportation, Cambridge, MA
R. Rosey, Westinghouse Electric Corp., Pittsburgh
J. Rossmon, Cornell University
G. Rowland, General Electric, Schenectady
J. Rubenzer, NASA-Ames Research Center, Moffett Field
P. H. Rubie, Electric Passenger Cars, Inc., San Diego
H. E. Ruskie, Naval Intelligence Support Center, Washington
A. J. Salkind, Exide Management & Technology Co., Yardley, PA
R. Schmidt, Volkswagen of America Inc., Englewood Cliffs, NJ
R. T. Schneider, RTS Laboratories, Gainesville, FL
L. W. Schopen, NASA-Lewis Research Center, Cleveland
H. J. Schwartz, NASA-Lewis Research Center, Cleveland
W. R. Scott, TRW Systems Inc., Redondo Beach
H. Seigel, South Coast Technology Inc., Santa Barbara
H. Seiger, Harvey Seiger Associates, Waterford, CT
J. Seliber, Fluid Drive Engineering Co., Wilmette, IL
E. Seo, Gates Energy Products, Denver, CO
L. Shahnasarian, Elcar Corp., Elkhart, IN
R. C. Shair, CENTREC Corporation, Fort Lauderdale
H. Shalit, ARCO Chemical Corp., Glendolden, PA
D. W. Sheibley, NASA-Lewis Research Center, Cleveland
E. Small, Ametran Corporation, Washington
G. A. Smith, Englehard Industries, Iselin, NJ
S. Smith, St. Joe Minerals Corp., Monaca, PA
V. Smith, Delco-Remy Div. GMC, Anderson, IN
J. Smits, Nevada Operations Office, Las Vegas, NV
I. J. Soloman, IIT Research Institute, Chicago
W. C. Spindler, Electric Power Research Institute, Palo Alto
J. S. Stanley, Dept. of the Army, U.S. Army Foreign Sci. & Tech. Center, Charlottesville, VA
E. J. Steeve, Commonwealth Edison Co., Chicago
I. Stein, Jet Propulsion Laboratory, Pasadena
T. A. Stoneham, Marathon Battery Company, Waco, TX
R. Strauss, Communications Satellite Corp., Clarksburg, MD
W. E. Strawbridge, Caterpiller Tractor Co., Peoria, IL
R. L. Strombotne, Transportation Systems Center, Cambridge, MA
S. Sudar, Rockwell International, Canoga Park
P. C. Symons, Energy Development Associates, Madison Heights, MI
F. Tepper, Catalyst Research Corp., Baltimore
R. Thacker, General Motors Research Labs, Warren, MI
C. E. Thomas, Chrysler Corp., New Orleans, LA
F. Thomas, Grumman Aerospace Corp., Bethpage, NY
G. M. Thur, DOE, Office of Transportation Programs, Washington
W. H. Tiedemann, Globe-Union Inc. Milwaukee, WI
C. W. Tobias, University of California, Berkeley
M. Thorpe, Towson, MD
A. Topouzian, Ford Motor Co., Dearborn, MI

W. Toth, Society of Automotive Engineers, Inc., Warrendale, PA
H. Toulmin, Bloomfield, MI
I. Trachtenberg, Texas Instruments, Dallas
G. W. Tuffnell, The International Nickel Co., Troy, MI
D. Turford, Western Mining Corp., Pittsburgh
G. H. Turney, Western Research Industries, Las Vegas, NV
E. A. Ulrich, Creative Automotive Research, Whittier, CA
R. L. Ulrich, General Services Administration, Washington
T. Ulrich, McGraw-Edison Co., Bloomfield, NJ
G. Underhill, A. D. Little, Cambridge, MA
H. B. Urbach, Naval Ship R&D Center, Annapolis, MD
H. Vaidyanathan, Energy Research Corp., Danbury, CT
C. J. Venuto, C&D Batteries, Plymouth Meeting, PA
S. W. Vreeland, General Dynamics, Convair Division, San Diego
A. Waddell, EBCO Battery Co., Columbus, GA
E. H. Wakefield, Linear Alpha Inc., Evanston, IL
R. Walker, University of Florida, Gainesville
C. H. Waterman, C. H. Waterman Industries, Althol, MA
G. Way, Troy, MI
W. Webster, DOE, Divison of Energy Storage Systems, Washington
R. D. Wehrle, Sandia Labs, Albuquerque, NM
C. Weinlein, Globe-Union Inc., Milwaukee
S. A. Weinter, Ford Motor Co., Detroit, MI
M. Weinreb, Consolidated Edison, New York
E. Y. Weissman, GASF Wynadotte Corp., Wynadotte, MI
I. Wender, Bureau of Mines, Pittsburgh, PA
H. B. West, McGraw-Edison Company, Bloomfield, NJ
M. E. Wilke, Burgess Battery Company, Freeport, IL
R. Wilks, Lavelle Aircraft Co., Newton, PA
C. F. Williams, Teledyne Isotopes, Timonium, MD
H. R. Williams, Detroit Edison Co., Detroit
J. M. Williams, E. I. DuPont De Nemours & Co., Wilmington, DE
E. Willhnganz, C&D Batteries, Plymouth Meeting, PA
N. L. Willmann, Delco-Remy Div. of GMC, Anderson, IN
R. Willow, Office of Technology Assessment, U.S. Congress, Washington, DC
J. F. Wing, Booz-Allen & Hamilton Inc., Bethesda, MD
K. Winters, Chrysler Corp., New Orleans, LA
T. J. Wissing, Eaton Corp., Southfield, MI
J. Wooldrige, Boeing Corp., Seattle
V. Wouk, Petro-Electric Motor Ltd., New York
R. A. Wynveen, Life Systems Inc., Cleveland
L. S. Yao, University of Illinois, Urbana
H. Yoder, Battronic Truck Corp., Boyertown, PA
M. Yontar, Jersey City, NJ
J. E. Zanks, NASA-Langley Research Center, Hampton, VA

☆ U.S. GOVERNMENT PRINTING OFFICE: 1980 — 651-118/15